New Uzbekistan University

UDC: 530.12:531.51

Davlataliev Akbar

Relativistic astrophysical processes around compact objects coupled with scalar field

01.03.01 - Astronomy

01.04.02 – Theoretical Physics

DISSERTATION OF THE DOCTOR OF PHILOSOPHY(PHD)

IN PHYSICS AND MATHEMATICS

Supervisors:

B. J. AHMEDOV

doctor of sciences in physics and mathematics, professor

A. A. ABDUJABBAROV

doctor of sciences in physics and mathematics, professor

TASHKENT - 2025

Contents

Acronyms

JNW	**J**anis-**N**ewman-**W**inicour
ISCO	**I**nnermost-**S**table- **C**ircular- **O**rbit
MSCO	**M**arginally-**S**table- **C**ircular- **O**rbit
SMBH	**S**uper-**M**assive- **B**lack- **H**oles
LMXB	**L**ow- **M**ass- **X**-ray- **B**inaries
MBO	**M**arginally- **B**ound- **O**rbit
VLBI	**V**ery- **L**ong- **B**aseline- **I**nterferometry

Physical constants & other definitions

Bohr radius	$a_B = \frac{4\pi\varepsilon_0\hbar^2}{m_e e^2} = \frac{\hbar}{m_e c\alpha} \approx 5.292 \times 10^{-9}\text{cm}$
Reduced Plank constant	$\hbar = h/2\pi \approx 1.054.. \times 10^{-27}$ g cm^2 s^{-1}
Vacuum permittivity	$\varepsilon_0 = 8.854 \times 10^{-12}$ F $\cdot$ m^{-1}
Electron rest mass	$m_e \approx 0.9109 \times 10^{-34}$ g
Elementary charge	$e = 1.602^{-19}$ C
Speed of Light	$c = 2.998 \times 10^{10}$ cm $\cdot$ s^{-1}
Fine structure constant	$\alpha \approx 7.297 \times 10^{-3}$
Avogadro's Constant	$N_A = 6.02214076 \times 10^{23}\text{mol}^{-1}$
Condensate initial width	$a_0 = (\hbar/M\omega)^{1/2}$
Mass of atom	M (^{87}Rb $= 87/N_A \approx 1.444 \times 10^{-22}$ g)
Harmonic oscillator frequency	ω ($\sim 10 - 100$ Hz)
Self-interaction parameter	$g = 4\pi\hbar^2\lvert a_s\rvert/Ma_z$ (for 2D)
s -wave scattering length	$\lvert a_s\rvert \approx 100a_B \approx 5 \times 10^{-7}\text{cm}$
Condensate extension along z-axis	a_z ($\sim 10^{-4}$ cm for 2D)

Introduction

Topicality and demand of the theme of the dissertation.

With the increasing precision of astronomical observations – such as gravitational wave detections (LIGO/Virgo) and high-frequency quasi-periodic oscillations (QPOs) from X-ray binaries—there is a growing demand for theoretical frameworks that extend beyond classical general relativity. This work provides essential insights into how scalar fields and external magnetic fields modify spacetime dynamics, offering testable predictions for future observations. The study of exotic compact objects (e.g. JNW naked singularities, Ellis wormholes) also aligns with ongoing efforts to probe the limits of Einstein theory and explore alternative gravity models. The dissertation addresses critical questions in modern relativistic astrophysics, particularly the interplay between compact objects (black holes, naked singularities, and wormholes) and scalar fields.

The dissertation's focus on scalar-tensor couplings and their astrophysical implications is highly relevant, given recent developments in modified gravity, dark matter, and dark energy research. Scalar fields are fundamental in theories like $f(R)$ gravity and string-inspired models, making this work pertinent to both theoretical and observational cosmology. Additionally, the analysis of quasi-resonant modes and QPOs contributes to the interpretation of data from next-generation telescopes (e.g., LISA, Athena) and X-ray observatories (e.g., NICER). The unusual late-time tails of perturbations in magnetized black holes, as explored in

Chapter IV, could even shed light on anomalies in pulsar timing array (PTA) signals, such as those reported by NANOGrav.

By bridging particle dynamics, perturbation theory, and observational constraints, this dissertation advances the toolkit for studying compact objects in extreme environments. Its methodologies, such as the WKB approximation for quasinormal modes and MCMC analysis for QPOs, are transferable to other compact object scenarios, including neutron stars and exotic horizonless objects. The work also underscores the importance of interdisciplinary approaches, combining general relativity, quantum field theory, and data science to tackle open problems in astrophysics. As the community seeks to resolve tensions between general relativity and quantum mechanics, studies like this pave the way for new physics beyond the Standard Model. The topicality, demand, and actuality of the dissertation lie in its direct engagement with cutting-edge questions in relativistic astrophysics, its applicability to current and future observational campaigns, and its potential to influence theoretical paradigms in gravity and cosmology.

Furthermore, the dissertation aligns with the strategic scientific priorities in Uzbekistan and the broader international community. This dissertation work corresponds to the tasks of the following state regulatory documents: Decree of the President of the Republic of Uzbekistan No. UP-4947 "On the Strategy of Actions for the Further Development of the Republic of Uzbekistan" dated February 07, 2017, Decree of the President of the Republic of Uzbekistan No. PP-2789 "On Measures for Further Improvement of Academy of Sciences, Organization, Management, and Financing of Research Activities from 18.02.2017.

Relevance of the research to the priority areas of science and technology development of the Republic of Uzbekistan. Dissertation research has been carried out in accordance with the priority areas of science and technology in the

Republic of Uzbekistan: II. “Power, energy and resource-saving”.

Degree of study of the problem

While the motion of test particles in black hole spacetimes has been extensively studied in general relativity (Subrahmanyan Chandrasekhar, Brandon Carter, James Bardeen, Valeri Frolov, Andrei Zelnikov, Pankaj S. Joshi, Remo Ruffini), the inclusion of scalar fields, particularly in the context of naked singularities (JNW spacetime) and wormholes (Ellis spacetime) – introduces novel complexities. This research work builds on foundational studies by Misner, Wheeler, and others but extends them by incorporating scalar couplings, radiation reaction effects, and magnetic fields, which have not been systematically explored in these spacetimes. This represents a significant advance beyond the classical treatments of geodesic motion.

Prior research on scalar fields in astrophysics has largely focused on cosmological applications or black hole perturbations (Claudia de Rham, Thomas P. Sotiriou, Vitor Cardoso, Kostas D. Kokkotas, Toby Crisford, Hideo Kodama), leaving gaps in understanding their role in naked singularities and wormholes. This dissertation fills these gaps by deriving exact analytical solutions (e.g., ISCO radii in JNW spacetime), numerical simulations of particle trajectories, and perturbation analyses (e.g., quasinormal modes in magnetized black holes). The study of quasiperiodic oscillations (QPOs) in scalar-modified spacetimes is particularly original, as it connects theoretical predictions with observational data from X-ray binaries, a link that has rarely been explored in the earlier literature. The inclusion of MCMC methods to constrain spacetime parameters further demonstrates a modern, data-driven approach to testing theoretical models.

Compared with similar studies, this work stands out by integrating scalar fields, electromagnetic interactions, and radiation reaction into a unified framework for

multiple types of compact objects. However, certain limitations remain, such as the assumption of weak backreaction (neglecting particle effects on spacetime geometry) and the restriction to static, spherically symmetric solutions. Rotating compact objects (e.g., Kerr-like naked singularities) and nonlinear scalar couplings remain open challenges. Future research could extend this work by incorporating numerical relativity techniques or higher-dimensional theories (e.g., braneworld models), which would deepen the exploration of scalar-field dynamics in more realistic astrophysical scenarios. The dissertation provides a comprehensive but not exhaustive study of the problem, balancing analytical rigor with innovative applications while identifying clear pathways for future research.

Connection of the topic of the dissertation with the scientific research of the higher educational/research institutions, where the dissertation was carried out. The dissertation was done in the framework of the scientific projects funded by the Ministry of Innovative Development: F-FA-2021-510 "Investigations of nuclear matter of neutron stars in modified gravity" (2021-2026).

The aim of the research is develop a new theoretical model to study scalar field couplings and reveal new findings on particle dynamics near compact objects.

The tasks of the research:

- to develop a theoretical model coupling scalar fields to particle dynamics in JNW and Ellis spacetimes;
- to derive equations of motion for massive particles under scalar field influence;
- to analyze ISCO modifications due to scalar coupling parameters;
- to investigate radiation reaction effects on particle trajectories near naked singularities;

- to compute fundamental frequencies (orbital, radial, vertical) for QPO applications;

- to conduct MCMC analysis to constrain spacetime parameters using X-ray binary data;

- to explore charged particle dynamics in magnetized wormhole and black hole spacetimes.

- to study perturbation spectra (quasinormal modes, late-time tails) in scalar-modified geometries.

The objects of the research are the Janis-Newman-Winicour (JNW) naked singularity spacetime with scalar field coupling; the Ellis wormhole geometry interacting with external scalar fields; Schwarzschild-like regular black holes immersed in external magnetic fields; test particles (neutral and charged) in these modified spacetime geometries.

The subjects of the research are dynamics of massive particles under scalar field influence in exotic spacetimes; modification of orbital mechanics and fundamental frequencies due to scalar couplings; astrophysical implications of scalar-field modified compact objects (QPOs, ISCOs, etc.); perturbation spectra and stability properties of scalar-coupled compact objects.

The methods of the research. Analytical modeling was used to derive exact equations of motion and effective potentials for particles in scalar-coupled spacetimes (JNW, Ellis). Numerical simulations (Runge-Kutta integration) were used to solve geodesic equations and analyze particle trajectories under radiation reaction effects. Semi-analytical WKB approximation and time-domain integration techniques were applied to compute quasinormal modes and perturbation spectra.

Bayesian MCMC analysis was conducted to fit theoretical QPO frequencies to observational data from X-ray binaries.

The scientific novelty of the research is as follows:

- The research establishes the first complete theoretical model of particle dynamics in JNW naked singularity spacetime with scalar coupling, revealing unique ISCO behavior that distinguishes it from black holes.

- Novel findings demonstrate how scalar fields modify Ellis wormhole physics, including radiation-driven particle escape and characteristic QPO frequencies that differentiate exotic compact objects from black holes.

- The work pioneers MCMC-based constraints on scalar field parameters using X-ray binary data and identifies new spectral signatures for testing modified gravity theories in strong-field regimes.

Practical results of the research are as follows:

- The analytical expressions derived for particle dynamics in scalar-modified spacetimes enable the precise modeling of accretion-disk structures and emission profiles around exotic compact objects.

- The computed QPO frequencies and ISCO radii provide observable signatures to distinguish JNW naked singularities and Ellis wormholes from black holes using X-ray binary data.

- The MCMC-fitted scalar field parameters ($n \sim 0.75$, $g_s \sim 0.2$) offer testable constraints for future gravitational wave and multi-messenger astrophysics campaigns.

- The identified perturbation spectra (e.g., confluent Heun solutions, oscillatory tails) serve as benchmarks for detecting scalar-tensor gravity effects in next-generation observatories.

Reliability of the research results is provided by the following:

- The analytical framework was rigorously derived from first principles and cross-verified against established results in general relativity, ensuring mathematical consistency throughout all calculations.
- Numerical simulations employed multiple independent methods (Runge-Kutta integration, WKB approximation) that produced consistent results, confirming the robustness of the particle dynamics and perturbation analyses.
- The MCMC parameter estimation was validated through convergence tests and comparison with existing astrophysical constraints, demonstrating statistical reliability of the scalar field coupling values.
- All theoretical predictions maintain consistency with observational data from X-ray binaries and known black hole phenomenology, while clearly identifying testable deviations for future verification.

Scientific and practical significance of the research.

- The research establishes a comprehensive framework for analyzing scalar field effects in exotic compact objects, providing new insights into the interplay between gravity and fundamental fields beyond classical black hole paradigms.
- The derived QPO frequencies and ISCO modifications serve as crucial observational discriminators between black holes, naked singularities, and wormholes, which are directly applicable to current X-ray telescope data analysis.

- The developed MCMC-QPO analysis technique and perturbation methods offer powerful new tools for constraining modified gravity theories using astrophysical data, significantly enhancing precision gravity tests.

- Technological Guidance: By identifying unique spectral signatures of scalar-tensor interactions, the results inform the design requirements for next-generation gravitational wave detectors and multimessenger astronomy campaigns.

Application of the research results.

The results of the study of the dynamics of particles around black holes in modified gravity theories have been applied as follows:

the theoretical research results and methods, published in the scientific paper "A. Davlataliev, B. Narzilloev, I. Hussain, A. Abdujabbarov, B. Ahmedov, "Probing the Starobinsky-Bel-Robinson gravity by photon motion around the Kerr-type black hole in non-uniform plasma," // Phys.Dark Univ. 42 (2023) 101340, https://doi.org/ 10.1016/j.dark.2023.101340" and presented in the Doctorate (PhD) thesis of Mr. A. Davlataliev have been used in the frame of the programs supported by the Fudan University (Letter from Prof. Cosimo Bambi)

Approbation of the research results

The dissertation results have been discussed in 3 international conferences.

Publication of the research results

11 scientific publications have been made on research results

Volume and structure of the dissertation

Consists of an introduction, four chapters, a conclusion, and a list of references, all in 120 pages.

List of published papers [1–11].

1. **Akbar Davlataliev**, Bakhtiyor Narzilloev, Ibrar Hussain, Ahmadjon Abdujabbarov, Bobomurat Ahmedov, "Probing the Starobinsky-Bel-Robinson gravity by photon motion around the Kerr-type black hole in non-uniform plasma," // **Physics of Dark Universe** 42 (2023) 101340, (Web of Science IF:=5.0 **Q1**)

   https://doi.org/10.1016/j.dark.2023.101340

2. **Akbar Davlataliev**, Bakhtiyor Narzilloev, Ibrar Hussain, Ahmadjon Abdujabbarov, Bobomurat Ahmedov, "Quasi periodic oscillations around Kerr-type black hole in the Starobinsky–Bel–Robinson theory of gravity," //**Physics of Dark Universe** 46 (2024) 101569. (Web of Science IF:=5.0 **Q1**)

   https://doi.org/10.1016/j.dark.2024.101569

3. **Akbar Davlataliev**, Bakhtiyor Narzilloev, Ibrar Hussain, Ahmadjon Abdujabbarov, Bobomurat Ahmedov, "Charged and magnetized particle motion around a static black hole in the Starobinsky–Bel–Robinson gravity" // **The European Physics Journal C** 84 (2024) 7, 694. (Web of Science IF:=4.9 **Q1**)

   https://doi.org/10.1140/epjc/s10052-024-13039-3

4. **Akbar Davlataliev**, Javlon Rayimbaev, Farukh Abdulkhamidov, Zdenek Stuchlik, Ahmadjon Abdujabbarov, "Circular motion and collisions of charged spinning particles near Kerr Newman black holes", // **Physics of Dark Universe** 46 (2024) 101590. (Web of Science IF:=5.0 **Q1**)

   https://doi.org/10.1016/j.dark.2024.101590

5. **Akbar Davlataliev**, Farruh Atamurotov, Ahmadjon Abdujabbarov, Noz-

ima Juraeva, Vokhid Khamidov, "Constraints on Schwarzschild-like black hole from QPOs data", // **Physics of Dark Universe** 46 (2024) 101603. (Web of Science IF:=5.0 **Q1**)

https://doi.org/10.1016/j.dark.2024.101603

6. Bobur Turimov, **Akbar Davlataliev**, Ahmadjon Abdujabbarov, Bobomurat Ahmedov, "Influence of scalar field in massive particle motion in JNW spacetime", // **Physical Review D** 110 (2024) 8, 084053. (Web of Science IF:=5.29 **Q1**)

   https://doi.org/10.1103/PhysRevD.110.084053

7. G. Mustafa, Emre Demir, **Akbar Davlataliev**, Himanshu Chaudhary, Farruh Atamurotov, "Observational signature of QPOs with particle motion around non-commutative Schwarzschild black hole surrounded by perfect fluid dark matter", // **Physics of Dark Universe** 46 (2024) 101644. (Web of Science IF:=5.0 **Q1**)

   https://doi.org/10.1016/j.dark.2024.101644.

8. Bobur Turimov, **Akbar Davlataliev**, Bobomurat Ahmedov, Zdeněk Stuchlík, "Exploring a novel feature of ellis spacetime: Insights into scalar field dynamics", //**Chinese Journal of Physics** 94 (2025) 807-819. (Web of Science IF:=4.6 **Q1**)

   https://doi.org/10.1016/j.cjph.2024.09.030.

9. Bobur Turimov, **Akbar Davlataliev**, Yusuf Usmanov, Shavkat Karshiboev, Pulat Tadjimuratov, "Investigating new aspects of Bocharova–Bronnikov–Melnikov–Bekenstein spacetime: ionized thin accretion disk model", // **The European Physics Jouranl C** 84 (2024) 10,

1098, (Web of Science IF:=4.9 **Q1**)

https://doi.org/10.1140/epjc/s10052-024-13426-w.

10. Husanboy Hoshimov, **Akbar Davlataliev**, Farruh Atamurotov, Ahmadjon Abdujabbarov, Ali Övgün, "Particle dynamics and quasi-periodic oscillations in the Dyonic ModMax: Constraint using quasars data", // **Journal of High Energy Astrophysics** 45 (2025) 306-315. (Web of Science IF:=10.2 **Q1**)

https://doi.org/10.1016/j.jheap.2024.12.012 .

11. Bobur Turimov, Ozodbek Rahimov, **Akbar Davlataliev**, Pulat Tadjimuratov, Mukhiddin Norkobilov, "Analysing geodesic motion in Bocharova–Bronnikov–Melnikov–Bekenstein spacetime," // **Physics of Dark Universe** 48 (2025) 101855, (Web of Science IF:=5.0 **Q1**)

https://doi.org/10.1016/j.dark.2025.101855

Chapter I

Influence of scalar field in massive particle motion in JNW spacetime

1.1 Introduction

A fundamental unresolved issue in general relativity concerns the ultimate fate of the gravitational collapse of a massive astrophysical object. It is commonly believed that a complete gravitational collapse generally leads to the formation of a Kerr black hole, which is fully characterized by just its total mass and angular momentum. All other physical attributes—such as initial symmetries or matter field properties—are thought to be radiated away during the collapse process [12]. However, this remains a hypothesis that requires validation through detailed computational studies that incorporate all relevant physical influences. Therefore, one should approach this conjecture with caution, as it is not yet definitively proven that gravitational collapse always ends in the formation of a black hole. Indeed, numerous studies have demonstrated that under specific, physically acceptable initial conditions, gravitational collapse can instead result in the formation of a naked singularity [13–18].

To investigate the mechanism of gravitational collapse and its end products, it is

essential to examine the observational distinctions between black holes and naked singularities, under the assumption that both can arise through some formation processes. Currently, we have access to extensive electromagnetic data from astrophysical sources, which can help reveal the nature of compact objects located at galactic centers or within X-ray binary systems. In particular, Refs. [19–25]. Authors have explored the accretion disks properties around naked singularity. The studies described in Refs. [26–32] demonstrate that black holes and naked singularities exhibit distinct gravitational lensing characteristics, allowing them to be distinguished observationally [31,33–36]. Additionally, high-energy phenomena and particle collisions may provide further means to differentiate black holes from naked singularities [37].

The motion of particles in curved spacetime is a fundamental aspect of general relativity, illustrating how spacetime curvature—shaped by matter and energy—affects the trajectories of particles. In such a curved geometry, particles move along geodesics, which are determined by the geodesic equation. When a charged particle is subject to an external electromagnetic field, it undergoes acceleration and emits electromagnetic radiation. This results in motion that deviates from a geodesic and is governed by a modified equation that includes the effects of the electromagnetic field and radiation reaction. A detailed discussion of different types of electromagnetic radiation and their mathematical descriptions can be found in [38].

Furthermore, the study of particle motion under the influence of an external scalar field is both theoretically important and astrophysically relevant. Although the interaction between scalar fields and massive particles is not yet fully understood, it plays a critical role in modeling phenomena occurring near compact objects such as black holes and neutron stars. This issue has been addressed in [39],

where the self-force acting on particles in a scalar field background is analyzed. Some aspects of this self-force can be interpreted geometrically, offering insights into the puzzling case where a radiating particle does not feel a corresponding self-force. The acceleration of particles near black holes in the presence of scalar fields has been investigated in [40]. Additionally, the influence of scalar fields on massive particles was previously explored by Misner et al. [41] and Breuer et al. [42], particularly in the context of scalar perturbations and the phenomenon known as geodesic synchrotron radiation in Schwarzschild spacetime.

In this chapter, we plan to study the particle dynamics. around the Janis-Newman-Winicour (JNW) naked singularity. JNW naked singularity represents an exact solution of the Einstein's equations with a massless scalar field [43]. With the different parametrization the similar solution has been obtained by Fisher in Ref. [44] The stability of Fisher's solution has been studied in Ref. [45]

The chapter is organized as follows. In Sect.1.2 we briefly describe the Einstein-scalar field-massive particle system and derive the equation of motion for the whole system. In Sect.1.3 we consider the circular motion of massive particles in the presence of the scalar field in the JNW spacetime. In Sect.1.4 we study the circular motion of massive particles including the radiation reaction term and present particle trajectories. Finally, in Sect.1.5 we summarize the results of the investigation.

1.2 Einstein-scalar field-massive particle system

The action for the free relativistic particle of mass m can be expressed as [46]

$$S = -\int m ds \ , \tag{1.1}$$

while in the presence of the external scalar field φ, it reads [42]

$$S = -\int m_* ds \ , \qquad m_* = m(1 + g_s\varphi) \ , \tag{1.2}$$

where m_* is the effective mass of the test particle in the presence of a scalar field, and g_s is a dimensionless coupling constant between scalar and massive particle. Notice that in Ref. [41,42] that the action for massive particle and scalar field can be expressed as follows:

$$\begin{aligned} S[x^\mu, \varphi] = &-\frac{1}{8\pi}\int d^4x\, \partial_\mu\varphi\partial^\mu\varphi \\ &- m\int ds(1 + g_s\varphi)\sqrt{-u_\mu u^\mu} \ . \end{aligned} \tag{1.3}$$

One has to emphasise that the action for massive particle in equation (1.3) is also valid in curved spacetime. The generalized form of the action for the Einstein-scalar field system, including massive particles, is given as

$$\begin{aligned} S[g_{\mu\nu}, x^\mu, \varphi] = &\frac{1}{16\pi}\int d^4x\sqrt{-g}(R - 2\nabla_\mu\varphi\nabla^\mu\varphi) \\ &- m\int ds(1 + g_s\varphi)\sqrt{-u_\mu u^\mu} \ , \end{aligned} \tag{1.4}$$

where R is the Ricci scalar, ∇_μ stands for a covariant derivative from a scalar field and $u^\mu = \dot{x}^\mu$ is the four-velocity of particle normalized as $u_\mu u^\mu = -1$. Hereafter minimizing the action (1.4), equations of motion for whole system, namely Einstein field equations, Klein-Gordon equation and geodesic equation, can be derived as

$$\begin{aligned} R_{\mu\nu} - \frac{1}{2}g_{\mu\nu}R = &\ 2\nabla_\mu\varphi\nabla_\nu\varphi - g_{\mu\nu}\nabla_\lambda\varphi\nabla^\lambda\varphi \\ &+ \frac{8\pi m}{\sqrt{-g}}\int ds(1 + g_s\varphi)\delta^{(4)}[x - z(s)]u_\mu u_\nu \ , \end{aligned} \tag{1.5}$$

$$\nabla_\mu\nabla^\mu\varphi = \frac{4\pi m g_s}{\sqrt{-g}}\int ds\delta^{(4)}[x - z(s)] \ , \tag{1.6}$$

$$u^\mu\nabla_\mu u^\nu = \frac{g_s}{1 + g_s\varphi}(g^{\mu\nu} + u^\mu u^\nu)\nabla_\mu\varphi \ . \tag{1.7}$$

For simplicity, we assume that the contribution of particle motion in the background spacetime and scalar field is negligibly small, and it does not alter the background geometry or the configuration of the scalar field. Consequently, equations of motion for the system reduces to

$$R_{\mu\nu} = 2\nabla_\mu\varphi\nabla_\nu\varphi \ , \tag{1.8}$$

$$\nabla_\mu\nabla^\mu\varphi = 0 \ , \tag{1.9}$$

$$u^\mu\nabla_\mu u^\nu = \frac{g_s}{1+g_s\varphi}(g^{\mu\nu}+u^\mu u^\nu)\nabla_\mu\varphi \ . \tag{1.10}$$

which are rather simply system of equations. In next section, we will discuss the explicit solution of above equations.

1.3 Background spacetime and particle dynamics

In this section, we will explore the motion of a massive particle within scalar and gravitational fields. The system of equations (3.51) and (1.9) is straightforward, allowing for an exact analytical solution. One of the simplest solutions to these Einstein-scalar field equations is represented by the Janis-Newman-Winicour naked singularity. The corresponding line element is given as [47]

$$\begin{aligned} ds^2 =& -f^n dt^2 + f^{-n}dr^2 + f^{1-n}r^2(d\theta^2+\sin^2\theta d\phi^2) \ , \\ \varphi(r) =& \frac{\sqrt{1-n^2}}{2}\ln f \ , \qquad f = 1-\frac{2M}{nr} \ , \end{aligned} \tag{1.11}$$

where M is the mass of the gravitational object, n is parameter of the scalar field. The singularity of the spacetime is located at $r_* = 2M/n$. The components Ricci

tensor are expressed by

$$R_{\mu\nu} = \frac{2(1-n^2)M^2}{f^2 n^2 r^4} \begin{pmatrix} 0 & 0 & 0 & 0 \\ 0 & 1 & 0 & 0 \\ 0 & 0 & 0 & 0 \\ 0 & 0 & 0 & 0 \end{pmatrix} . \tag{1.12}$$

When $n = 1$, the solution (3.1) reduces to the Schwarzschild spacetime, characterized by a horizon at $r = 2M$ and satisfying $R_{\mu\nu} = 0$.

The equation of motion for a massive particle in equation (1.10) in the background spacetime (3.1), can be explicitly written as:

$$\ddot{t} + \frac{2M\dot{t}\dot{r}}{fr^2}(1-B) = 0 , \tag{1.13}$$

$$\ddot{r} + \frac{Mf^n}{fr^2}\left(f^n\dot{t}^2 - 2B\right) - \frac{M\dot{r}^2}{fr^2}(1+2B) + \left(\frac{M(n+1)}{n} - r\right)\left(\dot{\theta}^2 + \sin^2\theta\dot{\phi}^2\right) = 0 , \tag{1.14}$$

$$\ddot{\theta} - \frac{1}{2}\sin 2\theta\dot{\phi}^2 - \frac{2M\dot{\theta}\dot{r}}{fr^2}\left(1 + \frac{1}{n} - \frac{r}{M} + B\right) = 0 , \tag{1.15}$$

$$\ddot{\phi} + 2\cot\theta\dot{\theta}\dot{\phi} - \frac{2M\dot{r}\dot{\phi}}{fr^2}\left(1 + \frac{1}{n} - \frac{r}{M} + B\right) = 0 , \tag{1.16}$$

where B is defined as

$$B = \frac{2g_s\sqrt{1-n^2}}{n(g_s\sqrt{1-n^2}\ln f + 2)} .$$

On the other hand, using the equation of motion (1.10), the Lagrangian for a massive particle in the presence of the scalar field can be expressed as:

$$L = \frac{1}{2}(1+g_s\varphi)g_{\mu\nu}u^\mu u^\nu , \tag{1.17}$$

and the four-momentum of the massive particle is

$$P_\mu = \frac{\partial L}{\partial u^\mu} = (1+g_s\varphi)g_{\mu\nu}u^\nu . \tag{1.18}$$

Since the spacetime is independent of the coordinates t and ϕ, the corresponding components of the four-momentum, P_t and P_ϕ, are conserved. These correspond to two conserved quantities: the energy and angular momentum of the massive particle. The explicit expressions for the specific energy $\mathcal{E}$ and specific angular momentum $\mathcal{L}$ are:

$$\mathcal{E} = -\frac{P_t}{m} = -(1 + g_s\varphi) g_{tt} u^t \ , \tag{1.19}$$

$$\mathcal{L} = \frac{P_\phi}{m} = (1 + g_s\varphi) g_{\phi\phi} u^\phi \ . \tag{1.20}$$

Using the normalization of the four-velocity of particle, one can obtain

$$g_{rr}\dot{r}^2 + g_{\theta\theta}\dot{\theta}^2 + 1 + \frac{1}{(1 + g_s\varphi)^2}\left(\frac{\mathcal{E}^2}{g_{tt}} + \frac{\mathcal{L}^2}{g_{\phi\phi}}\right) = 0 \ . \tag{1.21}$$

Here we focus on finding the ISCO position of massive particle in the JNW spacetime in the presence of the scalar field. For qualitative analyses, let us consider motion of massive particle in the equatorial plane, (i.e. $\theta = \pi/2$ and $\dot{\theta} = 0$). Hereafter performing simple algebraic manipulations equation (3.14) can be rewritten as

$$\mathcal{E}^2 = (1 + g_s\varphi)^2\dot{r}^2 + U(r) \ , \tag{1.22}$$

where

$$U(r) = f^n(1 + g_s\varphi)^2 + \frac{\mathcal{L}^2}{r^2} f^{2n-1} \ , \tag{1.23}$$

is the effective potential for massive particle.

The ISCO radius of massive test particle is a crucial concept in the study of the dynamics around compact astrophysical objects such as black holes and neutron stars. It represents the smallest radius at which a test particle can stably orbit the central object. Inside this radius, any perturbation will cause the particle to spiral inward, leading to eventual accretion onto the central body. For the

Schwarzschild black hole, the ISCO radius is located at $r_{\rm ISCO} = 6M$. In the case of a rotating Kerr black hole, the ISCO radius depends on the black hole's spin parameter and the direction of the particle's orbit. For prograde orbits (orbits in the direction of the black hole's spin), the ISCO radius decreases with increasing spin, potentially reaching as close as the event horizon for an extremely spinning black hole. Conversely, for retrograde orbits (orbits opposite to the direction of the black hole's spin), the ISCO radius increases with the black hole's spin. The ISCO radius is significant in astrophysics for several reasons: (i) Accretion Disk Dynamics: It defines the inner edge of the accretion disk around compact objects. The region inside the ISCO is dynamically unstable, causing material to rapidly spiral inwards and potentially emit significant amounts of radiation, (ii) Gravitational Wave Emission: For compact binary systems, the ISCO sets a natural frequency cutoff for gravitational wave emission, influencing the waveforms detected by observatories like LIGO and Virgo. (iii) Astrophysical Observations: Observations of the X-ray spectra from accreting black holes can provide estimates of the ISCO radius, thereby offering insights into the spin and other properties of the black hole.

It is also interesting to probe how the scalar field influences to the ISCO position for massive particle in the JNW spacetime. Using the conditions $\mathcal{E}^2 = U(r)$ and $U'(r) = 0$, one obtains the critical specific energy and critical specific angular momentum as follows:

$$\mathcal{E}^2 = \frac{f^n(1+g_s\varphi)\left((1+g_s\varphi)\left(2f-(n-1)rf'\right)+2g_s rf\varphi'\right)}{(1-2n)rf'+2f}\,, \tag{1.24}$$

$$\mathcal{L}^2 = \frac{r^3 f^{1-n}(1+g_s\varphi)\left(f'n(1+g_s\varphi)+2g_s f\varphi'\right)}{(1-2n)rf'+2f}\,. \tag{1.25}$$

The stationary points of these expressions (1.24) and (1.25) represent the innermost stable circular orbit (ISCO). If one neglects the interaction term ($g_s = 0$),

the ISCO radius is determined as:

$$r_{\rm ISCO} = \left(3 + \frac{1}{n} + \sqrt{5 - \frac{1}{n^2}}\right) M \ . \tag{1.26}$$

The ISCO radius is also influenced by various factors including the presence of additional forces or fields. For example, in the presence of an interaction parameter g_s, the ISCO equation can become quite complex. Numerical calculations have shown that the ISCO radius for a massive particle decreases when $g_s > 0$ and increases when $g_s < 0$. This indicates that the nature of the interactions around the central object can significantly alter the orbital dynamics, providing a rich field of study in both theoretical and observational astrophysics. In Fig.1.1, we show dependence of the ISCO position for massive particle from scalar parameter n for different value of the interaction parameter g_s.

1.4 Radiation Reaction

Since the four-acceleration of massive particles in the presence of a scalar field is non-zero, i.e., $w^\nu = u^\mu \nabla_\mu u^\nu \neq 0$, these particles can emit either electromagnetic or gravitational radiation. However, we currently lack understanding of the specific type of radiation emitted by test particles in this scenario. In the classical limit of this radiation, the coupling parameter g_s is related to the Newtonian gravitational constant. Thus, this radiation can be considered analogous to gravitational radiation. The intensity of the radiation from particle in the presence of the scalar field is given by

$$I \sim w_\mu w^\mu = \frac{g_s^2}{(1 + g_s\varphi)^2}(g^{\mu\nu} + u^\mu u^\nu)\nabla_\mu\varphi\nabla_\nu\varphi \ . \tag{1.27}$$

Now we explore the dynamics of massive particles in the presence of a scalar field, incorporating a radiation reaction term. While the Lorentz-Abraham-Dirac (LAD)

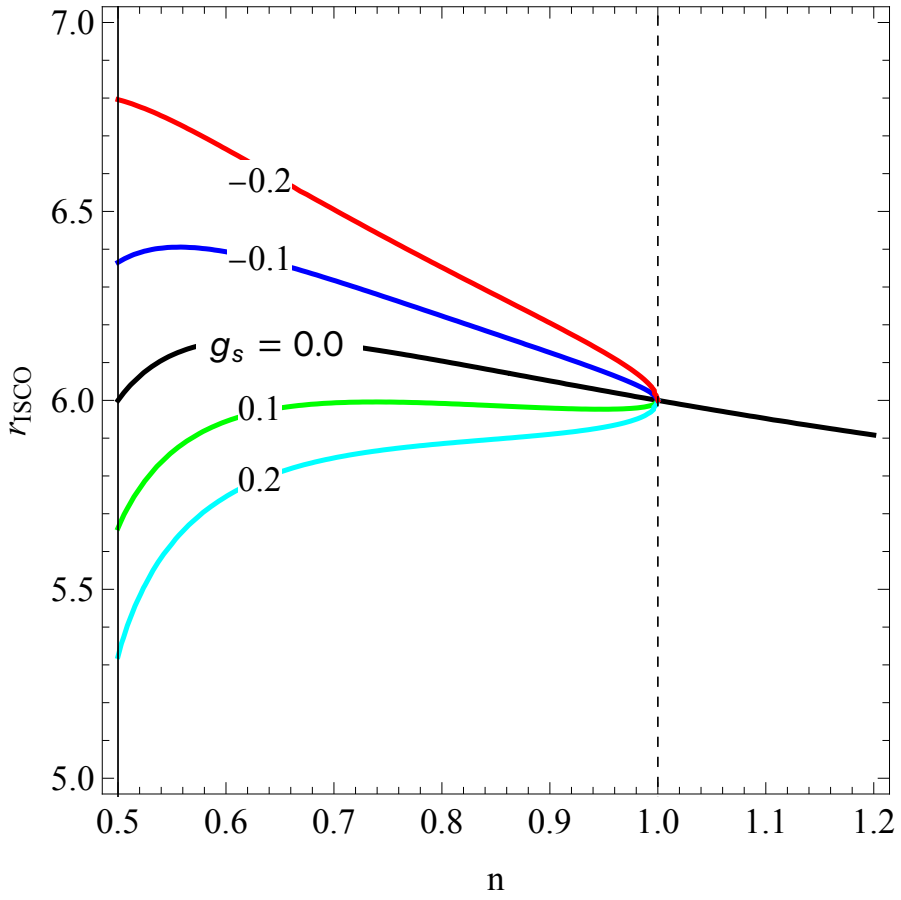

Figure 1.1: Dependence of the ISCO position of massive particle from the parameter n for the different values of the coupling parameter.

equation is widely recognized as the governing equation for radiation reaction in charged particles (see, for example, [48,49]), our study focuses on its gravitational counterpart. In this context, the equation of motion (3.14) can be modified as follows [39]:

$$\begin{aligned}\frac{Du^\mu}{ds} &= \frac{g_s}{1+g_s\varphi}(g^{\mu\nu}+u^\mu u^\nu)\partial_\nu\varphi \\ &+ \frac{1}{2}\tau_0\left(R^\mu{}_\nu + u^\mu u_\lambda R^\lambda{}_\nu\right)u^\nu \\ &+ \tau_0\left(\frac{D^2u^\mu}{ds^2} + u^\mu u_\lambda \frac{D^2u^\lambda}{ds^2}\right) \ , \end{aligned} \tag{1.28}$$

where τ_0 stands for the damping time of gravitational radiation defined as $\tau_0 << \tau$, and this parameter serves as an expansion factor.

Given that the final term of equation (1.28) is significantly smaller compared to the other terms, the Landau trick can be employed to expand the equation in terms of the damping time τ_0. By differentiating equation (1.28) and neglecting the highest-order terms related to the damping time τ_0, we obtain:

$$\begin{aligned}\frac{D^2u^\mu}{ds^2} &= \frac{g_s}{(1+g_s\varphi)}(g^{\mu\nu}+u^\mu u^\nu)u^\alpha\partial_\alpha\partial_\nu\varphi \\ &+ \frac{g_s^2}{(1+g_s\varphi)^2}(g^{\nu\alpha}+u^\nu u^\alpha)u^\mu\partial_\alpha\varphi\partial_\nu\varphi + \mathcal{O}(\tau_0) \ , \end{aligned} \tag{1.29}$$

Substituting expression (1.29) into (1.28) and after simple algebraic manipulations, the equation of motion can be reformulated as:

$$\begin{aligned}\frac{Du^\mu}{ds} &= \frac{g_s}{1+g_s\varphi}(g^{\mu\nu}+u^\mu u^\nu)(\partial_\nu\varphi + \tau_0 u^\alpha\partial_\alpha\partial_\nu\varphi) \\ &+ \frac{1}{2}\tau_0\left(R^\mu{}_\nu + u^\mu u_\lambda R^\lambda{}_\nu\right)u^\nu \ . \end{aligned} \tag{1.30}$$

The main idea behind reducing equation (1.28) to the form of (1.30) is to simplify the system into a second-order differential equation for four coordinates x^μ instead of a third-order system. This reduces the necessity of finding twelve constants of

motion, a primary challenge in particle motion in curved spacetime. By employing the Landau trick, the equation of motion can be expressed as a second-order system for the four coordinates x^μ. While the analytical form of the equations for each coordinate in (1.30) is extensive, we refrain from reporting them in this letter. Nevertheless, careful numerical analyses for given initial conditions $x_0^\mu = (0, r_0, \theta_0, 0)$ and $u_0^\mu = \left(\frac{\mathcal{E}}{f(r_0)^n}, 0, 0, \frac{\mathcal{L} f(r_0)^{n-1}}{(r_0 \sin\theta_0)^2}\right)$ enable the determination of each coordinate as a function of the affine parameter, i.e., $x^\mu = x^\mu(s)$.

In Fig. 1.2, we show the trajectory of a massive particle in the presence of a scalar field, including the radiation reaction term. Using numerical calculations, we have demonstrated that the contribution due to the radiation reaction is not significant. Therefore, to observe the effect of the radiation reaction term in circular motion, we set the damping time to $\tau_0 = 0$ s and $\tau_0 = 0.5$ s. This implies that the damping time is much shorter than 1 s, and the particle orbits many more times than shown in Fig. 1.2 around the compact object described by JNW spacetime before eventually escaping due to the radiation reaction force. It is shown that unlike a black hole [50], a naked singularity generates a repulsive effect in the radiation reaction due to the scalar field. In Fig. 1.3, we demonstrate the trajectory of a massive particle in two scenarios: (i) considering effect from the scalar field but without the radiation reaction term, and (ii) neglecting effect from the scalar field but including the radiation reaction term. This result show that indeed the scalar field generates attractive effect however radiation reaction repulsive effect in the motion of massive particle orbiting around the naked singularity.

1.5 Conclusions

In this chapter, we have studied the motion of a massive particle in the presence of scalar and gravitational fields, focusing on the Janis-Newman-Winicour (JNW)

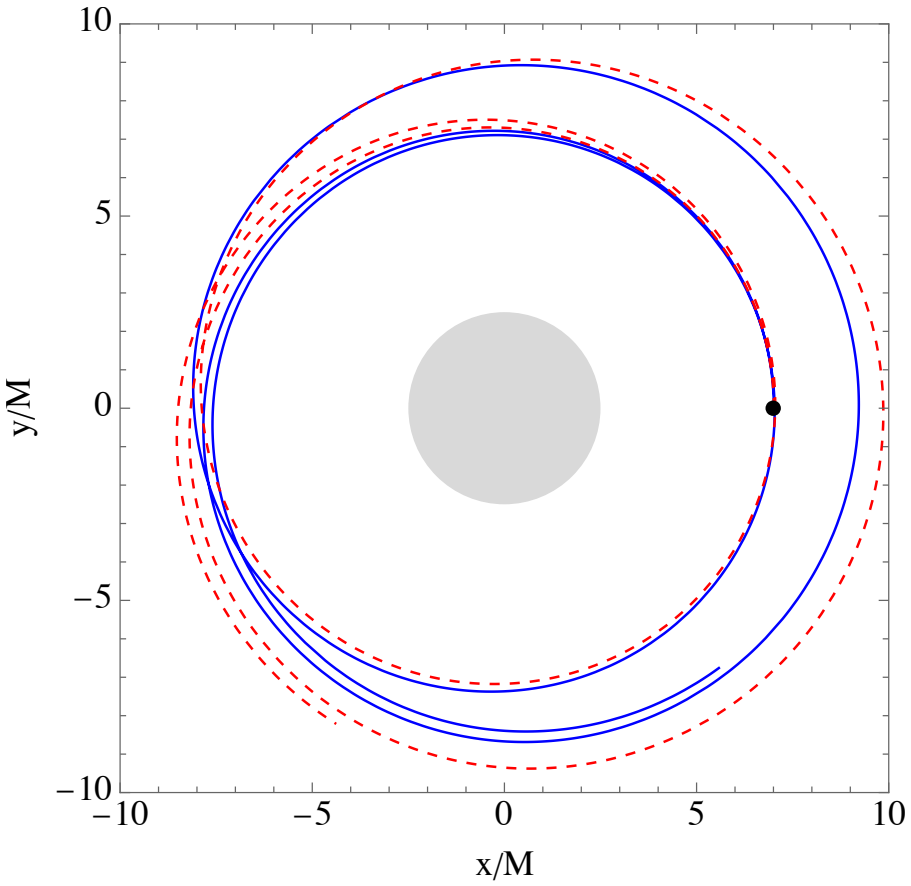

Figure 1.2: Particle trajectories near the JNW naked singularity without ($\tau_0 = 0$, solid blue line) and with ($\tau_0 = 1.0$, dashed red line) radiation reaction term for the particular choice of parameters $g_s = 0.03$ and $n = 0.8$

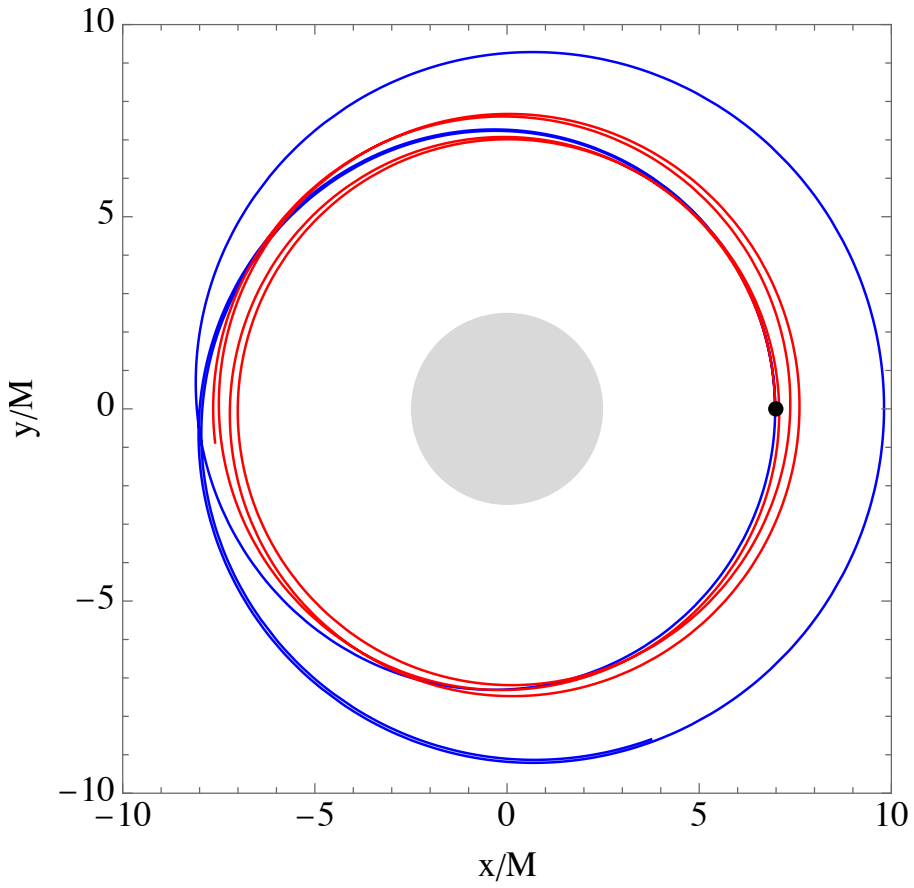

Figure 1.3: Particle trajectories near the JNW naked singularity the particular choice of parameters. Blue solid line represents for $g_s = 0.03$ and $\tau_0 = 0$ s and red solid line represents for $g_s = 0$ and $\tau_0 = 0.5$ s.

naked singularity solution. By deriving the equations of motion and the effective potential for a massive particle, we analyzed the innermost stable circular orbit (ISCO) radius in this spacetime. The ISCO radius, crucial for understanding dynamics around compact objects, was shown to be influenced by the scalar field and interaction parameter g_s. Our findings indicate that the ISCO radius decreases with positive g_s and increases with negative g_s, highlighting the significant impact of scalar interactions on orbital dynamics.

We have investigated the dynamics of massive particles in the presence of a scalar field including the effects of radiation reaction. The particles emit radiation due to their non-zero four-acceleration, with the intensity of the radiation depending on the coupling parameter g_s. By incorporating a radiation reaction term into the equation of motion, we derived a modified form that simplifies the analysis. Numerical calculations showed that the radiation reaction term has a minimal impact on the particle's trajectory. Our results indicate that the scalar field generates an attractive force, while the radiation reaction exerts a repulsive force. The trajectory of a massive particle around a naked singularity in the JNW spacetime is influenced by both these effects, as shown in our numerical simulations.

Chapter II

The Influence of the Scalar Field on Quasi-Periodic Oscillations (QPOs)

2.1 Introduction

It is worth to note that dynamics of massive test particles around black holes represent a great interest in Astrophysics [51]. Particularly, one may use circular geodesics in order to describe the accretion processes around compact objects. A huge number of works are devoted to explore the particle dynamics and geodesics around compact object in different gravity models (see, e.g. Refs. [3, 4, 52–93]). Furthermore, one may use the analysis of the geodesics to get constraints on different spacetime properties within different gravity theories [94–96].

One of the interesting features of the particle dynamics around compact objects is related to the observed QPOs from microquasars in X-ray band [97]. The analysis QPOs may be considered as a useful tool to test the gravity theories in strong field regime. Particularly it allows to get the values of mass and spin of the black holes [98, 99]. In order to describe QPOs various theoretical models have been proposed, namely the disc-seismic models, the warped disk models, the hot-spot models, the resonance models, etc. The different models and observations

have been used to test and get constraints on different parameters of gravity theories [2, 5, 100–107].

In this chapter, we aim to to apply the results of the particle dynamics to study the quasiperiodic oscillations (QPO) around JNW compact objects. The chapter is organized as follows. In Sec.2.2, we consider oscillatory motion of massive particle near the stable circular orbit in the JNW spacetime. As an astrophysical consequence we study application of the oscillatory motion of massive particle twin-peak QPO in Sec.2.3 and using these results obtain the constrains for two main parameters mass of the central object, scalar parameter and coupling constant in Sec.2.4. Finally, in Sect.2.5 we summarize the results of the investigation.

2.2 Oscillatory motion

Oscillatory motion of test particles around gravitational compact objects is a key aspect of relativistic astrophysics. This motion can be categorized into radial and vertical oscillations, and it provides crucial insights into the dynamics and structure of the spacetime around these objects. (i) Radial oscillations refer to the back-and-forth motion of a particle in the radial direction, i.e., towards and away from the central object. These oscillations occur around stable circular orbits. The stability and frequency of these oscillations are influenced by the spacetime geometry and the properties of the massive object. For the Schwarzschild black hole, the radial oscillation frequency depends on the mass of the black hole and the radial distance from it. Closer to the black hole, the stronger gravitational pull leads to higher oscillation frequencies. (ii) Vertical oscillations, also known as latitudinal or epicyclic oscillations, refer to the motion of a particle perpendicular to the plane of the orbit. These oscillations provide information about the vertical stability of the orbit and are influenced by the angular momentum and spin of

the central object. The vertical epicyclic frequency is the frequency at which a particle oscillates vertically around the equatorial plane of the central object. These two kind frequencies are related to the orbital frequency also known as Keplerian frequency. All together they are called fundamental frequencies and in the Schwarzschild black hole, these fundamental frequencies are expressed as $\Omega_r = \Omega_K\sqrt{1-6M/r}$, and $\Omega_\theta = \Omega_K = \sqrt{M/r^3}$, where Ω_K is Keplerian frequency in the Schwarzschild spacetime.

Here we will focus on oscillatory motion of massive particle near the stable circular orbit in the JNW spacetime in the presence of the scalar field. In this case four-velocity of particle takes a form: $u^\mu = \dot{t}(1,0,0,\Omega)$, where $\Omega = d\phi/dt$ is the angular velocity of the particle. The radial equation reduces to

$$\Omega^2 = -\frac{(1+g_s\varphi)\partial_r g_{tt} - 2g_s g_{tt}\varphi'(r)}{(1+g_s\varphi)\partial_r g_{\phi\phi} - 2g_s g_{\phi\phi}\varphi'(r)} \ . \tag{2.1}$$

Notice that in absence of the scalar field the explicit expression for the angular velocity of massive particle in JNW spacetime reduces to $\Omega = \Omega_K f^{n-1/2}\left[1 - M(1+n)/nr\right]^{-1}$. Consequently, expressions for the specific energy and angular momentum of massive particle yield

$$\mathcal{E} = -(1+g_s\varphi)g_{tt}\dot{t} = -\frac{(1+g_s\varphi)g_{tt}}{\sqrt{-g_{tt}-\Omega^2 g_{\phi\phi}}} \ , \tag{2.2}$$

$$\mathcal{L} = (1+g_s\varphi)g_{\phi\phi}\Omega\dot{t} = \frac{(1+g_s\varphi)g_{\phi\phi}\Omega}{\sqrt{-g_{tt}-\Omega^2 g_{\phi\phi}}} \ . \tag{2.3}$$

By using the normalization of the four-velocity of massive particle, one can obtain

$$g_{rr}\dot{r}^2 + g_{\theta\theta}\dot{\theta}^2 + V(r,\theta) = 0 \ , \tag{2.4}$$

where $V(r,\theta)$ is the effective potential explicitly given in equation (3.14). From the expression (2.4) equation for $2D$-harmonic oscillator can be derived after ex-

panding it up to leading order as follows

$$
\begin{aligned}
&g_{rr}(\dot{r}_0+\dot{\delta r})^2+g_{\theta\theta}(\dot{\theta}_0+\dot{\delta\theta})^2+V(r_0,\theta_0)\\
&+\partial_r V(r_0,\theta_0)\delta r+\partial_\theta V(r_0,\theta_0)\delta\theta+\partial_r\partial_\theta V(r_0,\theta_0)\delta r\delta\theta\\
&+\frac{1}{2}\partial_r^2 V(r_0,\theta_0)\delta r^2+\frac{1}{2}\partial_\theta^2 V(r_0,\theta_0)\delta\theta^2+...=0\ .
\end{aligned}
\tag{2.5}
$$

Consequently, equations of oscillatory motion for radial and vertical displacements δr and $\delta\theta$ from the stationary point read as follows:

$$
g_{rr}\left(\frac{d^2}{dt^2}+\Omega_r^2\right)\delta r+g_{\theta\theta}\left(\frac{d^2}{dt^2}+\Omega_\theta^2\right)\delta\theta=0\ ,
$$

where

$$
\Omega_r^2=\frac{1}{2g_{rr}\dot{t}^2}\partial_r^2 V=\frac{-g_{tt}-\Omega_\phi^2 g_{\phi\phi}}{2g_{rr}}\partial_r^2 V \tag{2.6}
$$

$$
\Omega_\theta^2=\frac{1}{2g_{rr}\dot{t}^2}\partial_\theta^2 V=\frac{-g_{tt}-\Omega_\phi^2 g_{\phi\phi}}{2g_{\theta\theta}}\partial_\theta^2 V\ . \tag{2.7}
$$

Our analysis showed that vertical frequency in (2.7) is the same as orbital angular velocity in (2.1) (i.e. $\Omega_\theta=\Omega$). We express all fundamental frequencies in Hz throughout our analysis. Therefore we restore fundamental constants in all frequencies as follows

$$
\nu_i=\frac{1}{2\pi}\frac{c^3}{GM}\Omega_i
$$

where $c=3\times10^{10}\mathrm{cms}^{-1}$ is the speed of light in a vacuum and $G=6.67\times10^{-8}\mathrm{cm}^3\mathrm{g}^{-1}\mathrm{s}^{-2}$ is the Newtonian gravitational constant.

The radial dependence of fundamental frequencies is illustrated in Fig. 2.1 with specific parameter settings. The left panel displays plots for different values of the coupling parameters with a fixed value of the n parameter, while the right panel shows similar plots for varying values of the n parameter with a fixed coupling parameter g_s. It can be observed that the fundamental frequencies increase due to the interaction of the massive particle with the scalar field, but they decrease with an increase in the n parameter.

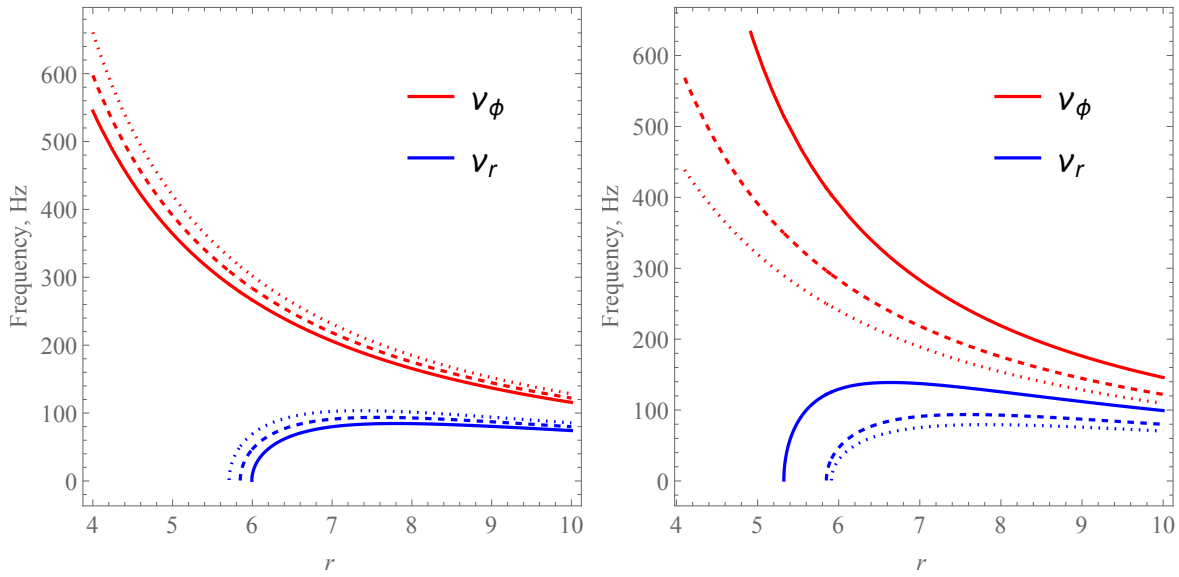

Figure 2.1: (Left panel) Radial dependence of fundamental frequencies of massive particle for different values of the coupling parameter ($g_s = 0.1$ - solid line, $g_s = 0.2$ - dashed line, and $g_s = 0.3$ -dotted line) for fixed $n = 0.7$. (Right panel) Radial dependence of fundamental frequencies of massive particle for different values of the n parameter ($n = 0.5$ - solid line, $n = 0.7$ - dashed line, and $n = 0.9$ -dotted line) for fixed $g_s = 0.2$. In both cases, the mass of the central object is taken as $M = 10M_\odot$.

2.3 QUASI-PERIODIC OSCILLATION

The combined effect of orbital, radial and vertical oscillations can lead to complex trajectories for test particles. These oscillations are crucial for understanding phenomena such as quasi-periodic oscillations (QPOs) observed in X-ray binaries. QPOs are believed to be related to the oscillatory motion of matter in the accretion disk around a black hole or neutron star. The oscillatory motion affects the stability and structure of accretion disks. Understanding these oscillations helps in modeling the emission spectra and variability of the disks. Observing the frequencies and modes of oscillations can provide insights into the properties of black holes and neutron stars, such as their mass, spin, and the geometry of the surrounding spacetime.

Astrophysical compact objects like black holes do not directly emit electromagnetic radiation. However, their strong gravitational pull distorts spacetime, significantly affecting the motion of nearby matter. This gravitational influence can lead to the formation of an accretion disk a rotating mass of gas, dust, and other debris caught in the black hole's gravitational field. As the material within the accretion disk orbits the black hole, friction and other forces generate extreme heat and pressure, causing the disk to emit large amounts of electromagnetic radiation across various wavelengths. Thus, while black holes themselves cannot be observed directly, the luminous emissions from their accretion disks offer valuable insights into their presence and properties in the universe.

The Relativistic Precession (RP) model offers a theoretical framework to explain the occurrence of quasi-periodic oscillations (QPOs), attributing them to the quasi-harmonic oscillations of charged particles as they move radially and angularly around black holes and wormholes. This model posits a direct connection between the dynamics of these charged particles and the manifestation of QPO

phenomena, providing valuable insights into the mechanisms driving oscillatory behavior in astrophysical systems with strong gravitational fields.

Within the RP model, the interpretation of twin-peaked QPOs is explained as follows: the higher frequency corresponds to the orbital frequency of the particle, denoted as $\nu_U = \nu_\phi$, while the lower frequency corresponds to the difference between the orbital frequency and the radial oscillation frequency, expressed as $\nu_L = \nu_\phi - \nu_r$. In other words, for twin-peaked QPOs, the upper frequency reflects the particle's orbital frequency, and the lower frequency is obtained by subtracting the radial oscillation frequency from the orbital frequency. This provides a clear understanding of the frequency components observed in twin-peaked QPO phenomena within the RP model, enabling insightful analysis of astrophysical systems.

Figure 2.2 illustrates the radial dependence of the upper and lower frequencies of twin QPOs within the RP model, shown by blue and black lines, respectively. In the left panel, the solid line represents $n = 0.5$, while the dashed line represents $n = 0.7$ with a fixed coupling parameter $g_s = 0.2$. In the right panel, the solid line represents $g_s = 0.1$, while the dashed line represents $g_s = 0.3$ with a fixed $n = 0.7$. It is evident from the figures that the radial position at which the frequency ratio of 3:2 QPOs is observed shifts slightly toward the naked singularity as the two main parameters, n and g_s, are increased.

In Fig. 2.3, we examine the relationships between the upper and lower frequencies of twin peak QPOs for various n and g_s values. The analysis shows that as n increases, both the upper and lower frequencies decrease. Conversely, the effect of g_s is opposite, leading to an increase in these frequencies. As can be seen from Fig. 2.3, the frequencies of the twin peak QPOs are not observable in the shaded area in both plots because these correspond to distances inside the ISCO position.

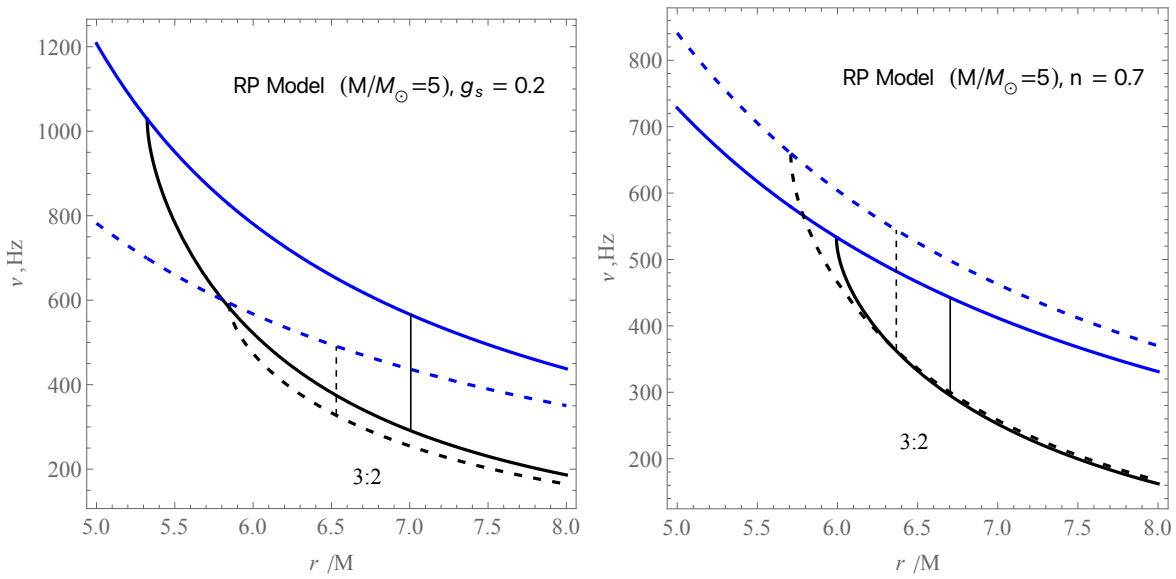

Figure 2.2: The radial dependence of upper and lower frequencies in RP model that are observed at ratio of 3:2.

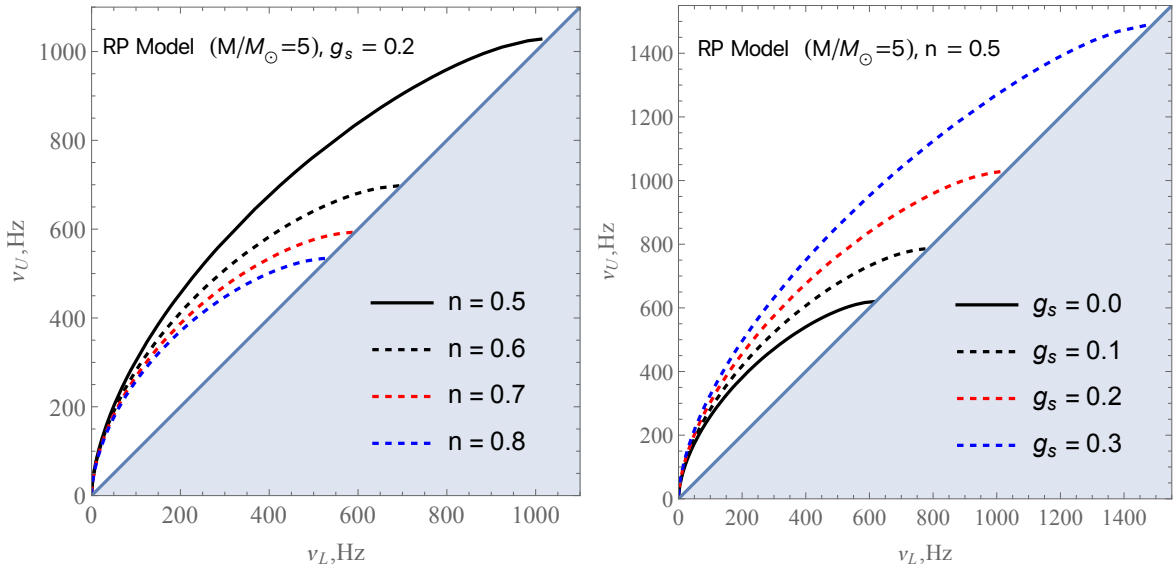

Figure 2.3: Relationships between the upper and lower peak frequencies of twin-peak QPOs in the RP model with mass $M = 5M_\odot$

2.4 Constraints

In this section, we analyze four X-ray binary systems to constrain the parameters associated with our JNW by examining Quasi-Periodic Oscillations (QPOs) data from these systems. The celestial objects under study include XTE J1550-564, GRO J1655-40 and GRS J1915+105. We will ultimately present the best-fit values within the parameter space, obtained through Markov Chain Monte Carlo (MCMC) code analysis.

We used the Python library emcee [108] for MCMC analysis to derive constraints on the JNW parameters in our study, which is based on the relativistic precession (RP) model.

The posterior is defined as described in reference [109]:

$$\mathcal{P}(\Theta|D,M) = \frac{P(D|\Theta,M)\pi(\Theta|M)}{P(D|M)} \quad , \tag{2.8}$$

Where: - $\pi(\Theta)$ is the prior. - $P(D|\Theta,M)$ is the likelihood.

The priors are Gaussian within specified boundaries, i.e.,

$$\pi(\Theta_i) \sim \exp\left(\frac{1}{2\sigma_i^2}(\Theta_i - \Theta_0)^2\right) \ , \tag{2.9}$$

Where $\Theta_{\mathrm{low},i} < \Theta_i < \Theta_{\mathrm{high},i}$ for the parameters $\Theta_i = [M, g_s, n, r/M]$, and σ_i are their corresponding standard deviations. We adopt the prior values of the parameters for the JNW as shown in Table 2.2.

Considering the upper and lower frequency data obtained in Section 2.3, our MCMC analysis incorporates two separate datasets. The core of this analysis is the likelihood function, denoted as $\mathcal{L}$, which is expressed as follows:

$$\log \mathcal{L} = \log \mathcal{L}_{\mathrm{up}} + \log \mathcal{L}_{\mathrm{low}} \ , \tag{2.10}$$

The logarithm of the likelihood function is the sum of the logarithms of the upper and lower frequency likelihoods. The logarithm of $\mathcal{L}_{\rm up}$ represents the likelihood associated with the upper-frequency data, given by:

$$\log \mathcal{L}_{\rm up} = -\frac{1}{2}\sum_i \left(\frac{(\nu^i_{\rm up,\,obs} - \nu^i_{\rm up,\,th})^2}{(\sigma^i_{\rm up,\,obs})^2} \right) \ , \tag{2.11}$$

Meanwhile, $\log \mathcal{L}_{\rm low}$ represents the likelihood associated with the lower frequency data, given by:

$$\log \mathcal{L}_{\rm low} = -\frac{1}{2}\sum_i \left(\frac{(\nu^i_{\rm low,\,obs} - \nu^i_{\rm low,\,th})^2}{(\sigma^i_{\rm low,\,obs})^2} \right) \ , \tag{2.12}$$

In these expressions, i ranges from 1 to an arbitrary integer, representing the number of measured upper and/or lower frequencies. $\nu^i_{\rm up,\,obs}$ and $\nu^i_{\rm low,\,obs}$ denote the observed results for the upper and lower frequencies, respectively, denoted as $\nu_{\rm up}$ and $\nu_{\rm low}$. Additionally, $\nu^i_{\rm up,\,th}$ and $\nu^i_{\rm low,\,th}$ correspond to their respective theoretical predictions. Furthermore, $\sigma^i_{\rm up}$ and $\sigma^i_{\rm low}$ represent the statistical uncertainties associated with these quantities.

Table 2.1: The mass, orbital frequencies, periastron precision frequencies and nodal precision frequencies of QPOs from the X-ray binaries selected for analysis.

	XTE J1550-564	GRO J1655-40	GRS 1915+105
$M(M_\odot)$	9.1 ± 0.61 [110, 111]	5.4±0.3 [112]	$12.4^{+2.0}_{-1.8}$ [113]
ν_{up}(Hz)	276 ± 3 [110]	441± 2 [112]	168 ± 3 [113]
ν_{low}(Hz)	184 ± 5 [110]	298 ± 4 [112]	113 ± 5 [113]

Using MCMC analyses at 1σ confidence level in Fig.2.4, we show the corner plots three different selected sources as mentioned before for the best-fit parameter

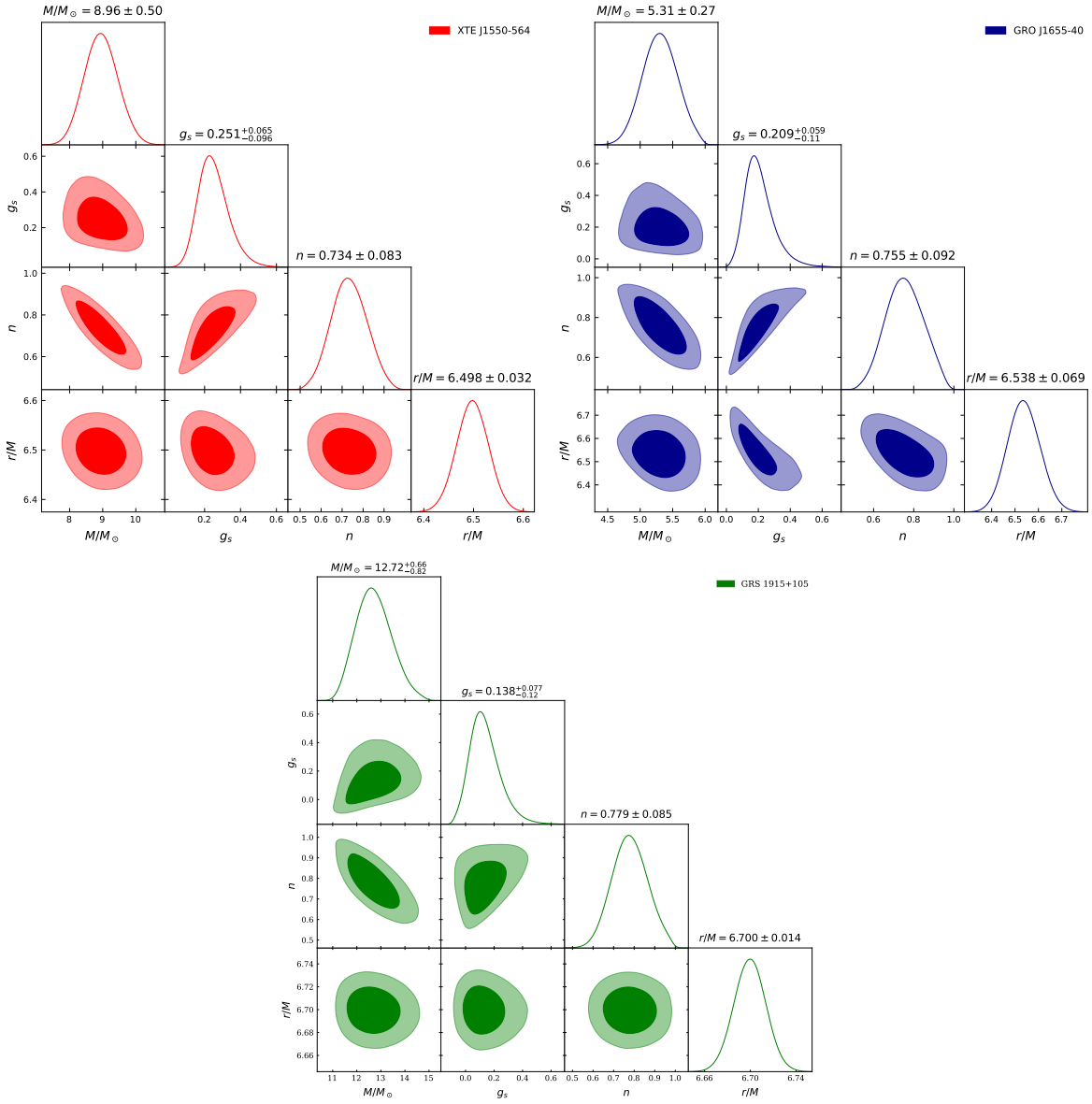

Figure 2.4: Constraints on JNW mass, the g_s and n parameters in the microquasars XTE J1550-564(upper left),GRO J1655-40 (upper right) and GRS 1915+105 (down) using MCMC analysis.

Table 2.2: The Gaussian prior of the JNW derived from QPOs for the selected X-ray sources.

	XTE J1550-564	GRO J1655-40	GRS 1915+105
$M(M_\odot)$	9.1 ± 0.6	5.4 ± 0.3	12.75 ± 1.25
g_s	0.25 ± 0.15	0.25 ± 0.2	0.225 ± 0.225
n	0.715 ± 0.175	0.7225 ± 0.1975	0.75 ± 0.1
r/M	6.5 ± 0.033	6.56 ± 0.08	6.7 ± 0.014

Table 2.3: The best-fit parameter values resembling those of JNW, deduced from the Quasi-Periodic Oscillations (QPOs) for the chosen X-ray sources.

	XTE J1550-564	GRO J1655-40	GRS 1915+105
$M(M_\odot)$	8.96 ± 0.50	5.31 ± 0.27	$12.72^{+0.66}_{-0.82}$
g_s	$0.251^{+0.065}_{-0.096}$	$0.209^{+0.059}_{-0.11}$	$0.138^{+0.077}_{-0.12}$
n	0.734 ± 0.083	0.755 ± 0.092	$0.779^{\pm}0.085$
r/M	6.498 ± 0.032	6.538 ± 0.069	6.700 ± 0.014

values (M, g_s, n, r) resembling those of JNW spacetime. Thus the best-fit values are listed in Tab. 2.3.

2.5 Conclusions

The oscillatory motion of test particles is a fundamental aspect of relativistic astrophysics, providing valuable information about the dynamics and characteristics of compact objects and their surrounding environments. We have examined the oscillatory motion of massive particles around compact gravitational objects within the JNW spacetime, influenced by the presence of a scalar field. Our analysis focused on radial and vertical oscillations, which are critical for understanding the dynamics and structure of spacetime around these objects. We derived the angular velocity and the expressions for specific energy and angular momentum of a massive particle in this spacetime, and further analyzed the effective potential

governing the motion. We found that the presence of a scalar field significantly alters the fundamental frequencies of particle oscillations. Specifically, the radial and vertical frequencies were influenced by the scalar field's coupling parameter g_s and the spacetime parameter n. Numerical results demonstrated that the interaction with the scalar field increases the fundamental frequencies, while higher values of the n parameter lead to a decrease in these frequencies. Our findings provide insights into the complex behavior of particles near compact objects, emphasizing the importance of considering scalar fields in relativistic astrophysics. This work contributes to a deeper understanding of the oscillatory dynamics and potential observational signatures of particles in scalar field-influenced spacetimes.

We have also explored the oscillatory motion of test particles around compact gravitational objects, emphasizing its relevance to quasi-periodic oscillations (QPOs) observed in X-ray binaries. QPOs, believed to result from the oscillatory motion of matter in accretion disks around black holes or neutron stars, provide critical insights into the stability and structure of these disks. Understanding these oscillations aids in modeling emission spectra and variability, shedding light on the properties of black holes and neutron stars, including their mass, spin, and surrounding spacetime geometry. According to the RP model, twin-peaked QPOs are characterized by two main frequencies: the upper frequency (ν_U) corresponding to the particle's orbital frequency, and the lower frequency (ν_L) representing the difference between the orbital and radial oscillation frequencies. This model provides a framework for analyzing QPO phenomena in astrophysical systems with strong gravitational fields. Our analysis showed the radial dependence and relationships between the upper and lower frequencies of twin-peaked QPOs. The results indicate that increasing the parameters n and g_s shifts the frequency ratio of 3:2 QPOs closer to the naked singularity. Additionally, while increasing n decreases

both frequencies, increasing g_s has the opposite effect.

Finally, we analyzed four X-ray binary systems to constrain the parameters associated with the Janis-Newman-Winicour (JNW) solution by examining Quasi-Periodic Oscillations (QPOs) data from these systems. The celestial objects under study included XTE J1550-564, GRO J1655-40, and GRS J1915+105. Using Markov Chain Monte Carlo (MCMC) analysis with the Python library 'emcee', we derived constraints on the JNW parameters based on the relativistic precession (RP) model. Our analysis utilized Gaussian priors within specified boundaries for the parameters. The likelihood function, combining upper and lower frequency data, was used to derive the posterior distributions of these parameters. The best-fit values were obtained through this MCMC analysis, providing insights into the mass, coupling parameter g_s, and the parameter n for each X-ray binary system. The obtained results demonstrate the constraints on the JNW parameters for each microquasar. It is also presented the best-fit parameter values derived from the QPOs data, reflecting the effectiveness of the RP model in describing the QPO phenomena in these X-ray binaries. This study enhances our understanding of the dynamics and properties of compact objects in strong gravitational fields.

Chapter III

Exploring a Novel Feature of Ellis Spacetime: Insights into Scalar Field Dynamics

3.1 Introduction

Wormholes are hypothetical tunnels in spacetime connecting two separate regions of the universe or even different universes. They are often depicted in science fiction as shortcuts through space and time, allowing for rapid travel between distant points or even different dimensions. These hypothetical tunnels in space-time are solutions to the equations of general relativity proposed by Albert Einstein. However, while wormholes are theoretically possible according to the laws of physics, they remain purely speculative as no observational evidence of their existence has been found yet. Despite their speculative nature, wormholes have captured the imagination of scientists, appearing frequently in science fiction as portals for interstellar travel or time travel. They remain an intriguing topic of study in theoretical physics, pushing the boundaries of our understanding of space-time and the universe.

The concept of a wormhole was initially introduced by John Wheeler in [114,115], who reinterpreted the Einstein-Rosen bridge as a link between distant points in spacetime without direct interaction [116]. In Ref. [117,118] it has been proposed a basic metric for a wormhole that, theoretically, could be traversed by humans. Since then, numerous publications have explored various types of wormholes, but they all share the common trait of violating the weak energy condition. For a more thorough examination, refer to works such as [].

The Ellis wormhole, also known as the Bronnikov-Ellis wormhole [119] or the Morris-Thorne wormhole [117], refers to a theoretical construct in the field of general relativity. It's a type of wormhole solution derived from Einstein's field equations, which describe the gravitational interaction between matter and spacetime. The Bronnikov-Ellis wormhole offers a mathematical description of a hypothetical tunnel-like structure in spacetime.

Another type of wormhole solution also known as the naked singularity has been studied in [47]. In Ref. [120] the construction of the related spherically-symmetric thin-shell traversable wormholes within the framework of general relativity has been studied. A "defect wormhole" solution has been extensively discussed in [121]. General wormhole solutions within Einstein gravity, featuring an exponential shape function around both an ultrastatic and a finite redshift geometry have been studied in Refs. [122–125]. Specific traversable wormhole solutions in Einstein-Dirac-Maxwell theory without including any exotic matter have been discussed in [126]. Charged wormhole solution in Einstein-Maxwell-scalar field theory has been studied in [127]. Three parametric wormhole solutions in Einstein-scalar field theory have been investigated in [128]. In Ref. [129], the spherically symmetric traversable wormhole solutions in the presence of the scalar field supported by a phantom field in the AdS spacetime have been studied. Possible wormhole

solutions in the Friedmann universe have been studied in [130]. A magnetized dusty wormhole is discussed in [131]. The exact geometric optics problems in the Ellis wormhole spacetime, namely, gravitational lensing effects including the computation of the deflection angle, have been studied in [67, 132–137]

In Ref. [138], an analysis is conducted on the characteristics of circular orbits for massive particles situated in the equatorial plane of symmetric rotating Ellis wormholes. This includes the determination of orbital frequencies as well as radial and vertical epicyclic frequencies. Additionally, in Ref. [139, 140], the study explores quasi-periodic oscillations emanating from the accretion disk surrounding rotating traversable wormholes. The focus lies on examining the linear stability of circular geodesic orbits in the equatorial plane across a broad class of wormhole geometries, leading to the derivation of analytical expressions for the epicyclic frequencies. The motion of spinning test particles around a wormhole is investigated in Ref. [141] using the Mathisson-Papapetrous-Dixon (MPD) equations, which couple the Riemann tensor with the anti-symmetric tensor.

A slowly rotating Ellis-Bronnikov wormhole has been discussed in [142]. The gravitational perturbations of the Morris-Thorne wormhole expanding up to the second order in rotation has been studied in Ref. [143]. It outlines the derivation process using the Newman-Penrose formalism and demonstrates the application of the Teukolsky equation to the wormhole spacetime. The article also details the computation of the perturbed Weyl scalars and the acquisition of its master equation. In Ref. [144], it has been introduced a comprehensive technique for deriving a gauge-invariant wave system of linearized perturbation equations in the context of the spherically symmetric Ellis-Bronnikov wormhole.

In general relativity, the motion of particles in curved spacetime is a fundamental concept, elucidating how matter and energy influence the curvature of spacetime

and, consequently, how this curvature governs the trajectories of objects. In such a curved spacetime, particles traverse paths known as geodesics, which are determined by the geodesic equation. However, when a charged particle is subjected to an external electromagnetic field, it experiences acceleration and emits electromagnetic radiation, a phenomenon described by a non-geodesic equation. Various forms of electromagnetic radiation and their corresponding mathematical formulations are detailed in [38]. Furthermore, the study of particle dynamics in the presence of an external scalar field is both intriguing and significant. The interaction between massive particles and scalar fields remains a topic of uncertainty, yet it is theoretically vital for comprehending astrophysical processes near compact objects such as black holes and neutron stars. This issue has been examined in Ref. [39], which includes the analysis of self-force effects in the presence of an external scalar field. Certain facets of this self-force can be interpreted through the geometry of spacetime, offering insights into the paradox of a particle radiating without experiencing a self-force. The acceleration of particles by black holes in the presence of a scalar field has been investigated in [40]. The interaction between scalar field and massive particle is also introduced by Misner et. al. [41] and by Breuer at. al. [42] to describe scalar perturbation or so-called geodesic synchrotron radiation in the Schwarzschild spacetime.

In this chapter, we are interested in testing the Ellis spacetime by considering particle motion around the wormhole in the presence of the external scalar field, using the technique mentioned in Ref. [39]. The Chapter is organized as follows: In Sec. 3.2, we provide the main equations that are related to background spacetime and dynamics motion of test particle in the presence of the external scalar field. In Sec. 3.3, we study particle motion including radiation reaction. In Sec. 3.4, we study wormhole perturbation. Finally, in Sec. 3.6 we summarize obtained results.

3.2 Background geometry and particle dynamics

The Ellis wormhole is governed by the spacetime line element [117, 119]:

$$ds^2 = -dt^2 + dr^2 + (r^2 + r_0^2)(d\theta^2 + \sin^2\theta d\phi^2) \ , \tag{3.1}$$

along with the associated scalar field

$$\Phi = \frac{\pi}{2} - \tan^{-1}\left(\frac{r}{r_0}\right) \ , \tag{3.2}$$

where r_0 is the throat of the wormhole. Here the radial coordinate r runs between r_0 and infinity, i.e. $r_0 < r < \infty$. One has to emphasise that it is one of the simple wormhole solutions of the Einstein-scalar field equation with the following energy-momentum tensor:

$$T^{\mu}_{\ \nu} = \frac{r_0^2}{\left(r^2 + r_0^2\right)^2} \begin{pmatrix} 1 & 0 & 0 & 0 \\ 0 & -1 & 0 & 0 \\ 0 & 0 & 1 & 0 \\ 0 & 0 & 0 & 1 \end{pmatrix} \ , \tag{3.3}$$

while the curvature scalar invariants of the spacetime such as Ricci scalar and Kretschmann scalar can be expressed as

$$R = -\frac{2r_0^2}{(r^2 + r_0^2)^2} \ , \qquad K = \frac{12r_0^4}{(r + r_0^2)^4} \ , \tag{3.4}$$

which are regular at any point of spacetime at $r > r_0$. The radial dependence of the scalar field and curvature invariants, Ricci and Kretchmann scalar is shown in Fig.3.1.

We can immediately observe that the motion of the test particle in the Ellis spacetime background lacks interest due to the absence of temporal and radial components in the metric tensor. However, when incorporating the interaction between a test particle and an external scalar field, the problem becomes intriguing. In

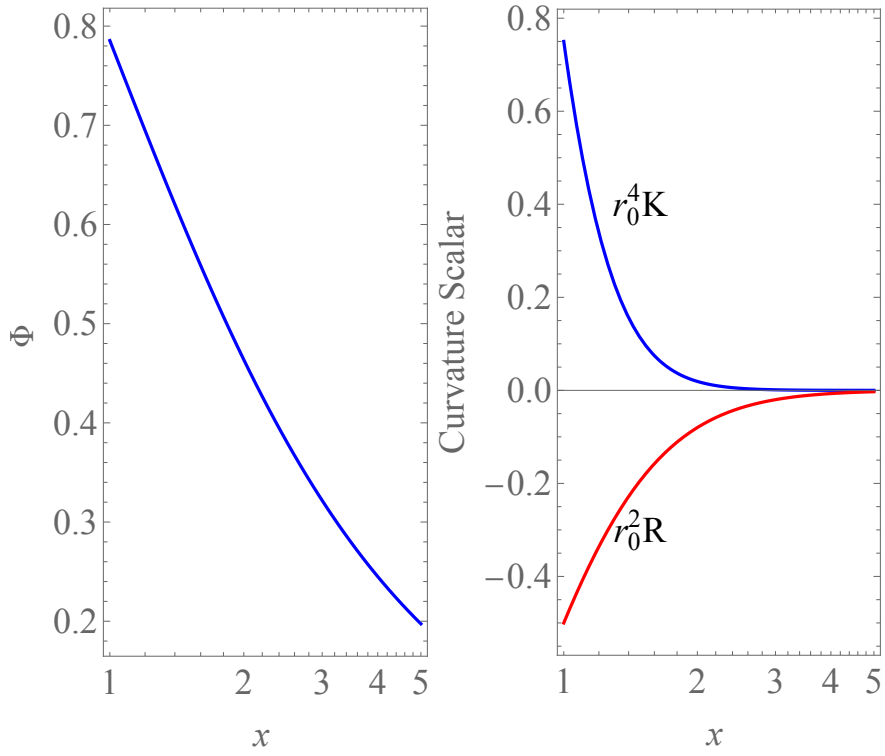

Figure 3.1: Radial dependence of the scalar field $\Phi(x)$ and curvature invariant, dimensionless Ricci scalar $r_0^2 R$ and dimensionless Kretschmann scalar $r_0^4 K$.

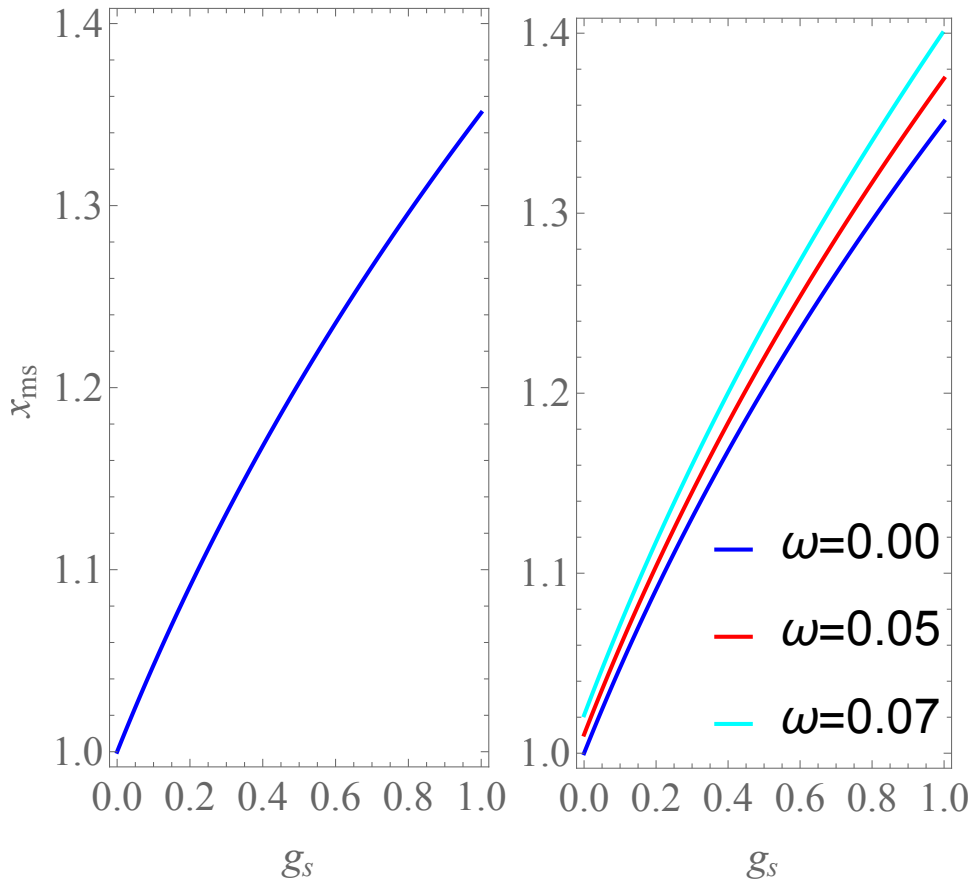

Figure 3.2: (Left panel) Dependence of the marginally bound orbit circular orbit of neutral particle $x_{\rm ms}$ from the coupling constant g_s. (Right panel) Dependence of the marginally bound orbit circular orbit of charged particle $x_{\rm ms}$ from the coupling constant g_s for the different values of the magnetic parameter.

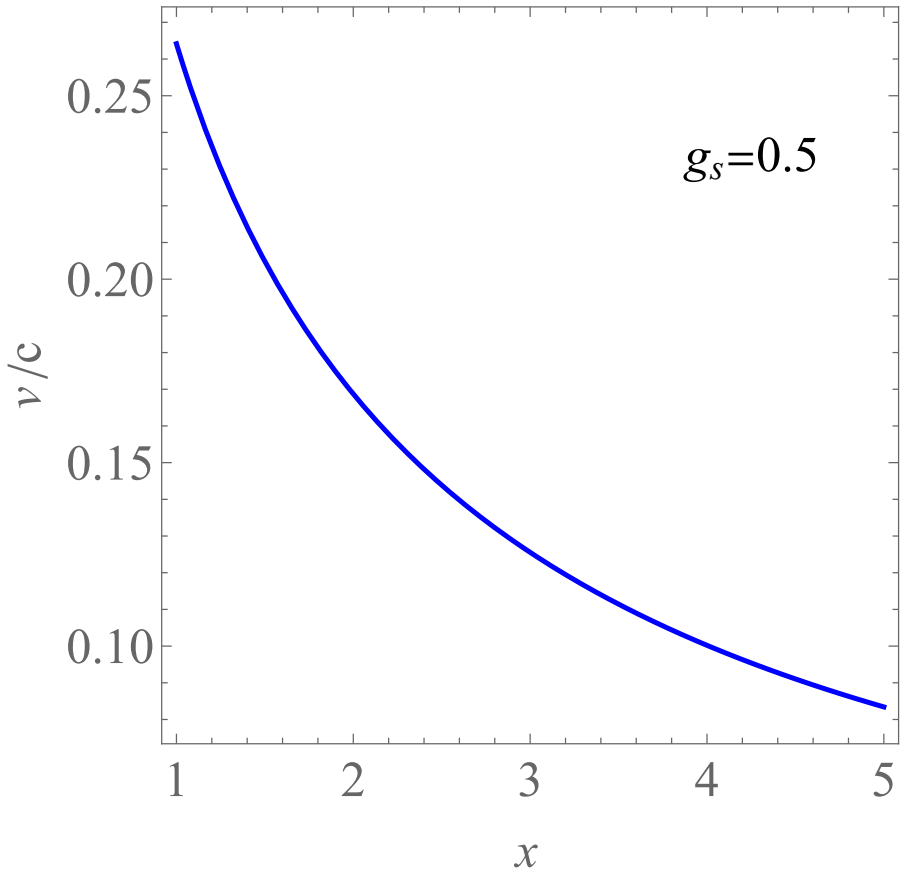

Figure 3.3: Radial dependence of the linear orbital velocity .

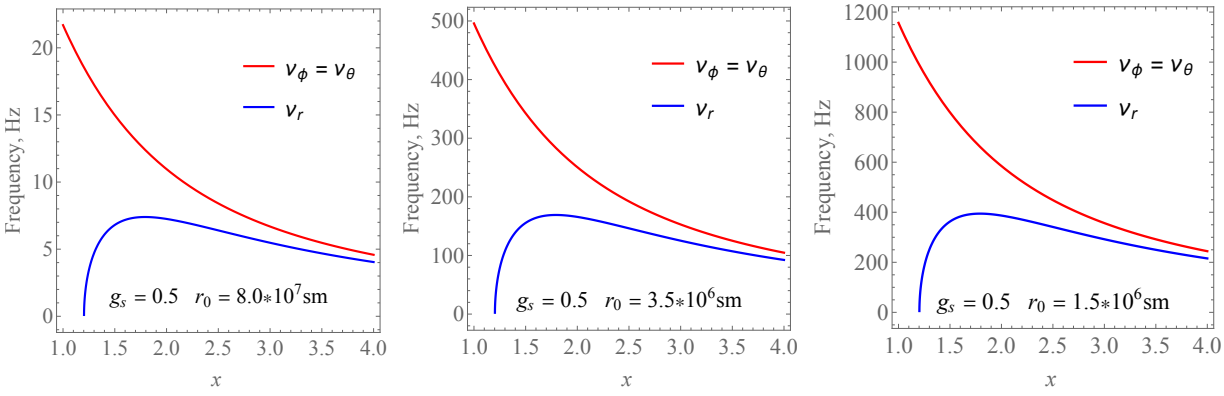

Figure 3.4: Radial dependence of the fundamental frequencies of a massive particle.

this case, the Lagrangian describing a test particle with mass m in the presence of the external scalar field Φ can be expressed as [39, 41, 42, 145]

$$L = \frac{1}{2} m_* g_{\mu\nu} u^\mu u^\nu \ , \qquad m_* = m(1 + \mathrm{g}_s \Phi) \ , \tag{3.5}$$

where m_* is the effective mass of a test particle in the presence of the external scalar field and influenced by a coupling constant, g_s, and $u^\mu = dx^\mu/d\tau$ is the four-velocity of test particle normalized as $u_\mu u^\mu = -1$. Here, τ is the particle's proper time. The constants of the motion namely, the specific energy $\mathcal{E}$ and specific angular momentum $\mathcal{L}$ of test particle are expressed as follows

$$\mathcal{E} = (1 + \mathrm{g}_s \Phi)\dot{t} \ , \qquad \mathcal{L} = (1 + \mathrm{g}_s \Phi)(r^2 + r_0^2)\dot{\phi} \ . \tag{3.6}$$

Hereafter using normalization of the four-velocity of massive test particle (i.e. $u_\mu u^\mu = -1$) along constants of motion in the expression (3.6), one can obtain

$$g_{rr}\dot{r}^2 + g_{\theta\theta}\dot{\theta}^2 + V(r, \theta) = 0 \ . \tag{3.7}$$

where $V(r, \theta)$ is defined as

$$V(r, \theta) = 1 - \frac{1}{(1 + \mathrm{g}_s \Phi)^2} \left[\mathcal{E}^2 - \frac{\mathcal{L}^2}{(r^2 + r_0^2) \sin^2 \theta} \right] \ , \tag{3.8}$$

which limits constants of motion.

3.2.1 Marginally stable circular orbit

The concept of stable and unstable orbits of test particle in the vicinity of compact and massive objects such as black holes, and neutron stars are well-described. It is also interesting to consider the marginally bound and marginally stable circular orbit of test particle motion near the wormhole. For simplicity, one can consider circular motion in the equatorial plane (i.e. $\theta = \pi/2$ and $\dot{\theta} = 0$), equation of

motion reduces to

$$\dot{t} = \frac{\mathcal{E}}{(1+\mathrm{g}_s\Phi)} \ , \tag{3.9}$$

$$\dot{\phi} = \frac{\mathcal{L}}{(1+\mathrm{g}_s\Phi)(r^2+r_0^2)} \ , \tag{3.10}$$

$$\dot{r}^2 = \frac{1}{(1+\mathrm{g}_s\Phi)^2}\left(\mathcal{E}^2 - \frac{\mathcal{L}^2}{r^2+r_0^2}\right) - 1 \ . \tag{3.11}$$

Using conditions $\dot{r} = \ddot{r} = 0$ and eliminating the specific angular momentum from the final expression, the critical value of the specific energy of a massive particle can be found as

$$\mathcal{E}^2 = \left(1 + \mathrm{g}_s\Phi - \mathrm{g}_s\frac{r_0}{r}\right)(1+\mathrm{g}_s\Phi) \ , \tag{3.12}$$

which is equal to 1 at the infinity. From this expression one can obtain two characteristic radii of particle, one is called marginally bound circular orbit and another one is marginally stable circular orbit.

The marginally bound circular orbit of particle can be found from the condition $\mathcal{E} = 1$ which does not exist around Ellis wormhole, while the stationary point of the specific energy is located at the marginally bound orbit of the massive particle (i.e. $\mathcal{E}'(r) = 0$) and determined from the following equation:

$$\mathrm{g}_s x + \left(1-x^2\right)\left[1 + \frac{\pi}{2}\mathrm{g}_s - \mathrm{g}_s\tan^{-1}(x)\right] = 0 \ , \tag{3.13}$$

where $x = r/r_0 > 1$ is the dimensional radial coordinate. It is impossible to obtain the analytical solution to equation (3.13), however, but employing numerical methods can yield the position of the marginally stable circular orbit of massive particle around the wormhole. Our numerical investigations showed that such orbits are smaller in size compared to the wormhole's throat (i.e. $x < 1$) when the coupling constant g_s takes a negative value, which is meaningless. Conversely, as the coupling constant g_s becomes positive, these orbits get larger (i.e. $x > 1$).

Figure 3.2 illustrates how the marginally bound circular orbit of a test particle varies with the coupling constant.

3.2.2 Fundamental frequencies

Here we will discuss fundamental frequencies, namely, orbital and epicyclic frequencies, of massive particle in the Ellis spacetime. From the Lagrangian (3.5) equation of motion for a massive particle in the presence of the external scalar field yields [39]

$$\frac{Du^{\mu}}{d\tau} = (g^{\mu\nu} + u^{\mu}u^{\nu})\partial_{\nu} \ln \frac{m_*}{m} \ , \qquad u_{\mu}\frac{Du^{\mu}}{d\tau} = 0 \ . \tag{3.14}$$

Now considering the circular motion with the four-velocity of $u^{\mu} = \dot{t}(1, 0, 0, \Omega)$ and angular velocity of test particle is derived from equation (3.14) as follows:

$$\Omega = \frac{d\phi}{dt} = \frac{1}{r_0} \frac{1}{\sqrt{(x^2+1)\left[1 + \frac{x}{\mathrm{g}_s}(1 + \mathrm{g}_s\Phi)\right]}} \ , \tag{3.15}$$

while the linear orbital velocity of particle measured by a local observer yields

$$v_{\phi} = \Omega\sqrt{\frac{g_{\phi\phi}}{-g_{tt}}} = \sqrt{\frac{1}{1 + \frac{x}{\mathrm{g}_s}(1 + \mathrm{g}_s\Phi)}} < 1 \ , \tag{3.16}$$

which is less than the speed of light for the positive value of the interaction parameter. The radial dependence of the linear velocity of massive particle orbiting around the Ellis wormhole in the presence of the scalar field is illustrated in Fig.3.3. It is also an interesting and important task to consider the radial and vertical oscillatory motion of test particle around the stationary stable orbit. Using equation (3.7), the radial and vertical epicyclic frequencies are [146]

$$\Omega_r = \sqrt{\frac{1}{2g_{rr}\dot{t}^2}\frac{\partial^2 V}{\partial r^2}} \ , \qquad \Omega_{\theta} = \sqrt{\frac{1}{2g_{\theta\theta}\dot{t}^2}\frac{\partial^2 V}{\partial \theta^2}} \ , \tag{3.17}$$

which satisfies the following $2D$-oscillator equations for displacements $(d^2/dt^2 + \Omega_r^2)\delta r = 0$ and $(d^2/dt^2 + \Omega_\theta^2)\delta\theta = 0$. To have an idea about the value of the fundamental frequencies of massive particle in the Ellis spacetime, we restore the fundamental constant in particular the speed of light. Our analyses showed that the vertical and orbital frequencies are equal to each other $\Omega = \Omega_\theta$. Now using the following notating $\nu_i = \Omega_i/2\pi$, measurable fundamental frequencies of massive particle can be determined as

$$\nu_r = \frac{c}{2\pi r_0}\sqrt{\frac{(1+\mathrm{g}_s\Phi)\,(x^2-1)-\mathrm{g}_s}{(x^2+1)\left[1+\frac{x}{\mathrm{g}_s}\,(1+\mathrm{g}_s\Phi)\right]}}\,, \tag{3.18}$$

$$\nu_\theta = \nu_\phi = \frac{c}{2\pi r_0}\frac{1}{\sqrt{(x^2+1)\left[1+\frac{x}{\mathrm{g}_s}\,(1+\mathrm{g}_s\Phi)\right]}}\,. \tag{3.19}$$

As one can easily check that the frequencies are sensitive to the wormhole's throat. To compare the theoretical results with observational data we have restored the speed of the light in (3.18) and (3.19). As an astrophysical consequence, we make constraints on the throat of the Ellis wormhole by comparing the above expression with observational evidence of the fundamental frequencies. We can make constraints on wormhole parameters using observation evidence of the fundamental frequency for quasars and micro-quasars. In Fig.3.4 radial dependence of the fundamental frequencies, namely, orbital, radial and vertical frequencies are illustrated.

3.3 Charged particle dynamics

Now we discuss the orbital motion of a charged particle around Ellis wormhole in the presence external uniform magnetic field. Assuming the wormhole is embedded in the asymptotically uniform magnetic field. By utilizing the Wald method [147],

it is possible to identify the elements of the four-vector potential that align with the magnetic field, in the following manner: $A^{\mu} = (0, 0, 0, B/2)$, where B is the strength of the asymptotically uniform magnetic field. Consequently, the azimuthal component of the vector potential of the electromagnetic field is given by $A_{\phi} = (B/2)(r^2+r_0^2)\sin^2\theta$ and fully satisfies Maxwell equation. The Lagrangian for a charged particle in the presence of the external magnetic field is

$$L = \frac{1}{2} m_* g_{\mu\nu} u^{\mu} u^{\nu} + q A_{\mu} u^{\mu} \ , \tag{3.20}$$

where q is a charge of the test particle. The Lagrangian equation of motion is derived as

$$\frac{Du^{\mu}}{d\tau} = \frac{q}{m} F^{\mu}_{\ \nu} u^{\nu} + (g^{\mu\nu} + u^{\mu}u^{\nu})\partial_{\nu} \ln \frac{m_*}{m} \ , \tag{3.21}$$

and after simple algebraic manipulations equation of the radial motion yields

$$\dot{r}^2 = \frac{1}{(1+\mathrm{g}_s\Phi)^2} \left[\mathcal{E}^2 - \left(r^2 + r_0^2\right) \left(\frac{\mathcal{L}}{r^2+r_0^2} - \omega \right)^2 \right] - 1 \ , \tag{3.22}$$

where $\omega = qB/2m$ is a magnetic parameter. The marginally bound circular radius for a charged test particle takes using conditions $\dot{r} = \ddot{r} = 0$:

$$\mathrm{g}_s x + \left(1 - x^2\right)(1 + \mathrm{g}_s\Phi) + 4\omega^2 x^3 (1 + x^2) = 0 \ . \tag{3.23}$$

Using the numerical calculation one can find the dependence of the marginally bound circular orbit radius of a charged particle orbiting wormhole from the interaction parameter g_s from the different values of the magnetic parameter ω is shown in Fig.3.2.

The fundamental frequencies of the charged particle in the vicinity of Ellis wormhole in the presence of the external magnetic field can be easily done. The Keplerian frequency of charged particle is derived from the following expression:

$$\Omega^2 + \omega\Omega\sqrt{1 - \Omega^2(x^2+1)} = \frac{\mathrm{g}_s\left[1 - \Omega^2(x^2+1)\right]}{x(x^2+1)(1+\mathrm{g}_s\Phi)} \ . \tag{3.24}$$

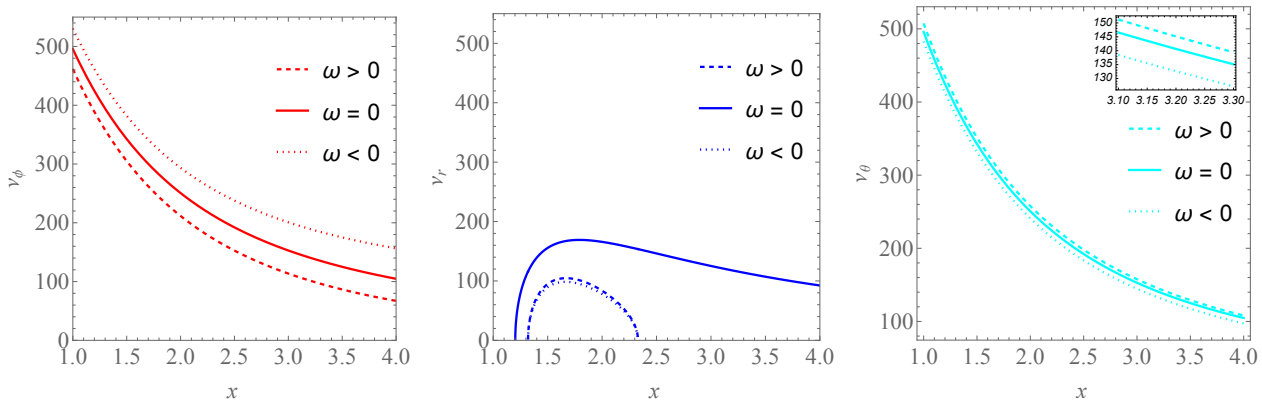

Figure 3.5: Fundamental frequencies of charged particle around Ellis wormhole on $\omega = \pm 0.4$, parameter $g_s = 0.5$.

Similarly, epicyclic frequencies for charged particle orbiting around the Ellis wormhole in the presence magnetic field, however we will skip the detailed calculations. The radial dependence of the fundamental frequencies is shown in Fig. 3.5. As one can see from this figure the fundamental frequencies of charged particle are split due to the external magnetic field. On the other hand, our results show that Keplerian frequencies strongly depend on the magnetic parameter.

Here we will discuss about radiation from massive particle in the Ellis spacetime in the presence of the scalar field. From the equation of motion (3.14) one can see that the four-acceleration is non-zero $w^\mu = Du^\mu/d\tau$. The intensity of the radiating particle is proportional to the square of the acceleration of particle:

$$I \sim \frac{Du_\mu}{d\tau}\frac{Du^\mu}{d\tau} = \frac{q}{m}F_{\mu\lambda}F^\mu_{\ \nu}u^\nu u^\lambda + (g^{\mu\nu} + u^\mu u^\nu)\partial_\mu\frac{m_*}{m}\partial_\nu\frac{m_*}{m} \ . \tag{3.25}$$

Here the first term of the last equation denotes electromagnetic radiation from charged particle while the second term is the intensity of radiation from massive particle due to interaction with the external scalar field.

Now we consider charged particle motion including the radiation reaction along massive particle trajectories in the presence of the scalar field. The Lorentz-

Abraham-Dirac equation can be expressed as

$$\frac{Du^\mu}{d\tau} = \frac{q}{m}F^\mu{}_\nu u^\nu + (g^{\mu\nu} + u^\mu u^\nu)\partial_\nu \ln\frac{m_*}{m} + \frac{1}{2}\tau_0\left(R^\mu{}_\nu + u^\mu u_\lambda R^\lambda{}_\nu\right)u^\nu + \tau_0 \ , \tag{3.26}$$

where $R_{\mu\nu}$ represents the Ricci tensor. Parameter τ_0 is rather small parameter than all other terms therefore it can serve as an expansion parameter. Hereafter applying the Landau trick equation of motion in the presence of the external scalar field reads

$$\begin{aligned}\frac{Du^\mu}{d\tau} = &\frac{q}{m}F^\mu{}_\nu u^\nu + h^{\mu\nu}\partial_\nu \ln\frac{m_*}{m} \\ &+ \tau_0\left[\frac{1}{2}h^\mu_\lambda R^\lambda{}_\nu u^\nu + h^{\mu\nu}\left(\frac{D}{d\tau} + u^\alpha\partial_\alpha \ln\frac{m_*}{m}\right)\partial_\nu \ln\frac{m_*}{m}\right] \\ &+ \tau_0\left[\frac{q}{m}\left(u^\alpha\nabla_\alpha F^\mu{}_\nu + \frac{q}{m}h^{\mu\lambda}F_{\lambda\alpha}F^\alpha{}_\nu\right)u^\nu\right] \ ,\end{aligned} \tag{3.27}$$

where $h^{\mu\nu} = g^{\mu\nu} + u^\mu u^\nu$.

The fundamental concept behind transforming equation (3.26) into the form depicted in (3.27) is to represent it as a third-order system of differential equations concerning four coordinates. This implies the necessity of determining twelve constants of motion, a pivotal aspect in understanding particle dynamics within curved spacetime. However, avoiding this issue is achievable through the Landau trick, resulting in the equation of motion being simplified to a second-order system concerning the four coordinates x^μ. While the explicit expressions for each coordinate in (3.27) are considerably lengthy, they will not be elaborated upon in this correspondence. Nevertheless, through careful numerical analysis, employing prescribed initial conditions: $(0, r_i, \theta_i, 0)$ and $\left\{-\mathcal{E}, 0, 0, \mathcal{L}/(r_i^2 + r_0^2)\sin^2\theta_i\right\}$, it becomes feasible to ascertain the dependency of each coordinate on the affine parameter, denoted as $x^\mu = x^\mu(s)$, where (r_i, θ_i) are the initial position of test particle. Subsequently, by implementing a coordinate transformation such as $x = r\cos\phi$a

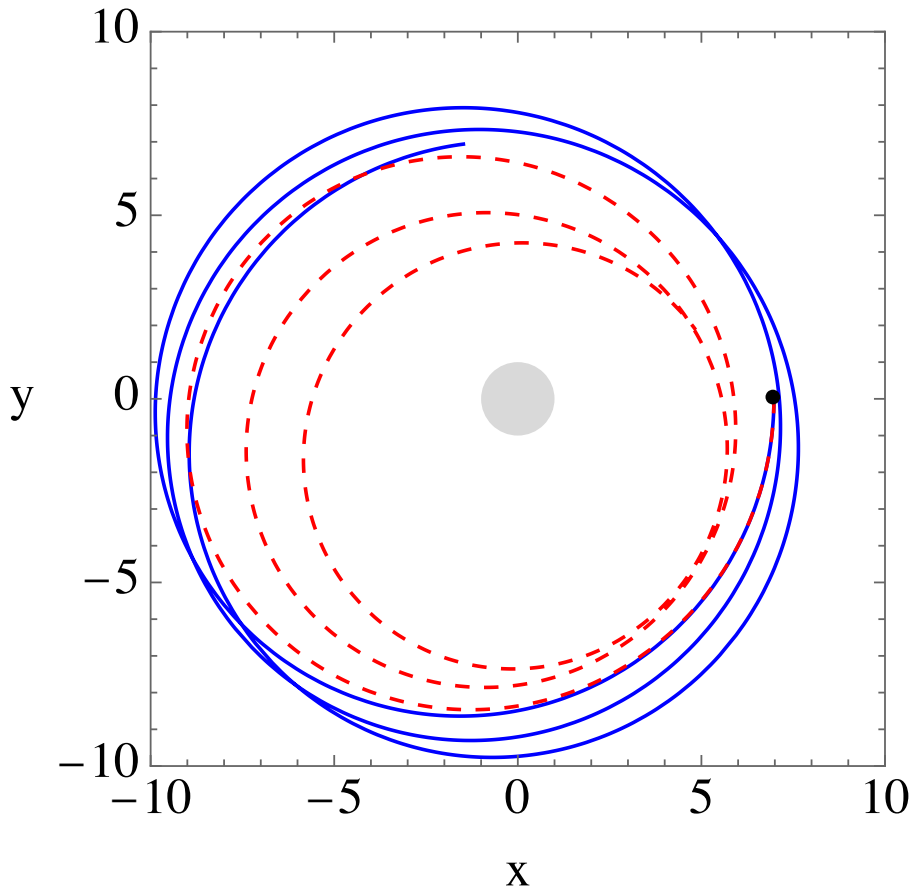

Figure 3.6: Particle trajectories near Ellis wormhole the radiation trajectory without ($\tau_0 = 0$, solid blue line) and with ($\tau_0 = 0.05$, dashed red line) radiation reaction term. $g_s = 0.4$ and $\omega = 0.1$

and $y = r\sin\phi$, the trajectories of particles can be visualized in Cartesian coordinates through parametric plots. The trajectory of particle in the Ellis spacetime in the presence of the scalar field is shown in Fig.3.6. Interestingly, it turns out that radiation allows massive particle to escape the wormhole by exploiting the absence of a gravitational field. However, in Ref. [50] it is shown that due to radiation particle starts to fall onto the black hole in the scalar-tensor-vector gravity.

3.4 Wormhole perturbation

The black hole perturbation is one of the hot topic, in particular, after LIGO and Virgo collaboration start detect the gravitational wave from the binary systems. This kind of perturbation cab also be applicable to wormhole spacetime. Here we are interested in considering perturbation of the Ellis spacetime. We have mentioned before that the Ellis spacetime is the solution of Einstein-scalar field equations. So that the scalar field and metric tensor can be expressed as $\tilde{\Phi} = \Phi + \delta\Phi$ and $\tilde{g}_{\mu\nu} = g_{\mu\nu} + h_{\mu\nu}$, where Φ and $g_{\mu\nu}$ are the scalar field and background spacetime metric given in Eqs. (3.1) and (3.2), while $\delta\Phi$ is perturbed scalar field is

$$\delta\Phi = e^{-i\omega t}F(r)P_\ell(\cos\theta)\ , \tag{3.28}$$

and perturbed metric tensor components are defined as [148]

$$h_{\mu\nu} = e^{-i\omega t}\begin{pmatrix} H_0 & H_1 & 0 & 0 \\ H_1 & H_2 & 0 & 0 \\ 0 & 0 & K(r^2+r_0^2) & 0 \\ 0 & 0 & 0 & K(r^2+r_0^2)\sin^2\theta \end{pmatrix} P_\ell(\cos\theta)\ , \tag{3.29}$$

where $H_0(r)$, $H_1(r)$, $H_2(r)$, $K(r)$ and $F(r)$ are unknown radial functions and $P_\ell = P_\ell(\cos\theta)$ is the Legendre polynomial which satisfies the following equation:

$$\frac{1}{\sin\theta}\frac{d}{d\theta}(\sin\theta\frac{d}{d\theta})P_\ell + \ell(\ell+1)P_\ell = 0 \ . \tag{3.30}$$

After applying the property of the Legendre polynomial (3.30), the explicit field equations for the radial functions are presented in Appendix 3.5. Notice that referring to Ref. [148], it's observed that the perturbation described in equation (3.29) is termed as the "polar perturbation" while another perturbation, known as the "axial perturbation," is mentioned for the metric tensor in the reference. However, our investigation confirms the absence of this axial perturbation in the Ellis spacetime.

3.4.1 Time-independent solutions

We first focus on finding the stationary solutions for the radial profile functions (i.e. $\omega = 0$). In this case, the function H_1 vanishes, (i.e. $H_1 = 0$), and from Eqs. (3.51)-(3.58), one can obtain equations for the remaining functions in the form:

$$\left[\left(x^2+1\right)H'\right]' - \ell(\ell+1)H = 0 \ , \tag{3.31}$$

$$\left[\left(x^2+1\right)F'\right]' - \ell(\ell+1)F + \frac{4}{x^2+1}F = 0 \ , \tag{3.32}$$

$$K = H - \frac{4}{(\ell+2)(\ell-1)}\left(F' + \frac{2x}{x^2+1}F\right) \ , \tag{3.33}$$

where primes denote the derivative with respect to the dimensionless radial coordinate x. Solutions to Eqs. (3.31) and (3.32) are rather simple and can be expressed as read

$$H(x) = i^\ell \left[C_{1\ell}P_\ell(ix) + C_{2\ell}iQ_\ell(ix)\right] \ , \tag{3.34}$$

$$F(x) = i^\ell \left[C_{3\ell}P^2_\ell(ix) + C_{4\ell}iQ^2_\ell(ix)\right] \ , \tag{3.35}$$

where $C_{1\ell}$, $C_{2\ell}$, $C_{3\ell}$ and $C_{4\ell}$ are constants of integration. $P_\ell(ix)$, $Q_\ell(ix)$ are Legendre functions of the first, and second kinds while $P^2_\ell(ix)$ and $Q^2_\ell(ix)$ are associated Legendre functions of the first and second kind, respectively. Note that the coefficients i^ℓ in equations (3.31) and (3.32) ensure that the solution remains real at all points in spacetime. Finally, from Eq.(3.33) the function K can be found as

$$K(x) = C_{1\ell}P_\ell\left(ix\right) + C_{2\ell}Q_\ell\left(ix\right) + \frac{4C_{3\ell}}{\left(\ell+2\right)\left(x^2+1\right)}[xP^2_\ell(ix) + iP^2_{\ell+1}(ix)] + \frac{4C_\ell 4}{\left(\ell+2\right)\left(x^2+1\right)}[xQ^2_\ell(ix) + iQ^2_{\ell+1}(ix)] \ . \tag{3.36}$$

3.4.2 Wave solution

Here we will discuss the wave solution of the field equations for radial functions. Before going further we introduce a dimensionless frequency which is defined as $\omega_0 = \omega r_0$. Now using expressions (3.57), (3.58) and taking into account the fact that $H = H_0 = H_2$, the equation for the function F can be easily derived as

$$\left[\left(x^2+1\right)F'\right]' + \left[\omega_0^2 x^2 + \frac{4}{x^2+1} - 4\eta\right]F = 0 \ ,$$

where $\eta = \ell^2 + \ell - \omega_0^2$ and the analytical solution to the above equation can be presented in terms of the confluent Heun function (i.e. $\mathrm{HeunC}(a,b,c,d,x)$) as follows:

$$F(r) = \left(x^2+1\right)\left[c_1 F_{1\ell}(x) + c_2 x F_{2\ell}(x)\right] \ , \tag{3.37}$$

where

$$F_{1\ell}(x) = \mathrm{HeunC}\left[\eta - \frac{3}{2}, -\frac{\omega_0^2}{4}, \frac{1}{2}, 3, 0, -x^2\right] \ , \tag{3.38}$$

$$F_{2\ell}(x) = \mathrm{HeunC}\left[\eta - 3, -\frac{\omega_0^2}{4}, \frac{3}{2}, 3, 0, -x^2\right] \ . \tag{3.39}$$

As we found that in the Ellis spacetime, the solution to scalar perturbation is described by the analytical expression, namely, confluent Heun function. The radial dependence of the function $F(x)$ is shown in Fig. 3.7. The radial profile function $F(x)$ oscillates while simultaneously decreasing.

Now we concentrate on the equations for the remaining radial functions $H(r)$, $H_1(r)$ and $K(r)$. The components of Einstein field equations for those functions yield

$$K'' + \frac{3x}{x^2+1}K' - \frac{\ell^2+\ell-2}{2\left(x^2+1\right)}K - \frac{x}{x^2+1}H' - \frac{\ell^2+\ell+2}{2\left(x^2+1\right)}H = -\frac{2}{x^2+1}F' \ , \tag{3.40}$$

$$K' - H' - \frac{\ell(\ell+1)-2}{2x}(K-H) + \frac{\omega_0^2\left(x^2+1\right)}{x}K - 2i\omega_0 H_1 = \frac{2}{x}F' \ , \tag{3.41}$$

$$K'' - H'' + \frac{2x}{x^2+1}(K'-H') + \omega_0^2(K+H) - \frac{2ix\omega_0 H_1}{x^2+1} - 2i\omega_0 H_1' = -\frac{4}{x^2+1}F' \ , \tag{3.42}$$

$$K' + \frac{x}{x^2+1}(K-H) - \frac{i\ell(\ell+1)}{2\omega_0\left(x^2+1\right)}H_1 = -\frac{2}{x^2+1}F \ , \tag{3.43}$$

$$H_1' + i\omega_0\left(K+H\right) = 0 \ , \tag{3.44}$$

$$K' - H' - i\omega_0 H_1 = -\frac{4}{x^2+1}F \ . \tag{3.45}$$

Hereafter introducing new radial functions $X = K + H$ and $Y = K - H$, and performing simple algebraic manipulations, one obtains

$$Y'' - \frac{2xY'}{x^2+1} + Y\left(\omega_0^2 - \frac{\ell^2+\ell-2}{x^2+1}\right) = \frac{24xF}{\left(x^2+1\right)^2} \ , \tag{3.46}$$

$$X = \frac{1}{\omega_0^2}\left[Y'' + 4\left(\frac{F}{x^2+1}\right)'\right] \ , \tag{3.47}$$

$$H_1 = \frac{1}{i\omega_0}\left[Y' + \frac{4}{x^2+1}F\right] \ . \tag{3.48}$$

Since the explicit expression of the function F is already obtained, the task

remains to solve Eq.(3.46) exclusively. Hereafter introducing a new function $Y = y\sqrt{x^2+1}$, this equation can be simplified to the Regge–Wheeler–Zerilli equation (See, e.g. [148, 149]) including a source term in this form:

$$\left[\frac{d^2}{dx^2} + \omega^2 - V\right] y = \frac{24xF}{(x^2+1)^{3/2}} \ , \tag{3.49}$$

where V is the effective potential defined as

$$V(x) = \frac{\ell(\ell+1)}{x^2} - \frac{5x^2+2}{x^2(x^2+1)^2} \ . \tag{3.50}$$

It is difficult to find the analytical solution to equation (3.49), however numerical solution of this equation can be easily obtained. As s result radial dependence of the profile function $X(x)$, $Y(x)$ and $H_1(r)$ is shown in Fig.3.8. As one can see all profile functions oscillate with damping and disappear towards infinity. As one sees there is not any gravitational potential in the Ellis spacetime wave propagate like in a flat spacetime, in particular, if we see $r_0 = 0$.

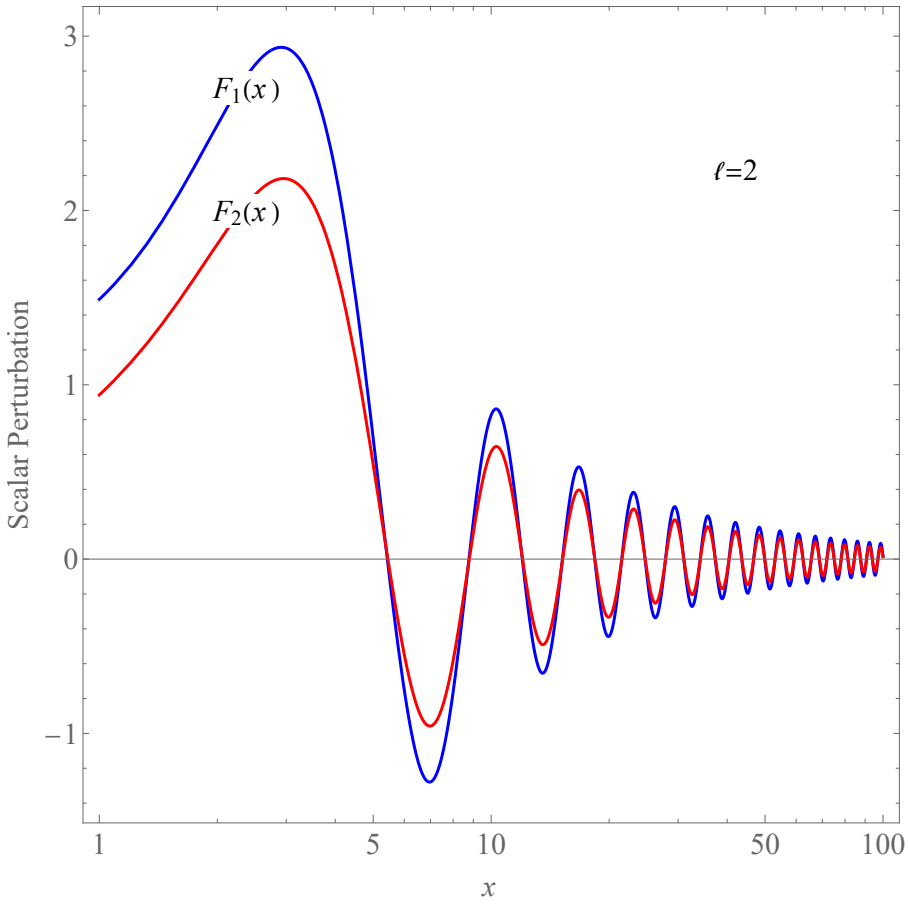

Figure 3.7: Radial dependence of the scalar perturbation at $\ell = 2$.

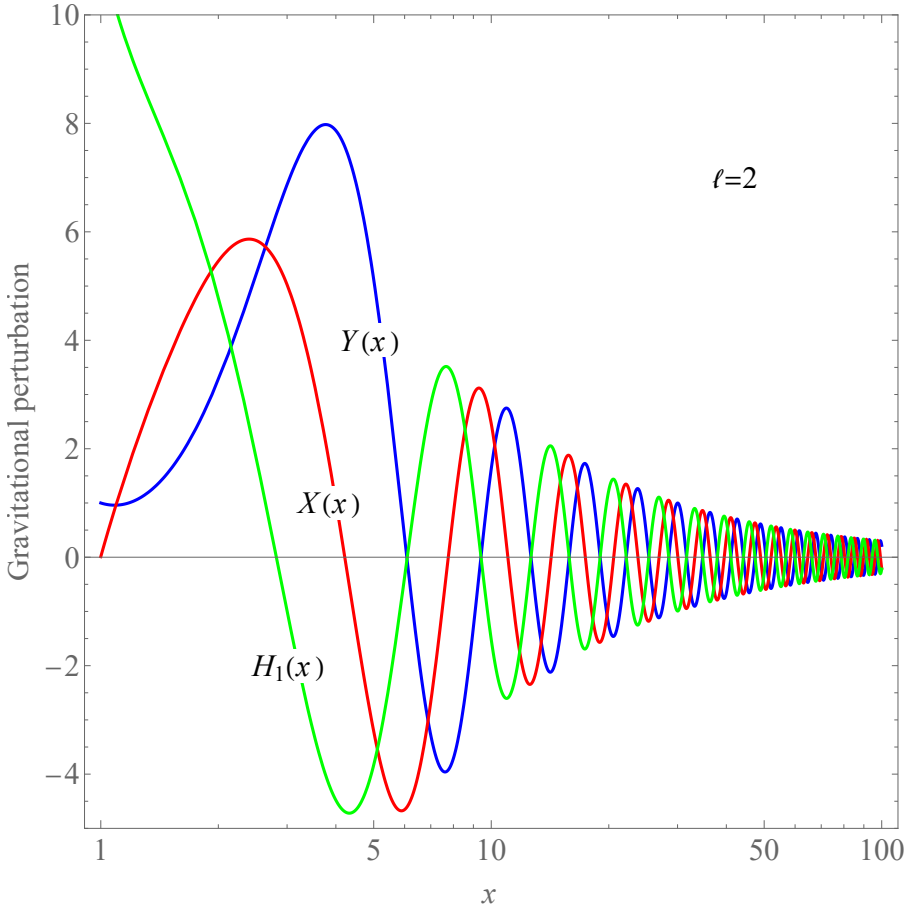

Figure 3.8: Radial dependence of the gravitational perturbation at $\ell = 2$.

3.5 List of radial equations

The list of Einstein-scalar field equations for unknown radial function are

$$K'' + \frac{3r}{r^2+r_0^2}K' - \frac{\ell^2+\ell-2}{2\left(r^2+r_0^2\right)}K - \frac{r}{r^2+r_0^2}H_2' - \frac{\ell^2+\ell+2}{2\left(r^2+r_0^2\right)}H_2 = -\frac{2r_0}{r^2+r_0^2}F' \ , \tag{3.51}$$

$$K' - H_0' + \frac{2\omega^2\left(r^2+r_0^2\right)-\ell^2-\ell+2}{2r}K + \frac{\ell(\ell+1)}{2r}H_0 - 2i\omega H_1 - \frac{H_2}{r} = \frac{2r_0}{r}F' \ , \tag{3.52}$$

$$\left[K'' - H_0'' + \frac{2rK'}{r^2+r_0^2} - \frac{rH_0'}{r^2+r_0^2} - \frac{rH_2'}{r^2+r_0^2} + \frac{4r_0F'}{r^2+r_0^2} - \frac{2ir\omega H_1}{r^2+r_0^2} - 2i\omega H_1' + \omega^2(K+H_2)\right]$$
$$\times P_\ell(\cos\theta) = \frac{H_0-H_2}{r^2+r_0^2}\cot\theta\frac{d}{d\theta}P_\ell(\cos\theta) \ , \tag{3.53}$$

$$\left[K'' - H_0'' + \frac{2rK'}{r^2+r_0^2} - \frac{rH_0'}{r^2+r_0^2} - \frac{rH_2'}{r^2+r_0^2} + \frac{4r_0F'(r)}{r^2+r_0^2} - \frac{2ir\omega H_1}{r^2+r_0^2} - 2i\omega H_1' + \omega^2(K+H_2\right.$$
$$\times P_\ell(\cos\theta) = -\frac{H_0-H_2}{r^2+r_0^2}\frac{d^2}{d\theta^2}P_\ell(\cos\theta) \ , \tag{3.54}$$

$$K' + \frac{r}{r^2+r_0^2}K - \frac{i\ell(\ell+1)}{2\omega\left(r^2+r_0^2\right)}H_1 - \frac{r}{a^2+r^2}H_2 = -\frac{2r_0}{r^2+r_0^2}F \ , \tag{3.55}$$

$$H_1' + i\omega\left(K+H_2\right) = 0 \ , \tag{3.56}$$

$$K' - H_0' + \frac{r}{r^2+r_0^2}H_0 - \frac{r}{r^2+r_0^2}H_2 - i\omega H_1 = -\frac{4r_0}{r^2+r_0^2}F \ , \tag{3.57}$$

$$\left[\left(r^2+r_0^2\right)F'\right]' + \left[\omega^2\left(r^2+r_0^2\right) - \ell(\ell+1)\right]F = r_0\left(K' - i\omega H_1 - \frac{H_0'+H_2'}{2}\right) \ . \tag{3.58}$$

From Eqs. (3.53) and (3.54), one can easily find that $H_0 = H_2 = H$ which is useful in further calculations.

3.6 Conclusion

In this chapter, we have investigated Ellis spacetime by considering neutral and charged particle dynamics in the presence of the external scalar field. As well as

the perturbation of the Ellis spacetime is also explored. Our main findings are summarized as follows:

- We have studied the circular motion of a massive particle in the Ellis spacetime, initially considering its potential interaction with an external scalar field for a more focused analysis. This spacetime is distinguished by two primary factors: the wormhole throat and the interaction parameter between the scalar field and the massive particle. Our study concentrated particularly on the particle's motion within the equatorial plane and aimed to ascertain how the ISCO position is influenced by these parameters.

- We have examined the oscillating movement of a massive particle within Ellis spacetime, focusing on understanding the equations governing its orbital and epicyclic motion. By employing perturbation techniques, we've derived linear oscillator equations describing the radial and angular displacements near the stable orbit. Exact analytical expressions for the frequencies of these oscillations along both the radial and vertical directions have been derived as well. To impose constraints on the throat of the wormhole, we've compared our theoretical findings with observational data. Our analysis showed that for low-frequency sources, the wormhole throat is no larger than $\sim$ 800km, whereas for high-frequency sources, it resembles approximately the size of a neutron star $\sim$ 15km.

- We also examined a charged particle motion around the Ellis wormhole, presuming it to be situated within a consistently uniform magnetic field. Employing the Wald method, we've presented a precise analytical solution for the azimuthal component of the vector potential of the electromagnetic field, derived from Maxwell's equations. Furthermore, we've established analytical

formulas for the ISCO equation, contingent upon two primary interaction factors: the scalar field parameter g_s and the magnetic parameter ω, governing the interaction between charged massive particles with electromagnetic field and scalar field.

- Finally, we have explored scalar and gravitational perturbations in the Ellis spacetime. We assume that both scalar gravitational waves propagate at identical frequencies and expressions for these are expanded in terms of the spherical harmonics. It is shown that the equation for the scalar profile function is totally independent from the tensor profile functions, however equations for the tensor profile functions strongly depend on the scalar profile functions in the Ellis spacetime. We have discovered that time-independent solutions for scalar and gravitational disturbances can be expressed using Legendre and associated Legendre functions, where the argument is complex. However, when considering stationary solutions within the wave zone, the exact analytical solution for scalar disturbances can be achieved, described by the confluent Heun function. It's noteworthy that the equations governing gravitational disturbances are considerably intricate, but they can be simplified to the familiar Regge–Wheeler–Zerilli equation for the tensor profile function. Finally, we present numerical solutions to the Regge–Wheeler–Zerilli equation for the radial functions.

Chapter IV

Long-lived quasinormal modes and asymptotic tails of regular Schwarzschild-like black holes in the presence of a magnetic field

4.1 Introduction

Quasinormal modes (QNMs) [150–153] are fundamental features of black holes, representing the oscillatory decay of perturbations in their surrounding spacetime. These modes emerge from disturbances such as binary mergers, producing gravitational waves with characteristic frequencies that encode critical information about the mass and spin of black holes. Observations from LIGO, starting with GW150914, have confirmed the presence of these QNMs in gravitational wave signals, offering strong evidence to support the predictions of General Relativity (GR) [154–157]. Future observations with advanced detectors like LISA aim to refine our understanding, testing the no-hair theorem, and investigating deviations that could indicate new physics beyond GR [152, 158].

Perturbations and the quasinormal spectrum of a massive or effectively massive

field differ qualitatively from those of a massless field. First, the mass term significantly suppresses the damping rate of frequencies [159–162], which can sometimes lead to the existence of arbitrarily long-lived modes, known as quasi-resonances [163, 164].

This phenomenon is quite broad and encompasses various spherically and axially symmetric black holes in four and higher dimensions, as well as fields with different spin [165–169]. However, there are configurations in which quasi-resonances do not occur, despite considerable suppression of the decay rate [170–172]. Therefore, determining the existence of arbitrarily long-lived modes must be done on a case-by-case basis.

It is also noteworthy that initially massless fields may acquire an effective mass term due to various factors, such as tidal forces from extra dimensions in brane-world models [173, 174] or the presence of an external magnetic field [161, 175], which may induce a strong superradiant instability [176, 177]. The influence of a magnetic field will be relevant in our analysis as well.

In the time domain, massive fields also exhibit distinctive decay characteristics. Although massless fields typically transition from quasinormal ringing to power-law decay, massive fields decay in a slow, oscillatory manner with a power-law envelope [178–185].

These slowly decaying oscillatory tails were employed in [186] to suggest that a massive graviton or other massive particles, whether in the framework of massive gravity or as an effective force, could contribute to the very long gravitational waves currently observed by the Pulsar Timing Array [187].

However, most of the studies mentioned above, with the exception of [188], focus on perturbations and spectra of massive fields in the background of singular black holes. In [188], the quasinormal modes of a massive scalar field around the regular,

ad hoc Bardeen black hole were examined. In this work, we aim to take a further step by investigating the spectrum of a massive scalar field near other regular black holes with an asymptotically Minkowski core, incorporating the effects of an external magnetic field.

It is worth noting that the literature on perturbations and quasinormal modes of regular black holes is now quite extensive (see, for instance, [189–196] and references therein). However, these studies generally do not consider perturbations of massive fields.

The regular black hole of interest in our study was introduced in [197] and differs from the well-known Bardeen and other regular black hole models in several respects.

The chapter is organized as follows: Section 4.2 provides an overview of Schwarzschild-like spacetime and discusses the associated magnetic field configuration. In Section 4.3, we analyze the dynamics of a charged scalar field within this framework. Section 4.4 presents the numerical results obtained using both the WKB approximation and the time-domain analysis.

4.2 Schwarzschild-like Black Hole

The gravitational field of a Schwarzschild-like compact object in Boyer–Lindquist coordinates can be expressed through the following line element [197]:

$$ds^2 = -f\,dt^2 + f^{-1}\,dr^2 + r^2\left(d\theta^2 + \sin^2\theta\,d\phi^2\right)\,, \tag{4.1}$$

where the metric function f is defined as:

$$f = 1 - \frac{2Me^{-\mathrm{a}/r}}{r}\,. \tag{4.2}$$

In this context, the parameter M represents the mass of the black hole, while a is a deviation parameter introduced by Simpson and Visser [197, 198]. It is important

to note that the spacetime metric described above corresponds to the standard Schwarzschild black hole in general relativity when a $\rightarrow 0$.

4.2.1 Magnetic Field Configuration

In realistic astrophysical scenarios, the magnetic field configuration near a gravitationally compact object is highly complex. However, for simplicity, one can consider an analytical expression for the magnetic field. A straightforward approach is provided by Wald [147]. According to this approach, the black hole is placed in an asymptotically uniform magnetic field, and the exact analytical expression for the vector potential in Schwarzschild space is given as:

$$A_{\phi,Sch} = \frac{1}{2} B r^2 \sin^2\theta \ , \tag{4.3}$$

where B is the magnetic field strength. Note that the expression (4.3) is independent of the mass of the Schwarzschild black hole and fully satisfies Maxwell's equations in curved spacetime, given as:

$$\nabla_\alpha F^{\alpha\beta} = 0 \ . \tag{4.4}$$

Similarly, in the background of the Schwarzschild-like spacetime, Maxwell's equation can be analytically solved, and the expression for the vector potential can be found as:

$$A_\phi = \frac{1}{2} B \psi(r) \sin^2\theta \ , \tag{4.5}$$

which is similar to the solution in the Schwarzschild spacetime in (4.3), but with a new radial function $\psi(r)$ substituting r^2. By inserting equation (4.5) into (4.4), one can obtain:

$$r^2 \left[f \psi'(r) \right]' - 2\psi(r) = 0 \tag{4.6}$$

where a prime denotes the derivative with respect to the radial coordinate. The solution to equation (4.6) can be expressed as $\psi(r) = C(r^2 - 2aM)$, where C is a constant of integration, which can be set to 1. Finally, the exact analytical solution of Maxwell's equation for the vector potential near the Schwarzschild-like black hole can be found as:

$$A_\phi = \frac{1}{2} B \left(r^2 - 2aM\right) \sin^2\theta \ , \tag{4.7}$$

To study the magnetic field configuration in the vicinity of the black hole, we can analyze the magnetic field lines represented by the equation $A_\phi = \text{const}$. Figure 4.1 provides a visualization of the magnetic field lines near the Schwarzschild-like black hole. It is apparent that due to the additional term in the metric function, the magnetic field lines extend outward from the black hole in a more uniform manner.

4.3 charged scalar field

The relativistic Klein-Gordon equation for a massive, charged scalar field Ψ, in the presence of an electromagnetic field, is expressed as follows:

$$g^{\alpha\beta}(\Delta_\alpha - iqA_\alpha)(\Delta_\beta - iqA_\beta)\Psi - \mu^2\Psi = 0 \ , \tag{4.8}$$

Here, μ represents the mass of the scalar field, q is the charge coupling constant between the scalar and electromagnetic fields,∇_α denotes the covariant derivative and i is imaginary number. Although separating variables in equation (4.8) is quite challenging, we can simplify the problem by applying the following physically reasonable assumptions:

- Lorentz gauge condition for the vector potential: $\nabla_\alpha A^\alpha = 0$;

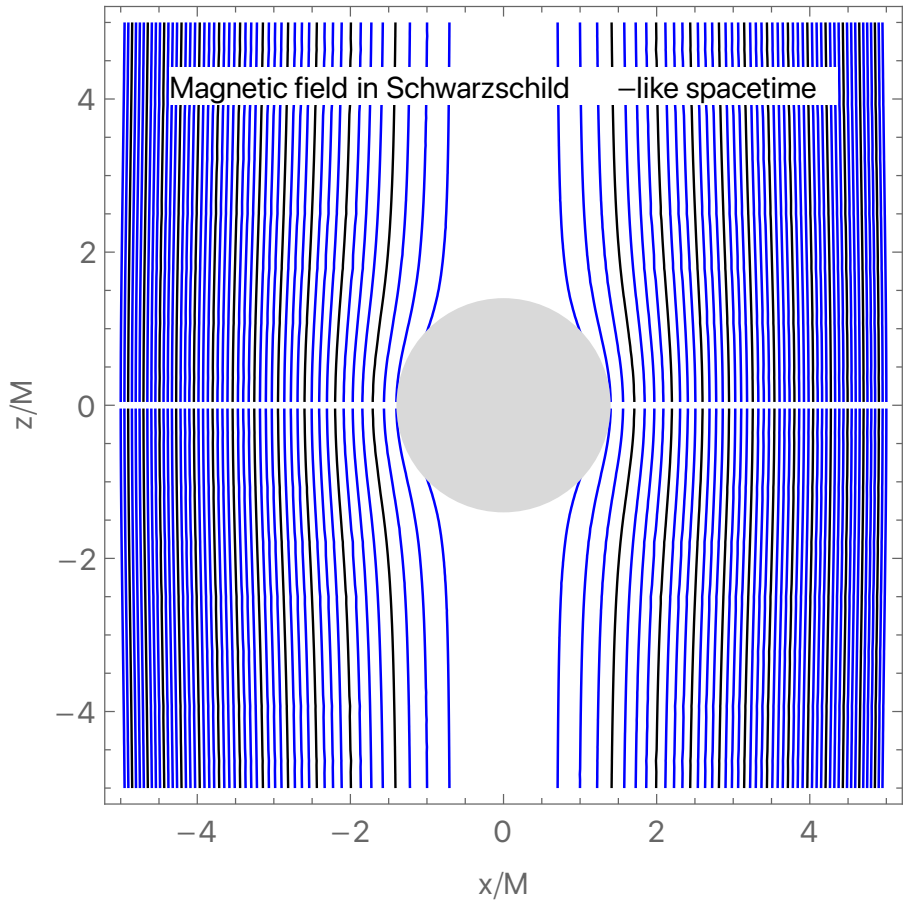

Figure 4.1: The magnetic field lines in the vicinity of the Schwarzschild-like spacetime (a/M = 0.5).

- In the weak interaction limit, higher-order terms, such as q^2B^2, can be neglected, i.e., $q^2B^2 \to 0$. Then, eq.(4.8) becomes

$$\frac{1}{\sqrt{-g}}\partial_\alpha(\sqrt{-g}g^{\alpha\beta}\partial_\beta\Psi) - 2iqA^\alpha\partial_\alpha\Psi - \mu^2\Psi = 0 \ , \tag{4.9}$$

We can write the solution as:

$$\Psi(t, r, \theta, \phi) = e^{-i\omega t}Y_{lm}(\theta, \phi)\frac{R(r)}{r}. \tag{4.10}$$

With the use the following notation:

$$\nabla^2_\Omega = \frac{1}{\sin\theta}\partial_\theta\left(\sin\theta\partial_\theta\right) + \frac{1}{\sin^2\theta}\partial^2_\phi \tag{4.11}$$

one can then obtain the following

$$\nabla^2_\Omega\Psi = -l(l+1)\Psi. \tag{4.12}$$

Then, in tortoise coordinate system with $dx = dr/f$, one can write

$$\left[\frac{d^2}{dx^2} + \omega^2 - V\right]R(r) = 0 \tag{4.13}$$

where the effective potential is defined as

$$V = f\left[\frac{l(l+1)}{r^2} + \frac{f'}{r} + mqB\frac{2\mathrm{a}M}{r^2} + \mu^2_{eff}\right] \tag{4.14}$$

with

$$\mu^2_{eff} = \mu^2 - mqB \ . \tag{4.15}$$

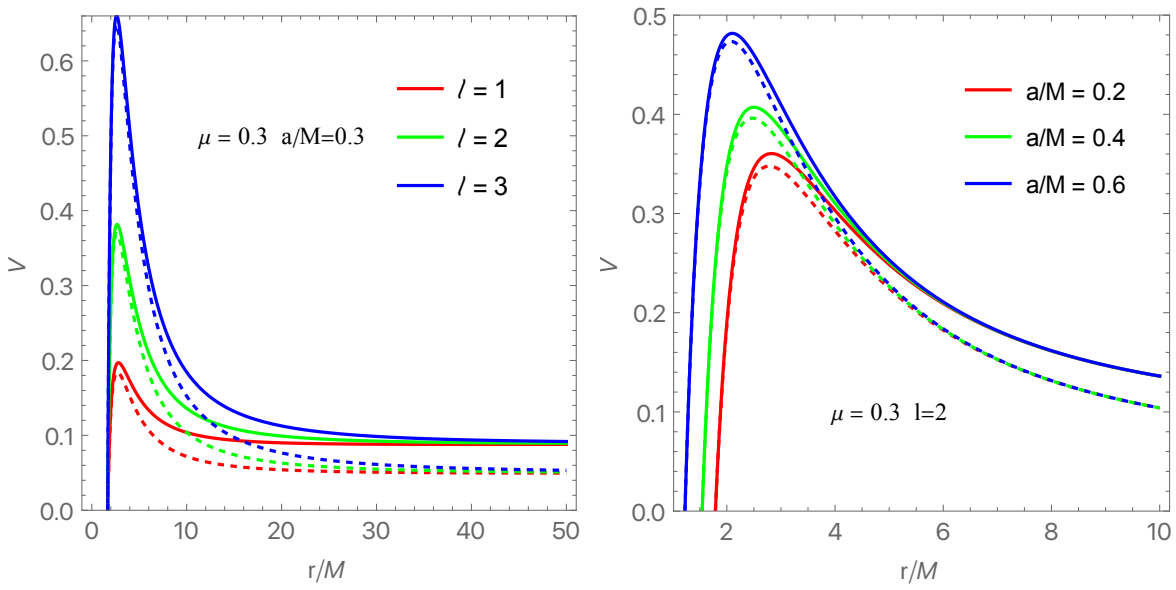

Figure 4.2: Radial profile of effective potential. Solid lines for neutral ($qB = 0$) particle, dashed lines for charged ($qB = 0.2$) particle.

l	m	a = 0, $\mu = 0$, $qB = 0$	a = 0.3, $\mu = 0$, $qB = 0$	a = 0.3, $\mu = 0.1$, $qB = 0$	a = 0.5, $\mu = 0.1$, $qB = 0.1$	a=0.3, $\mu = 0.0$, $qB = 0.45$
0	0	0.111946 -0.104579 i	0.125072 - 0.106152i	0.127077 - 0.0992083i	0.139158 - 0.0990972i	0.124967-0.105965i
	1				0.364317 - 0.10033i	0.264653-0.136211 i
1	0	0.292931 - 0.0976602 i	0.328766 - 0.100271 i	0.332542 - 0.0981747 i	0.366747 - 0.0987235i	0.328762-0.100294 i
	-1				0.36919 - 0.0970796i	
	2				0.598773 - 0.100327i	0.452369-0.12924 i
	1				0.600472 - 0.0997012i	0.496175-0.115227 i
2	0	0.483643 -0.096759 i	0.542474 - 0.0994879 i	0.54509 - 0.0986551 i	0.602177 - 0.0990695i	0.542474-0.099488 i
	-1				0.603889 - 0.0984322i	0.591758-0.081276 i
	-2				0.605608 - 0.0977892i	0.644421-0.059118 i
	3				0.835555 - 0.100175i	0.655526-0.123318 i
	2				0.836821 - 0.0998474i	0.688443-0.115782 i
	1				0.838089 - 0.0995185i	0.722359-0.107792 i
3	0	0.675366 - 0.0964997 i	0.757385 - 0.0992644 i	0.75933 - 0.0988275 i	0.839361 - 0.0991881i	0.757385-0.0992643 i
	-1				0.840635 - 0.0988562i	0.793655-0.0900815 i
	-2				0.841912 - 0.0985228i	0.831329-0.080071 i
	-3				0.843192 - 0.0981878i	0.870599-0.0689605 i

Table 4.1: Fundamental quasinormal modes of charged scalar field for Schwarzschild-like black hole obtained by the 6th order WKB ($\tilde{n} = 3$, $\tilde{m} = 3$, $M = 1$).

l	m	6th order WKB($\tilde{n}=3, \tilde{m}=3$)	time domain	Relative error(Re(ω))	Relative error(Im(ω))
0	0	0.127077 - 0.0992083i			
	1	0.32919 - 0.100268i			
1	0	0.332542 - 0.0981747i	$0.332491 - 0.0987287i$	-0.015%	-0.56%
	-1	0.33591 - 0.0960409i			
	2	0.54038 - 0.100314i			
	1	0.542732 - 0.0994874i			
2	0	0.54509 - 0.0986551i	$0.54509 - 0.0986532i$	0.00%	0.0019%
	-1	0.547456 - 0.0978167i			
	-2	0.549829 - 0.0969722i			
	3	0.754058 - 0.100133i	$0.75407 - 0.100128i$	0.0016%	0.0049%
	2	0.755813 - 0.0996994i	$0.755825 - 0.0996941i$	0.0016%	0.0053%
	1	0.75757 - 0.0992642i	$0.757582 - 0.0992592i$	0.0016%	0.0050%
3	0	0.75933 - 0.0988275i	$0.759342 - 0.0988225i$	0.0016%	0.0051%
	-1	0.761093 - 0.0983891i	$0.761106 - 0.0983841i$	0.0017%	0.0051%
	-2	0.76286 - 0.0979492i	$0.762872 - 0.0979442i$	0.0016%	0.0051%
	-3	0.764629 - 0.0975076i	$0.764642 - 0.0975025i$	0.0017%	0.0052%

Table 4.2: Fundamental quasinormal modes of charged scalar field for Schwarzschild-like black hole obtained by the 6th order WKB (a= 0.3, $\mu = 0.1$, $qB = 0.1$, $M = 1$).

4.4 Numerical Results

In this section, we briefly present the results of numerical calculations of the quasinormal modes for a Schwarzschild-like black hole immersed in an external asymptotically uniform magnetic field. To solve the Schrödinger-like wave equation (4.13), we impose the following boundary conditions: the wave exhibits purely incoming behavior at the event horizon and purely outgoing behavior at spatial infinity, as

$$R(r) = \begin{cases} e^{-i\omega x}, & \text{as } x \to -\infty \, (r \to -\frac{\mathrm{a}}{W\left(-\frac{\mathrm{a}}{2}\right)}), \\ e^{i\chi x}, & \text{as } x \to \infty \, (r \to \infty), \end{cases}$$

where $\chi = \sqrt{\omega^2 - \mu_{eff}^2}$.

4.4.1 WKB method

For frequency-domain analysis, we employ the semi-analytical WKB method [199–203]. This method involves expanding the solution at both infinities in a WKB series and matching these asymptotic expansions with a Taylor series near the peak of the effective potential. Additionally, as suggested in [201], we enhance the WKB expansion by representing it with the Padé approximation, which significantly improves the accuracy of the WKB method in most cases.

The higher order WKB formula is given by [202]:

$$\begin{aligned} \omega^2 &= V_0 + A_2(K^2) + A_4(K^2) + A_6(K^2) + \dots \\ &- iK\left(-2V_1 + A_3(K^2) + A_5(K^2) + A_7(K^2) + \dots\right) \end{aligned} \tag{4.16}$$

where $K = n + 1/2$, with $n = 0, 1, 2, 3, \dots$.

Corrections $A_k(K^2)$ of order k to the eikonal formula are polynomials in K^2 with rational coefficients, depending on the values $V_2, V_3, \dots$ of higher derivatives of

the potential $V(r)$ at its maximum. To further improve the accuracy of the WKB formula, we use the procedure proposed by Matyjasek and Opala [201], which involves applying the Padé approximation. For a given order k of the WKB formula (4.16), we define a polynomial $P_k(\epsilon)$ as follows:

$$\begin{aligned} P_k(\epsilon) &= V_0 + A_2(K^2)\epsilon^2 + A_4(K^2)\epsilon^4 + A_6(K^2)\epsilon^6 + \dots \\ &- iK\left(-2V_1\epsilon + A_3(K^2)\epsilon^3 + A_5(K^2)\epsilon^5 + \dots\right) \end{aligned} \tag{4.17}$$

and the squared frequency is then obtained by setting $\epsilon = 1$:

$$\omega^2 = P_k(1). \tag{4.18}$$

To improve the approximation of $P_k(\epsilon)$, we apply the Padé approximation:

$$\tilde{P}_{\tilde{n}/\tilde{m}}(\epsilon) = \frac{Q_0 + Q_1\epsilon + \dots + Q_{\tilde{n}}\epsilon^{\tilde{n}}}{R_0 + R_1\epsilon + \dots + R_{\tilde{m}}\epsilon^{\tilde{m}}}, \tag{4.19}$$

where $\tilde{n} + \tilde{m} = k$, ensuring that near $\epsilon = 0$, $\tilde{P}_{\tilde{n}/\tilde{m}}(\epsilon) - P_k(\epsilon) = O(\epsilon^{k+1})$.

For finding the fundamental mode ($n = 0$), Padé approximation with $\tilde{n} \approx \tilde{m}$ generally yield the best results. In [201], the approximation $P_{6/6}(1)$ and $P_{6/7}(1)$ were compared for this purpose. The 6th-order WKB formula $P_{6/0}(1)$ is commonly used, but as noted in [202], even the Padé approximation $P_{3/3}(1)$ of the 6th order often yields a more accurate value for the squared frequency than $P_{6/0}(1)$. In this work, we will use the 6th WKB expansions.

Using the sixth-order WKB approximation, we compute the quasinormal mode frequencies of electrically charged scalar perturbations in the field of a magnetized Schwarzschild-like black hole. Table 4.1 displays the real and imaginary components of these frequencies for various azimuthal (m) and multipole (l) numbers, as well as for different values of the parameter qB and the spacetime parameter a.

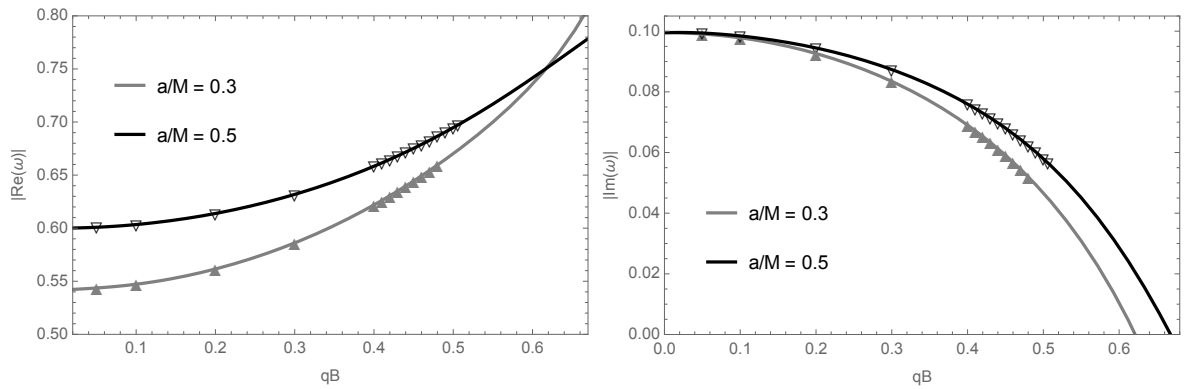

Figure 4.3: Best fitting polynomial functions of WKB data for different values of spacetime values($l = 2, m = -2$).

Furthermore, in Table 4.2, we compare the results obtained using the sixth-order WKB method with those derived from the time-domain method. The relative errors in the real (third column) and imaginary (fourth column) parts are shown to be negligible, demonstrating the high accuracy of the WKB results.

Fig.4.3 illustrates the best-fit polynomial function for data obtained using the WKB method, applied to a massless scalar field in an external magnetic field. The figure shows two curves, gray and black, corresponding to different spacetime parameter values ($a/M = 0.3$ and $a/M = 0.5$, respectively). The imaginary parts of the quasinormal mode frequency ω for these parameter values are shown on the right-hand side. Each curve intersects the zero value of qB at approximately 0.611711 (gray line) and 0.651842 (black line), respectively.

The WKB data is checked here by time-domain integration. However, two aspects must be taken into account for such a comparison. First of all, the period of quasi-normal ringing is very short for $\ell = 0$ perturbations because it is quickly followed by oscillatory power-law tails, as shown in Fig. 4.5. Therefore, it is difficult to extract the frequency from the time-domain profile with sufficient accuracy in this case. The second aspect is the growth of the perturbation at late times Fig. 4.4. One could think that this means an instability caused by the negative value of the

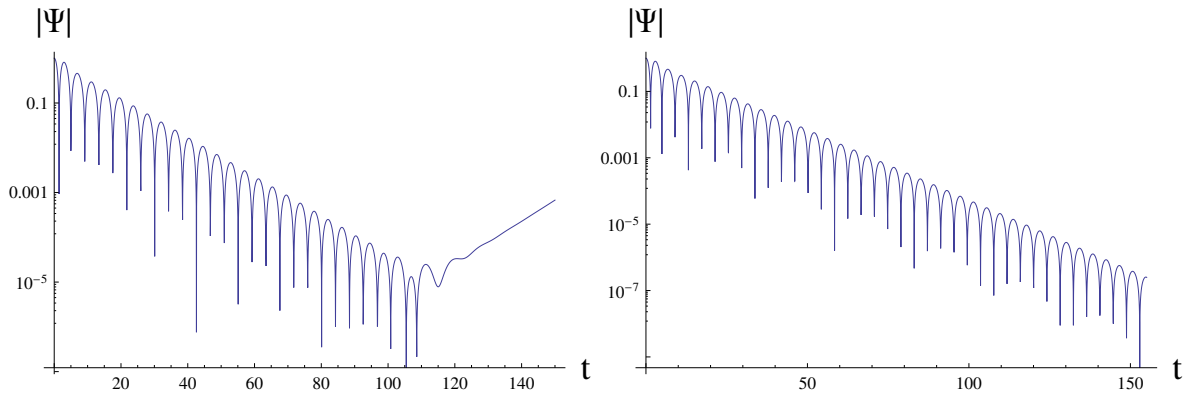

Figure 4.4: Semi-logarithmic plots of time-domain profiles for $m = 3$ (left) and $m = -3$ (right) perturbations; $l = 3$, $qB = 0.1$, a $= 0.3$, $\mu = 0.1$, $M = 1$. The instability at late times for $m > 0$ is the artifact of the approximation for the effective potential which is valid only until some distance from the black hole (see discussion in [204]). At the ringdown phase the WKB data is reproduced with high accuracy.

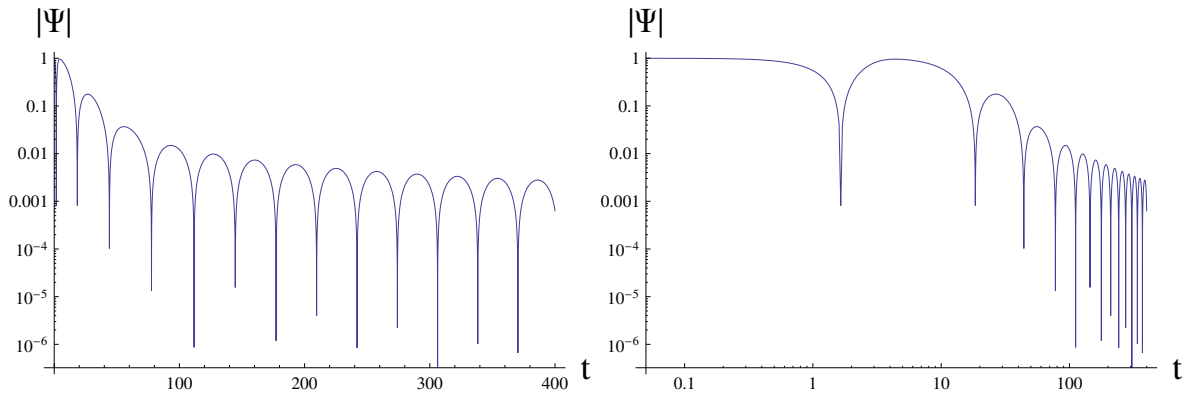

Figure 4.5: Semi-logarithmic plots of time-domain profiles (left) and logarithmic plot (right); $l = m = 0$, $qB = 0.1$, a $= 0.3$, $\mu = 0.1$, $M = 1$. The short period of quasinormal ringing is quickly changed by an asymptotic tails, making it unable to extract the frequency from the profile with sufficient accuracy.

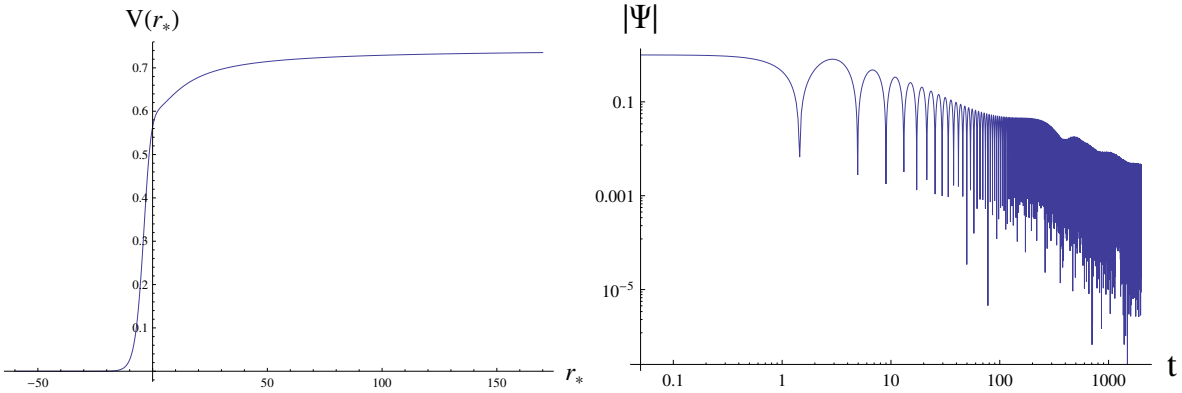

Figure 4.6: Effective potential and logarithmic plots of time-domain profiles for $m = -2$ perturbations; $l = 2$, $qB = 0.61$, a $= 0.3$, $\mu = 0$, $M = 1$.

effective potential at large r when $m > 0$. However, as shown in [204], the effective potential itself is valid only up to some range that is inversely proportional to the asymptotic value of the magnetic field B. Thus, we conclude, in the same way as in [204], that the instability is false and is simply an artifact of treating the effective potential which is determined only in some range near the black hole valid throughout the whole space instead. Even in that case, the quasinormal ringing period before the "instability" is in very good agreement with the WKB data.

4.4.2 The time-domain integration

We rewrite the wave equation (4.13) without assuming the stationary ansatz ($\Psi \sim e^{-i\omega t}$) as:

$$\frac{\partial^2\Psi}{\partial t^2} - \frac{\partial^2\Psi}{\partial x^2} + V(t,x)\Psi = 0 \tag{4.20}$$

where x is the tortoise coordinate. The method for integrating this wave equation in the time domain was developed by Gundlach, Price, and Pullin [205]. We now express equation (4.13) in terms of the light-cone coordinates $du = dt - dx$ and $dv = dt + dx$, resulting in:

$$\left(4\frac{\partial^2}{\partial u\partial v}+V(u,v)\right)\Psi(u,v)=0 \tag{4.21}$$

This equation is solved numerically using a discretization scheme as follows [205]:

$$\begin{aligned}\Psi\left(N\right) &= \Psi\left(W\right)+\Psi\left(E\right)-\Psi\left(S\right)\\ &\quad -\Delta^2 V\left(S\right)\frac{\Psi\left(W\right)+\Psi\left(E\right)}{4}+\mathcal{O}\left(\Delta^4\right),\end{aligned} \tag{4.22}$$

Here, we have the following points for the integration scheme: $N \equiv (u+\Delta, v+\Delta)$, $W \equiv (u+\Delta, v)$, $E \equiv (u, v+\Delta)$, $S \equiv (u, v)$, and Δ is a constant representing the separation between neighboring grid points (further details can be found in references [205, 206]). Initial conditions are specified on the two null surfaces, $u = u_0$ and $v = v_0$. For computations, we assume that the initial perturbation is a Gaussian pulse centered around v_c with width σ, given by:

$$\Psi(u=u_0,v)=A\exp\left(-\frac{(v-v_c)^2}{\sigma^2}\right). \tag{4.23}$$

Then, utilizing the Prony method [207] to represent the signal as a sum of exponential terms with associated weights , we extract the dominant quasinormal frequencies from the time-domain profile. The time-domain integration approach, known for its high precision, has been extensively employed in numerous studies (see, for example, [208–215]. Consequently, we will not elaborate on it further in this work.

As shown in Fig. 4.6, when ℓ and m are non-vanishing, and some values of other parameters are fixed, the asymptotic behavior qualitatively deviates from the usual massive tails, which are oscillatory with a power-law envelope [178–180, 182–185]. In our case, the presence of a magnetic field results in an oscillatory envelope instead of a power-law one, which cannot be easily fitted to a simple analytical

formula. A similar behavior was recently observed in the context of environmental effects on the late-time decay of massive fields [216]. In that case, however, the configuration did not involve a magnetic field; the environmental effects were instead modeled by Gaussian bumps in the effective potential. In our case this unusual behavior should not be determined by the limited approximation of the range of the effective potential. We believe this phenomenon occurs due to the specific behavior of the effective potential near the event horizon, as illustrated in Fig. 4.6. In terms of the tortoise coordinate, there is a distinct kink near the event horizon. As demonstrated in [216], deformations in the effective potential close to the horizon can significantly modify the late-time tails of massive fields. Additionally, given that massive tails decay slowly and are expected to contribute to the very long-wavelength radiation observed via the Pulsar Timing Array [186], the unusual late-time decay induced by magnetic fields opens up a new avenue for further investigation.

4.5 Conclusions

While the quasinormal modes of regular black holes have been extensively studied in numerous works, no comprehensive investigations have been conducted for regular black holes in the presence of an external magnetic field. In this paper, we address this gap and demonstrate that the magnetic field significantly alters the spectrum of a charged scalar field, leading to the emergence of arbitrarily long-lived quasinormal modes, known as quasi-resonances [163].

Another distinctive feature of the evolution of perturbations in the presence of a magnetic field is the unusual behavior of asymptotic tails. For certain parameter values, these tails do not exhibit a power-law envelope but instead display an oscillatory envelope. This behavior is most likely due to the peculiar deformation of

the effective potential near the event horizon and deserves a detailed investigation in future studies.

This work could be further extended by considering other regular black hole solutions and different magnetic field structures.

Main results and conclusions

Below we present the main results of the dissertation. The following conclusions were presented on the basis of research carried out on the topic of "Relativistic Astrophysics around Compact Objects Coupled with Scalar Field" for the Doctor of Philosophy (PhD) dissertation:

1. It has been shown that the Janis-Newman-Winicour (JNW) naked singularity spacetime exhibits a repulsive scalar field effect, altering the innermost stable circular orbit (ISCO) radius nonmonotonically with the scalar parameter n. Unlike Schwarzschild black holes, the ISCO vanishes for critical scalar strengths, indicating a breakdown of stable orbits near the singularity.

2. For the first time, analytical expressions for the effective potential, specific energy, and angular momentum of massive particles in the JNW spacetime have been derived, revealing that scalar coupling g_s reduces (increases) the ISCO for positive (negative) values. The radiative efficiency of the accretion disks in this space-time was found to exceed the Schwarzschild predictions by up to 12%.

3. It has been demonstrated that Ellis' throat wormhole r_0 and scalar coupling g_s govern marginally stable orbits, with particle trajectories exhibiting escape paths under radiation reaction, a stark contrast to black hole capture. The fundamental frequencies of oscillatory motion were computed, showing

distinct shifts observable in quasiperiodic oscillations (QPOs).

4. It has been found that charged particles in magnetized Ellis wormhole spacetimes follow split fundamental frequencies due to Lorentz forces, with quasi-resonant modes emerging at critical magnetic field strengths. The radiation intensity was shown to depend on both scalar and electromagnetic interactions.

5. For the first time, Markov Chain Monte Carlo (MCMC) analysis was applied to constrain the JNW spacetime parameters (M, g_s, n) using binary QPO X-ray data (e.g. GRO J1655-40), yielding best-fit values consistent with weak scalar dominance ($n \sim 0.75$, $g_s \sim 0.2$).

6. It has been shown that scalar perturbations in Ellis wormhole spacetime admit exact solutions in terms of confluent Heun functions, while gravitational perturbations obey a Regge-Wheeler-type equation with unusual oscillatory tails, which varies from power-law decay in black holes.

7. The quasinormal modes of Schwarzschild-like black holes in external magnetic fields were computed via WKB and time-domain methods, revealing long-lived quasiresonances and anomalous late-time tails. These signatures could distinguish scalar-modified spacetimes in future gravitational wave observations.

Bibliography

[1] A. Davlataliev, B. Narzilloev, I. Hussain, A. Abdujabbarov, and B. Ahmedov, "Probing the Starobinsky-Bel-Robinson gravity by photon motion around the Kerr-type black hole in non-uniform plasma," *Phys. Dark Univ.*, vol. 42, p. 101340, 2023.

[2] A. Davlataliev, B. Narzilloev, I. Hussain, A. Abdujabbarov, and B. Ahmedov, "Quasi periodic oscillations around Kerr-type black hole in the Starobinsky–Bel–Robinson theory of gravity," *Phys. Dark Univ.*, vol. 46, p. 101569, 2024.

[3] A. Davlataliev, B. Narzilloev, I. Hussain, A. Abdujabbarov, and B. Ahmedov, "Charged and magnetized particle motion around a static black hole in the Starobinsky–Bel–Robinson gravity," *Eur. Phys. J. C*, vol. 84, no. 7, p. 694, 2024.

[4] A. Davlataliev, J. Rayimbaev, F. Abdulkhamidov, Z. Stuchlik, and A. Abdujabbarov, "Circular motion and collisions of charged spinning particles near Kerr Newman black holes," *Phys. Dark Univ.*, vol. 46, p. 101590, 2024.

[5] A. Davlataliev, F. Atamurotov, A. Abdujabbarov, N. Juraeva, and V. Khamidov, "Constraints on Schwarzschild-like black hole from QPOs data," *Phys. Dark Univ.*, vol. 46, p. 101603, 2024.

[6] B. Turimov, A. Davlataliev, A. Abdujabbarov, and B. Ahmedov, "Influence of scalar field in massive particle motion in JNW spacetime," *Phys. Rev. D*, vol. 110, no. 8, p. 084053, 2024.

[7] G. Mustafa, E. Demir, A. Davlataliev, H. Chaudhary, F. Atamurotov, and E. Güdekli, "Observational signature of QPOs with particle motion around non-commutative Schwarzschild black hole surrounded by perfect fluid dark matter," *Phys. Dark Univ.*, vol. 46, p. 101644, 2024.

[8] B. Turimov, A. Davlataliev, B. Ahmedov, and Z. Stuchlík, "Exploring a novel feature of ellis spacetime: Insights into scalar field dynamics," *Chin. J. Phys.*, vol. 94, pp. 807–819, 2025.

[9] B. Turimov, A. Davlataliev, Y. Usmanov, S. Karshiboev, and P. Tadjimuratov, "Investigating new aspects of Bocharova–Bronnikov–Melnikov–Bekenstein spacetime: ionized thin accretion disk model," *Eur. Phys. J. C*, vol. 84, no. 10, p. 1098, 2024.

[10] H. Hoshimov, A. Davlataliev, F. Atamurotov, A. Abdujabbarov, and A. Övgün, "Particle dynamics and quasi-periodic oscillations in the Dyonic ModMax: Constraint using quasars data," *JHEAp*, vol. 45, pp. 306–315, 2025.

[11] B. Turimov, O. Rahimov, A. Davlataliev, P. Tadjimuratov, M. Norkobilov, and S. Rahimova, "Analysing geodesic motion in Bocharova–Bronnikov–Melnikov–Bekenstein spacetime," *Phys. Dark Univ.*, vol. 48, p. 101855, 2025.

[12] R. Penrose, ""Golden Oldie": Gravitational Collapse: The Role of General Relativity," *General Relativity and Gravitation*, vol. 7, pp. 1141–1165, Jul. 2002.

[13] P. S. Joshi and I. H. Dwivedi, "Naked singularities in spherically symmetric inhomogeneous Tolman-Bondi dust cloud collapse," *Phys. Rev. D*, vol. 47, no. 12, pp. 5357–5369, Jun. 1993.

[14] B. Waugh and K. Lake, "Strengths of shell-focusing singularities in marginally bound collapsing self-similar Tolman spacetimes," *Phys. Rev. D*, vol. 38, no. 4, pp. 1315–1316, Aug. 1988.

[15] D. M. Eardley and L. Smarr, "Time functions in numerical relativity: Marginally bound dust collapse," *Phys. Rev. D*, vol. 19, no. 8, pp. 2239–2259, Apr. 1979.

[16] R. Giambò, F. Giannoni, G. Magli, and P. Piccione, "Naked Singularities Formation in the Gravitational Collapse of Barotropic Spherical Fluids," *General Relativity and Gravitation*, vol. 36, no. 6, pp. 1279–1298, Jun. 2004.

[17] P. S. Joshi, N. Dadhich, and R. Maartens, "Why do naked singularities form in gravitational collapse?" *Phys. Rev. D*, vol. 65, no. 10, p. 101501, May 2002.

[18] T. Harada, H. Iguchi, and K.-I. Nakao, "Naked singularity formation in the collapse of a spherical cloud of counterrotating particles," *Phys. Rev. D*, vol. 58, no. 4, p. 041502, Aug. 1998.

[19] Z. Kovács, T. Harko, and S. Shahidi, "Reply to "Comment on 'Can accretion disk properties observationally distinguish black holes from naked singularities?"'," *Phys. Rev. D*, vol. 98, no. 8, p. 088502, Oct. 2018.

[20] M. Blaschke and Z. Stuchlík, "Efficiency of the Keplerian accretion in braneworld Kerr-Newman spacetimes and mining instability of some naked singularity spacetimes," *Phys. Rev. D*, vol. 94, no. 8, p. 086006, Oct. 2016.

[21] Z. Stuchlík and J. Schee, "Appearance of Keplerian discs orbiting Kerr superspinars," *Classical and Quantum Gravity*, vol. 27, no. 21, p. 215017, Nov. 2010.

[22] C. Bambi, D. Malafarina, and L. Modesto, "Non-singular quantum-inspired gravitational collapse," *Phys. Rev. D*, vol. 88, no. 4, p. 044009, Aug. 2013.

[23] P. S. Joshi, D. Malafarina, and R. Narayan, "Equilibrium configurations from gravitational collapse," *Classical and Quantum Gravity*, vol. 28, no. 23, p. 235018, Dec. 2011.

[24] D. Pugliese, H. Quevedo, and R. Ruffini, "Circular motion of neutral test particles in Reissner-Nordström spacetime," *Phys. Rev. D*, vol. 83, no. 2, p. 024021, Jan. 2011.

[25] P. Pradhan and P. Majumdar, "Circular orbits in extremal Reissner-Nordstrom spacetime," *Physics Letters A*, vol. 375, no. 3, pp. 474–479, Jan. 2011.

[26] K. Hioki and K.-I. Maeda, "Measurement of the Kerr spin parameter by observation of a compact object's shadow," *Phys. Rev. D*, vol. 80, no. 2, p. 024042, Jul. 2009.

[27] L. Yang and Z. Li, "Shadow of a dressed black hole and determination of spin and viewing angle," *Int. J. Mod. Phys. D*, vol. 25, no. 02, p. 1650026, 2015.

[28] R. Takahashi, "Black hole shadows in accretion disks and spin parameters of black holes: Massive black holes and stellar mass black holes," in *The Interplay Among Black Holes, Stars and ISM in Galactic Nuclei*, T. Storchi-Bergmann, L. C. Ho, and H. R. Schmitt, Eds., vol. 222, Nov. 2004, pp. 115–116.

[29] G. N. Gyulchev and S. S. Yazadjiev, "Gravitational lensing by rotating naked singularities," *Phys. Rev. D*, vol. 78, no. 8, p. 083004, Oct. 2008.

[30] K. S. Virbhadra and G. F. Ellis, "Gravitational lensing by naked singularities," *Phys. Rev. D*, vol. 65, no. 10, p. 103004, May 2002.

[31] K. S. Virbhadra, D. Narasimha, and S. M. Chitre, "Role of the scalar field in gravitational lensing," *Astronomy & Astrophysics*, vol. 337, pp. 1–8, Sep. 1998.

[32] K. S. Virbhadra and C. R. Keeton, "Time delay and magnification centroid due to gravitational lensing by black holes and naked singularities," *Phys. Rev. D*, vol. 77, no. 12, p. 124014, Jun. 2008.

[33] V. Deliyski, G. Gyulchev, P. Nedkova, and S. Yazadjiev, "Observing naked singularities by the present and next-generation Event Horizon Telescope," *arXiv e-prints*, p. arXiv:2401.14092, Jan. 2024.

[34] D. Chen, Y. Chen, P. Wang, T. Wu, and H. Wu, "Gravitational lensing by transparent Janis-Newman-Winicour naked singularities," *European Physical Journal C*, vol. 84, no. 6, p. 584, Jun. 2024.

[35] B. Chauvineau, "Erratum: Lensing by a Fisher-Janis-Newman-Winicour naked singularity: Observational issues related to the existence of caustic

bending in the strongly scalarized case [Phys. Rev. D 105, 024071 (2022)]," *Phys. Rev. D*, vol. 106, no. 12, p. 129901, Dec. 2022.

[36] G. Gyulchev, J. Kunz, P. Nedkova, T. Vetsov, and S. Yazadjiev, "Observational signatures of strongly naked singularities: image of the thin accretion disk," *European Physical Journal C*, vol. 80, no. 11, p. 1017, Nov. 2020.

[37] M. Patil and P. S. Joshi, "High energy particle collisions in superspinning Kerr geometry," *Phys. Rev. D*, vol. 84, p. 104001, 2011.

[38] L. D. Landau and E. M. Lifshitz, *The Classical Theory of Fields, Course of Theoretical Physics, Volume 2.* Oxford: Elsevier Butterworth-Heinemann, 2004.

[39] A. Noble, D. A. Burton, L. Docherty, and D. A. Jaroszynski, "Self-force on a charged particle in an external scalar field," *New Journal of Physics*, vol. 23, no. 11, p. 115007, Nov. 2021.

[40] O. B. Zaslavskii, "Black hole with a scalar field as a particle accelerator," *International Journal of Modern Physics D*, vol. 26, no. 10, p. 1750108, Jan. 2017.

[41] C. W. Misner, R. A. Breuer, D. R. Brill, P. L. Chrzanowski, H. G. Hughes, and C. M. Pereira, "Gravitational Synchrotron Radiation in the Schwarzschild Geometry," *prl*, vol. 28, no. 15, pp. 998–1001, Apr. 1972.

[42] R. A. Breuer, P. L. Chrzanowksi, H. G. Hughes, and C. W. Misner, "Geodesic Synchrotron Radiation," *prd*, vol. 8, no. 12, pp. 4309–4319, Dec. 1973.

[43] A. I. Janis, E. T. Newman, and J. Winicour, "Reality of the Schwarzschild Singularity," *Phys. Rev. Lett.*, vol. 20, pp. 878–880, 1968.

[44] I. Z. Fisher, "Scalar mesostatic field with regard for gravitational effects," *arXiv e-prints*, pp. gr–qc/9 911 008, Nov. 1999.

[45] K. A. Bronnikov and A. V. Khodunov, "SCALAR FIELD AND GRAVITATIONAL INSTABILITY," *Gen. Rel. Grav.*, vol. 11, pp. 13–18, 1979.

[46] L. D. Landau and E. M. Lifshitz, *The Classical Theory of Fields*, 4th ed. Butterworth-Heinemann, Jan. 1980. [Online]. Available: http://www.worldcat.org/isbn/0750627689

[47] A. I. Janis, E. T. Newman, and J. Winicour, "Reality of the Schwarzschild Singularity," *Physical Review Letters*, vol. 20, pp. 878–880, Apr. 1968.

[48] E. Poisson, "The Motion of Point Particles in Curved Spacetime," *Living Reviews in Relativity*, vol. 7, no. 1, p. 6, May 2004.

[49] A. Tursunov, M. Kološ, Z. Stuchlík, and D. V. Gal'tsov, "Radiation Reaction of Charged Particles Orbiting a Magnetized Schwarzschild Black Hole," *ApJ*, vol. 861, no. 1, p. 2, Jul. 2018.

[50] B. Turimov, A. Nosirov, and A. Abdujabbarov, "Gravitational analogue of radiation reaction in STVG," *Physics of the Dark Universe*, vol. 42, p. 101375, Dec. 2023.

[51] P. Bambhaniya, A. B. Joshi, D. Dey, and P. S. Joshi, "Timelike geodesics in naked singularity and black hole spacetimes," *Phys. Rev. D*, vol. 100, p. 124020, Dec 2019. [Online]. Available: https://link.aps.org/doi/10.1103/PhysRevD.100.124020

[52] R. M. Wald, "Black hole in a uniform magnetic field," *Phys. Rev. D*, vol. 10, pp. 1680–1685, Sep 1974. [Online]. Available: https://link.aps.org/doi/10.1103/PhysRevD.10.1680

[53] S. Shaymatov, F. Atamurotov, and B. Ahmedov, "Isofrequency pairing of circular orbits in Schwarzschild spacetime in the presence of magnetic field," *Astrophys. Space Sci.*, vol. 350, no. 1, pp. 413–419, 2014.

[54] S. Shaymatov, M. Patil, B. Ahmedov, and P. S. Joshi, "Destroying a near-extremal kerr black hole with a charged particle: Can a test magnetic field serve as a cosmic censor?" *Phys. Rev. D*, vol. 91, p. 064025, Mar 2015. [Online]. Available: https://link.aps.org/doi/10.1103/PhysRevD.91.064025

[55] I. Hussain and S. Ali, "Marginally stable circular orbits in the Schwarzschild black hole surrounded by quintessence matter," *Eur. Phys. J. Plus*, vol. 131, no. 8, p. 275, 2016.

[56] N. Dadhich, A. Tursunov, B. Ahmedov, and Z. Stuchlík, "The distinguishing signature of Magnetic Penrose Process," *Mon. Not. Roy. Astron. Soc.*, vol. 478, no. 1, pp. L89–L94, 2018.

[57] A. Hakimov, A. Abdujabbarov, and B. Narzilloev, "Quantum interference effects in conformal Weyl gravity," *International Journal of Modern Physics A*, vol. 32, p. 1750116, Jul. 2017.

[58] C. A. Benavides-Gallego, A. Abdujabbarov, D. Malafarina, B. Ahmedov, and C. Bambi, "Charged particle motion and electromagnetic field in γ spacetime," *Phys. Rev. D*, vol. 99, p. 044012, Feb 2019. [Online]. Available: https://link.aps.org/doi/10.1103/PhysRevD.99.044012

[59] S. Shaymatov, J. Vrba, D. Malafarina, B. Ahmedov, and Z. Stuchlík, "Charged particle and epicyclic motions around $4D$ Einstein–Gauss–Bonnet black hole immersed in an external magnetic field," *Phys. Dark Univ.*, vol. 30, p. 100648, 2020.

[60] S. Shaymatov, B. Narzilloev, A. Abdujabbarov, and C. Bambi, "Charged particle motion around a magnetized reissner-nordström black hole," *Phys. Rev. D*, vol. 103, p. 124066, Jun 2021. [Online]. Available: https://link.aps.org/doi/10.1103/PhysRevD.103.124066

[61] J. Rayimbaev, B. Narzilloev, A. Abdujabbarov, and B. Ahmedov, "Dynamics of magnetized and magnetically charged particles around regular nonminimal magnetic black holes," *Galaxies*, vol. 9, no. 4, 2021. [Online]. Available: https://www.mdpi.com/2075-4434/9/4/71

[62] B. Narzilloev, J. Rayimbaev, A. Abdujabbarov, and B. Ahmedov, "Regular bardeen black holes in anti-de sitter spacetime versus kerr black holes through particle dynamics," *Galaxies*, vol. 9, no. 3, 2021. [Online]. Available: https://www.mdpi.com/2075-4434/9/3/63

[63] B. Narzilloev and B. Ahmedov, "Regular black hole solution in PFDM environment to explain the radiative efficiency of black hole candidates," *New Astron.*, vol. 98, p. 101922, 2023.

[64] B. Narzilloev and B. Ahmedov, "Radiation properties of the accretion disk around a black hole surrounded by pfdm," *Symmetry*, vol. 14, no. 9, 2022. [Online]. Available: https://www.mdpi.com/2073-8994/14/9/1765

[65] B. Narzilloev and B. Ahmedov, "Observational and Energetic Properties of Astrophysical and Galactic Black Holes," *Symmetry*, vol. 15, no. 2, p. 293, Jan. 2023.

[66] B. Narzilloev, A. Abdujabbarov, and A. Hakimov, "Redshift of photons emitted from the accretion disk of a regular black hole surrounded by dark matter," *International Journal of Modern Physics*

A, vol. 37, no. 23, p. 2250144, 2022. [Online]. Available: https://doi.org/10.1142/S0217751X22501445

[67] A. Davlataliev, B. Narzilloev, I. Hussain, A. Abdujabbarov, and B. Ahmedov, "Probing the Starobinsky-Bel-Robinson gravity by photon motion around the Kerr-type black hole in non-uniform plasma," *Phys. Dark Univ.*, vol. 42, p. 101340, 2023.

[68] B. Narzilloev and B. Ahmedov, "The eye of the storm: Optical properties," *Int. J. Mod. Phys. A*, vol. 38, no. 04n05, p. 2350026, 2023.

[69] Abdulxamidov, Farrux, Benavides-Gallego, Carlos A., Narzilloev, Bakhtiyor, Hussain, Ibrar, Abdujabbarov, Ahmadjon, Ahmedov, Bobomurat, and Xu, Haiguang, "Dynamics of spinning test particles around the kerr-newman-nut black hole with quintessence in the rastall gravity," *Eur. Phys. J. Plus*, vol. 138, no. 7, p. 635, 2023. [Online]. Available: https://doi.org/10.1140/epjp/s13360-023-04283-9

[70] H. Alibekov, B. Narzilloev, A. Abdujabbarov, and B. Ahmedov, "Frequency shift of photons in the spacetime of deformed rn bh," *Symmetry*, vol. 15, no. 7, 2023. [Online]. Available: https://www.mdpi.com/2073-8994/15/7/1414

[71] M. Alloqulov, B. Narzilloev, I. Hussain, A. Abdujabbarov, and B. Ahmedov, "Energetic processes around electromagnetically charged black hole in the Rastall gravity," *Chin. J. Phys.*, vol. 85, pp. 302–317, 2023.

[72] B. Narzilloev and B. Ahmedov, "Thermal radiation of thin accretion disk around Taub-NUT black hole," *Int. J. Mod. Phys. D*, vol. 32, no. 10, p. 2350064, 2023.

[73] B. Narzilloev, A. Abdujabbarov, B. Ahmedov, and C. Bambi, "Kerr-taub-nut spacetime to explain the jet power and the radiative efficiency of astrophysical black holes," *Phys. Rev. D*, vol. 108, p. 103013, Nov 2023. [Online]. Available: https://link.aps.org/doi/10.1103/PhysRevD.108.103013

[74] J. Rayimbaev, F. Abdulxamidov, S. Tojiev, A. Abdujabbarov, and F. Holmurodov, "Test Particles and Quasiperiodic Oscillations around Gravitational Aether Black Holes," *Galaxies*, vol. 11, no. 5, p. 95, 2023.

[75] F. Abdulxamidov, J. Rayimbaev, A. Abdujabbarov, and Z. Stuchlík, "Spinning magnetized particles orbiting magnetized Schwarzschild black holes," *Phys. Rev. D*, vol. 108, no. 4, p. 044030, 2023.

[76] N. Kurbonov, J. Rayimbaev, M. Alloqulov, M. Zahid, F. Abdulxamidov, A. Abdujabbarov, and M. Kurbanova, "Charged particles and Penrose process near charged black holes in Einstein–Maxwell-scalar theory," *Eur. Phys. J. C*, vol. 83, no. 6, p. 506, 2023.

[77] F. Abdulxamidov, C. A. Benavides-Gallego, W.-B. Han, J. Rayimbaev, and A. Abdujabbarov, "Spinning test particle motion around a rotating wormhole," *Phys. Rev. D*, vol. 106, no. 2, p. 024012, 2022.

[78] F. Abdulkhamidov, P. Nedkova, J. Rayimbaev, J. Kunz, and B. Ahmedov, "Parameter constraints on traversable wormholes within beyond Horndeski theories through quasiperiodic oscillations," *Phys. Rev. D*, vol. 109, no. 10, p. 104074, 2024.

[79] J. Rayimbaev, A. Abdujabbarov, F. Abdulkhamidov, V. Khamidov, S. Djumanov, J. Toshov, and S. Inoyatov, "Quasiperiodic oscillation around

charged black holes in Einstein–Maxwell-scalar theory," *Eur. Phys. J. C*, vol. 82, no. 12, p. 1110, 2022.

[80] J. Rayimbaev, D. Bardiev, F. Abdulxamidov, A. Abdujabbarov, and B. Ahmedov, "Magnetized and Magnetically Charged Particles Motion around Regular Bardeen Black Hole in 4D Einstein Gauss–Bonnet Gravity," *Universe*, vol. 8, no. 10, p. 549, 2022.

[81] J. M. Ladino, C. A. Benavides-Gallego, E. Larrañaga, J. Rayimbaev, and F. Abdulxamidov, "Charged spinning and magnetized test particles orbiting quantum improved charged black holes," *Eur. Phys. J. C*, vol. 83, no. 11, p. 989, 2023.

[82] J. Rayimbaev, S. Shaymatov, F. Abdulxamidov, S. Ahmedov, and D. Begmatova, "Magnetized Particles with Electric Charge around Schwarzschild Black Holes in External Magnetic Fields," *Universe*, vol. 9, no. 3, p. 135, 2023.

[83] A. Ditta, X. Tiecheng, S. Mumtaz, F. Atamurotov, G. Mustafa, and A. Abdujabbarov, "Testing metric-affine gravity using particle dynamics and photon motion," *Physics of the Dark Universe*, vol. 41, p. 101248, 2023. [Online]. Available: https://www.sciencedirect.com/science/article/pii/S2212686423000821

[84] B. Narzilloev, I. Hussain, A. Abdujabbarov, B. Ahmedov, and C. Bambi, "Dynamics and fundamental frequencies of test particles orbiting Kerr–Newman–NUT–Kiselev black hole in Rastall gravity," *Eur. Phys. J. Plus*, vol. 136, no. 10, p. 1032, 2021.

[85] T. Mirzaev, S. Li, B. Narzilloev, I. Hussain, A. Abdujabbarov, and B. Ahmedov, "Simulated image of the shadow of the Kerr-Newman-NUT-Kiselev black hole in the Rastall gravity with a thin accretion disk," *European Physical Journal Plus*, vol. 138, no. 1, p. 47, Jan. 2023.

[86] E. Battista and G. Esposito, "Geodesic motion in Euclidean Schwarzschild geometry," *Eur. Phys. J. C*, vol. 82, no. 12, p. 1088, 2022.

[87] F. Atamurotov, I. Hussain, G. Mustafa, and K. Jusufi, "Shadow and quasinormal modes of the Kerr–Newman–Kiselev–Letelier black hole," *Eur. Phys. J. C*, vol. 82, no. 9, p. 831, 2022.

[88] G. Mustafa, F. Atamurotov, I. Hussain, S. Shaymatov, and A. Övgün, "Shadows and gravitational weak lensing by the Schwarzschild black hole in the string cloud background with quintessential field*," *Chin. Phys. C*, vol. 46, no. 12, p. 125107, 2022.

[89] B. Ahmedov, O. Rahimov, and B. Toshmatov, "Gravitational Capture Cross-Section of Particles by Schwarzschild-Tangherlini Black Holes," *Universe*, vol. 7, no. 8, p. 307, Aug. 2021.

[90] B. Turimov, O. Rahimov, B. Ahmedov, Z. Stuchlík, and K. Boymurodova, "Dynamical motion of matter around a charged black hole," *International Journal of Modern Physics D*, vol. 30, no. 5, pp. 2 150 037–407, Apr. 2021.

[91] B. Toshmatov, O. Rahimov, B. Ahmedov, and A. Ahmedov, "Capture of Massless and Massive Particles by Parameterized Black Holes," *Galaxies*, vol. 9, no. 3, p. 65, Sep. 2021.

[92] B. Turimov and O. Rahimov, "The Orbital and Epicyclic Frequencies in Axially Symmetric and Stationary Spacetime," *Universe*, vol. 8, no. 10, p. 507, Sep. 2022.

[93] Y.-Q. Lei and X.-H. Ge, "Circular motion of charged particles near a charged black hole," *Phys. Rev. D*, vol. 105, p. 084011, Apr 2022. [Online]. Available: https://link.aps.org/doi/10.1103/PhysRevD.105.084011

[94] T. W. Darling, F. Rossi, G. I. Opat, and G. F. Moorhead, "The fall of charged particles under gravity: A study of experimental problems," *Rev. Mod. Phys.*, vol. 64, pp. 237–257, Jan 1992. [Online]. Available: https://link.aps.org/doi/10.1103/RevModPhys.64.237

[95] T. R. P. Carames, E. R. Bezerra de Mello, and M. E. X. Guimaraes, "On the motion of a test particle around a global monopole in a modified gravity," *Mod. Phys. Lett. A*, vol. 27, p. 1250177, 2012.

[96] H. Zhang, N. Zhou, W. Liu, and X. Wu, "Charged Particle Motions near Non-Schwarzschild Black Holes with External Magnetic Fields in Modified Theories of Gravity," *Universe*, vol. 7, no. 12, p. 488, 2021.

[97] J. Homan, M. Klein-Wolt, S. Rossi, J. M. Miller, R. Wijnands, T. Belloni, M. van der Klis, and W. H. G. Lewin, "High frequency quasi-periodic oscillations in the black hole x-ray transient xte j1650-500," *Astrophys. J.*, vol. 586, pp. 1262–1267, 2003.

[98] J. Rayimbaev, B. Ahmedov, and A. H. Bokhari, "Constraints on charged black hole parameters using quasiperiodic oscillations data," *International Journal of Modern Physics D*, vol. 31, no. 11, p. 2240004, 2022. [Online]. Available: https://doi.org/10.1142/S0218271822400041

[99] M. Qi, J. Rayimbaev, and B. Ahmedov, "Charged particles and quasiperiodic oscillations around magnetized Schwarzschild black holes," *European Physical Journal C*, vol. 83, no. 8, p. 730, Aug. 2023.

[100] L. Rezzolla, S. Yoshida, T. J. Maccarone, and O. Zanotti, "A New simple model for high frequency quasi periodic oscillations in black hole candidates," *Mon. Not. Roy. Astron. Soc.*, vol. 344, p. L37, 2003.

[101] G. Torok, A. Kotrlova, E. Sramkova, and Z. Stuchlik, "Confronting the models of 3:2 quasiperiodic oscillations with the rapid spin of the microquasar GRS 1915+105," *Astron. Astrophys.*, vol. 531, p. A59, 2011.

[102] Z. Stuchlik, A. Kotrlova, and G. Torok, "Resonant radii of kHz quasi-periodic oscillations in Keplerian discs orbiting neutron stars," *Astron. Astrophys.*, vol. 525, p. A82, 2011.

[103] Z. Stuchlik, A. Kotrlova, and G. Torok, "Multi-resonance orbital model of high-frequency quasi-periodic oscillations: possible high-precision determination of black hole and neutron star spin," *Astron. Astrophys.*, vol. 552, p. A10, 2013.

[104] G. Mustafa, I. Hussain, and W.-M. Liu, "Quasi-periodic oscillations of test particles and red–blue shifts of photons in the charged-kiselev black hole with cloud of strings," *Chinese Journal of Physics*, vol. 80, pp. 148–166, 2022. [Online]. Available: https://www.sciencedirect.com/science/article/pii/S0577907322001319

[105] X. Jiang, P. Wang, H. Yang, and H. Wu, "Testing Kerr black hole mimickers with quasi-periodic oscillations from GRO J1655-40," *Eur. Phys. J. C*, vol. 81, no. 11, p. 1043, 2021, [Erratum: Eur.Phys.J.C 82, 5 (2022)].

[106] L. Amarilla, E. F. Eiroa, and G. Giribet, "Null geodesics and shadow of a rotating black hole in extended chern-simons modified gravity," *Phys. Rev. D*, vol. 81, p. 124045, Jun 2010. [Online]. Available: https://link.aps.org/doi/10.1103/PhysRevD.81.124045

[107] Y. Liu, G. Mustafa, S. K. Maurya, and F. Javed, "Orbital motion and quasi-periodic oscillations with periastron and Lense–Thirring precession of slowly rotating Einstein–Æther black hole," *Eur. Phys. J. C*, vol. 83, no. 7, p. 584, 2023.

[108] D. Foreman-Mackey, D. W. Hogg, D. Lang, and J. Goodman, "emcee: The MCMC Hammer," *Publications of the Astronomical Society of the Pacific*, vol. 125, no. 925, p. 306, Mar. 2013.

[109] C. Liu, H. Siew, T. Zhu, Q. Wu, Y. Sun, Y. Zhao, and H. Xu, "Constraints on the rotating self-dual black hole with quasi-periodic oscillations," *JCAP*, vol. 11, p. 096, 2023.

[110] R. Remillard, M. Muno, J. McClintock, and J. Orosz, "Evidence for Harmonic Relationships in the High Frequency QPOs of XTEJ1550-564 and GROJ1655-40," in *APS April Meeting Abstracts*, ser. APS Meeting Abstracts, Apr. 2002, p. N17.076.

[111] J. A. Orosz, J. F. Steiner, J. E. McClintock, M. A. P. Torres, R. A. Remillard, C. D. Bailyn, and J. M. Miller, "An Improved Dynamical Model for the Microquasar XTE J1550-564," *apj*, vol. 730, no. 2, p. 75, Apr. 2011.

[112] S. E. Motta, T. M. Belloni, L. Stella, T. Muñoz Darias, and R. Fender, "Precise mass and spin measurements for a stellar-mass black hole through

X-ray timing: the case of GRO J1655−40," *Mon. Not. Roy. Astron. Soc.*, vol. 437, no. 3, pp. 2554–2565, 2014.

[113] R. A. Remillard and J. E. McClintock, "X-ray Properties of Black-Hole Binaries," *Ann. Rev. Astron. Astrophys.*, vol. 44, pp. 49–92, 2006.

[114] J. A. Wheeler, "Geons," *Physical Review*, vol. 97, no. 2, pp. 511–536, Jan. 1955.

[115] C. W. Misner and J. A. Wheeler, "Classical physics as geometry," *Annals of Physics*, vol. 2, no. 6, pp. 525–603, Dec. 1957.

[116] A. Einstein and N. Rosen, "The Particle Problem in the General Theory of Relativity," *Physical Review*, vol. 48, no. 1, pp. 73–77, Jul. 1935.

[117] M. S. Morris and K. S. Thorne, "Wormholes in spacetime and their use for interstellar travel: A tool for teaching general relativity," *American Journal of Physics*, vol. 56, no. 5, pp. 395–412, May 1988.

[118] M. S. Morris, K. S. Thorne, and U. Yurtsever, "Wormholes, time machines, and the weak energy condition," *Phys. Rev. Lett.*, vol. 61, no. 13, pp. 1446–1449, Sep. 1988.

[119] H. G. Ellis, "Ether flow through a drainhole: A particle model in general relativity," *Journal of Mathematical Physics*, vol. 14, no. 1, pp. 104–118, Jan. 1973.

[120] F. S. N. Lobo, A. Simpson, and M. Visser, "Dynamic thin-shell black-bounce traversable wormholes," *Phys. Rev. D*, vol. 101, no. 12, p. 124035, Jun. 2020.

[121] J. Baines, R. Gaur, and M. Visser, "Defect Wormholes Are Defective," *Universe*, vol. 9, no. 10, p. 452, Oct. 2023.

[122] A. Papapetrou, "Eine Theorie des Gravitationsfeldes mit einer Feldfunktion," *Zeitschrift fur Physik*, vol. 139, no. 5, pp. 518–532, Oct. 1954.

[123] A. Dutta, D. Roy, and S. Chakraborty, "Particle motion around traversable wormholes: Possibility of closed timelike geodesics," *na*, vol. 111, p. 102236, Oct. 2024.

[124] P. Boonserm, T. Ngampitipan, A. Simpson, and M. Visser, "Exponential metric represents a traversable wormhole," *Phys. Rev. D*, vol. 98, no. 8, p. 084048, Oct. 2018.

[125] B. Turimov, Y. Turaev, B. Ahmedov, and Z. Stuchlík, "Circular motion of test particles around wormhole represented by exponential metric," *Physics of the Dark Universe*, vol. 35, p. 100946, Mar. 2022.

[126] J. L. Blázquez-Salcedo, C. Knoll, and E. Radu, "Traversable Wormholes in Einstein-Dirac-Maxwell Theory," *prl*, vol. 126, no. 10, p. 101102, Mar. 2021.

[127] B. Turimov, B. Ahmedov, and Z. Stuchlík, "On exact analytical solution of Einstein-Maxwell-scalar field equations," *Physics of the Dark Universe*, vol. 33, p. 100868, Sep. 2021.

[128] B. Turimov, A. Abdujabbarov, B. Ahmedov, and Z. Stuchlík, "Generic three-parameter wormhole solution in einstein-scalar field theory," *Particles*, vol. 5, no. 1, pp. 1–11, 2022. [Online]. Available: https://www.mdpi.com/2571-712X/5/1/1

[129] C.-H. Hao, X. Su, and Y.-Q. Wang, "AdS Ellis wormholes with scalar field," *arXiv e-prints*, p. arXiv:2404.11002, Apr. 2024.

[130] K. A. Bronnikov, P. E. Kashargin, and S. V. Sushkov, "Possible Wormholes in a Friedmann Universe," *Universe*, vol. 9, no. 11, p. 465, Oct. 2023.

[131] K. A. Bronnikov, P. E. Kashargin, and S. V. Sushkov, "Magnetized Dusty Black Holes and Wormholes," *Universe*, vol. 7, no. 11, p. 419, Nov. 2021.

[132] T. Müller, "Exact geometric optics in a Morris-Thorne wormhole spacetime," *prd*, vol. 77, no. 4, p. 044043, Feb. 2008.

[133] H. Ghaffarnejad, "Wave optics and weak gravitational lensing of lights from spherically symmetric static scalar vector tensor Brans Dicke wormholes," *General Relativity and Gravitation*, vol. 54, no. 1, p. 13, Jan. 2022.

[134] J. Zhang and Y. Xie, "Strong deflection gravitational lensing by the marginally unstable photon spheres of a wormhole," *prd*, vol. 109, no. 4, p. 043032, Feb. 2024.

[135] M. Alloqulov, F. Atamurotov, A. Abdujabbarov, B. Ahmedov, and V. Khamidov, "Shadow and weak gravitational lensing for Ellis-Bronnikov wormhole," *Chinese Physics C*, vol. 48, no. 2, p. 025104, Feb. 2024.

[136] R. Shaikh, P. Banerjee, S. Paul, and T. Sarkar, "Erratum: Strong gravitational lensing by wormholes," *jcap*, vol. 2023, no. 12, p. E01, Dec. 2023.

[137] T. Manna, F. Rahaman, and T. Chowdhury, "Strong lensing in the exponential wormhole spacetimes," *na*, vol. 102, p. 102040, Aug. 2023.

[138] E. Deligianni, B. Kleihaus, J. Kunz, P. Nedkova, and S. Yazadjiev, "Quasiperiodic oscillations in rotating Ellis wormhole spacetimes," *Phys. Rev. D*, vol. 104, no. 6, p. 064043, Sep. 2021.

[139] E. Deligianni, J. Kunz, P. Nedkova, S. Yazadjiev, and R. Zheleva, "Quasiperiodic oscillations around rotating traversable wormholes," *Phys. Rev. D*, vol. 104, no. 2, p. 024048, Jul. 2021.

[140] J. Vrba, J. Rayimbaev, Z. Stuchlik, and B. Ahmedov, "Charged particles motion and quasiperiodic oscillation in Simpson-Visser spacetime in the presence of external magnetic fields," *European Physical Journal C*, vol. 83, no. 9, p. 854, Sep. 2023.

[141] C. A. Benavides-Gallego, W.-B. Han, D. Malafarina, B. Ahmedov, and A. Abdujabbarov, "Spinning test particle motion around a traversable wormhole," *Phys. Rev. D*, vol. 104, no. 8, p. 084024, Oct. 2021.

[142] B. Azad, J. L. Blázquez-Salcedo, F. Scen Khoo, and J. Kunz, "Radial perturbations of Ellis-Bronnikov wormholes in slow rotation up to second order," *arXiv e-prints*, p. arXiv:2403.08387, Mar. 2024.

[143] Y. Kang and S.-W. Kim, "The gravitational perturbation of a Morris-Thorne wormhole and the Newman-Penrose formalism," *Classical and Quantum Gravity*, vol. 37, no. 10, p. 105012, May 2020.

[144] F. Cremona, L. Pizzocchero, and O. Sarbach, "Gauge-invariant spherical linear perturbations of wormholes in Einstein gravity minimally coupled to a self-interacting phantom scalar field," *Phys. Rev. D*, vol. 101, no. 10, p. 104061, May 2020.

[145] B. Turimov, A. Davlataliev, A. Abdujabbarov, and B. Ahmedov, "Influence of scalar field in massive particle motion in JNW spacetime," *Accepted to Phys. Rev. D*, p. https://journals.aps.org/prd/accepted/8d07fQ22H931e045a1c93965e8fa61def0ecd1a8b, Sep. 2024.

[146] B. Turimov and O. Rahimov, "The Orbital and Epicyclic Frequencies in Axially Symmetric and Stationary Spacetime," *Universe*, vol. 8, no. 10, p. 507, Sep. 2022.

[147] R. M. Wald, "Black hole in a uniform magnetic field," *Phys. Rev. D*, vol. 10, no. 6, pp. 1680–1685, Sep. 1974.

[148] T. Regge and J. A. Wheeler, "Stability of a Schwarzschild Singularity," *Physical Review*, vol. 108, no. 4, pp. 1063–1069, Nov. 1957.

[149] F. J. Zerilli, "Effective Potential for Even-Parity Regge-Wheeler Gravitational Perturbation Equations," *Phys. Rev. Lett*, vol. 24, no. 13, pp. 737–738, Mar. 1970.

[150] K. D. Kokkotas and B. G. Schmidt, "Quasinormal modes of stars and black holes," *Living Rev. Rel.*, vol. 2, p. 2, 1999.

[151] H.-P. Nollert, "Quasinormal modes: the characteristic 'sound' of black holes and neutron stars," *Class. Quant. Grav.*, vol. 16, pp. R159–R216, 1999.

[152] E. Berti, V. Cardoso, and A. O. Starinets, "Quasinormal modes of black holes and black branes," *Classical and Quantum Gravity*, vol. 26, no. 16, p. 163001, 2009.

[153] R. A. Konoplya and A. Zhidenko, "Quasinormal modes of black holes: From astrophysics to string theory," *Rev. Mod. Phys.*, vol. 83, pp. 793–836, 2011.

[154] B. Abbott *et al.*, "Observation of gravitational waves from a binary black hole merger," *Physical Review Letters*, vol. 116, no. 6, p. 061102, 2016.

[155] R. Abbott *et al.*, "GW190814: Gravitational Waves from the Coalescence of a 23 Solar Mass Black Hole with a 2.6 Solar Mass Compact Object," *Astrophys. J. Lett.*, vol. 896, no. 2, p. L44, 2020.

[156] B. P. Abbott *et al.*, "GW170817: Observation of Gravitational Waves from a Binary Neutron Star Inspiral," *Phys. Rev. Lett.*, vol. 119, no. 16, p. 161101, 2017.

[157] M. Isi, M. Giesler, W. M. Farr, M. A. Scheel, and S. A. Teukolsky, "Testing the no-hair theorem with gw150914," *Physical Review Letters*, vol. 123, no. 11, p. 111102, 2019.

[158] V. Cardoso *et al.*, "Testing the nature of dark compact objects: a status report," *Physical Review D*, vol. 104, no. 10, p. 103010, 2021.

[159] L. E. Simone and C. M. Will, "Massive scalar quasinormal modes of Schwarzschild and Kerr black holes," *Class. Quant. Grav.*, vol. 9, pp. 963–978, 1992.

[160] P. Burikham, S. Ponglertsakul, and L. Tannukij, "Charged scalar perturbations on charged black holes in de Rham-Gabadadze-Tolley massive gravity," *Phys. Rev. D*, vol. 96, no. 12, p. 124001, 2017.

[161] C. Wu and R. Xu, "Decay of massive scalar field in a black hole background immersed in magnetic field," *Eur. Phys. J. C*, vol. 75, no. 8, p. 391, 2015.

[162] A. Dubinsky and A. Zinhailo, "Asymptotic decay and quasinormal frequencies of scalar and Dirac fields around dilaton-de Sitter black holes," *Eur. Phys. J. C*, vol. 84, no. 8, p. 847, 2024.

[163] A. Ohashi and M.-a. Sakagami, "Massive quasi-normal mode," *Class. Quant. Grav.*, vol. 21, pp. 3973–3984, 2004.

[164] R. A. Konoplya and A. V. Zhidenko, "Decay of massive scalar field in a Schwarzschild background," *Phys. Lett. B*, vol. 609, pp. 377–384, 2005.

[165] R. A. Konoplya and A. Zhidenko, "Stability and quasinormal modes of the massive scalar field around Kerr black holes," *Phys. Rev. D*, vol. 73, p. 124040, 2006.

[166] A. Zhidenko, "Massive scalar field quasi-normal modes of higher dimensional black holes," *Phys. Rev. D*, vol. 74, p. 064017, 2006.

[167] M. Zhang, J. Jiang, and Z. Zhong, "The longlived charged massive scalar field in the higher-dimensional Reissner–Nordström spacetime," *Phys. Lett. B*, vol. 789, pp. 13–18, 2019.

[168] R. A. Konoplya and A. Zhidenko, "Quasinormal modes of massive fermions in Kerr spacetime: Long-lived modes and the fine structure," *Phys. Rev. D*, vol. 97, no. 8, p. 084034, 2018.

[169] S. V. Bolokhov, "Long-lived quasinormal modes and overtones' behavior of holonomy-corrected black holes," *Phys. Rev. D*, vol. 110, no. 2, p. 024010, 2024.

[170] R. A. Konoplya and A. Zhidenko, "Massive charged scalar field in the Kerr-Newman background I: quasinormal modes, late-time tails and stability," *Phys. Rev. D*, vol. 88, p. 024054, 2013.

[171] A. Aragón, R. Bécar, P. A. González, and Y. Vásquez, "Massive Dirac quasinormal modes in Schwarzschild–de Sitter black holes: Anomalous decay rate and fine structure," *Phys. Rev. D*, vol. 103, no. 6, p. 064006, 2021.

[172] A. F. Zinhailo, "Exploring unique quasinormal modes of a massive scalar field in brane-world scenarios," *Phys. Lett. B*, vol. 853, p. 138682, 2024.

[173] S. S. Seahra, C. Clarkson, and R. Maartens, "Detecting extra dimensions with gravity-wave spectroscopy: The black-string brane world," *Phys. Rev. Lett.*, vol. 94, p. 121302, Apr 2005. [Online]. Available: https://link.aps.org/doi/10.1103/PhysRevLett.94.121302

[174] C. G. Boehmer, G. De Risi, T. Harko, and F. S. N. Lobo, "Classical tests of general relativity in brane world models," *Class. Quant. Grav.*, vol. 27, p. 185013, 2010.

[175] R. A. Konoplya and R. D. B. Fontana, "Quasinormal modes of black holes immersed in a strong magnetic field," *Phys. Lett. B*, vol. 659, pp. 375–379, 2008.

[176] R. A. Konoplya, "Magnetic field creates strong superradiant instability," *Phys. Lett. B*, vol. 666, pp. 283–287, 2008.

[177] R. Brito, V. Cardoso, and P. Pani, "Superradiant instability of black holes immersed in a magnetic field," *Phys. Rev. D*, vol. 89, no. 10, p. 104045, 2014.

[178] S. Hod and T. Piran, "Late time tails in gravitational collapse of a selfinteracting (massive) scalar field and decay of a selfinteracting scalar hair," *Phys. Rev. D*, vol. 58, p. 044018, 1998.

[179] H. Koyama and A. Tomimatsu, "Slowly decaying tails of massive scalar fields in spherically symmetric space-times," *Phys. Rev. D*, vol. 65, p. 084031, 2002.

[180] H. Koyama and A. Tomimatsu, "Asymptotic tails of massive scalar fields in Schwarzschild background," *Phys. Rev. D*, vol. 64, p. 044014, 2001.

[181] M. Rogatko and A. Szyplowska, "Decay of massive scalar hair on brane black holes," *Phys. Rev. D*, vol. 76, p. 044010, 2007.

[182] R. Moderski and M. Rogatko, "Late time evolution of a selfinteracting scalar field in the space-time of dilaton black hole," *Phys. Rev. D*, vol. 64, p. 044024, 2001.

[183] G. W. Gibbons, M. Rogatko, and A. Szyplowska, "Decay of Massive Dirac Hair on a Brane-World Black Hole," *Phys. Rev. D*, vol. 77, p. 064024, 2008.

[184] J. Jing, "Late-time evolution of charged massive Dirac fields in the Reissner-Nordstrom black-hole background," *Phys. Rev. D*, vol. 72, p. 027501, 2005.

[185] R. A. Konoplya, A. Zhidenko, and C. Molina, "Late time tails of the massive vector field in a black hole background," *Phys. Rev. D*, vol. 75, p. 084004, 2007.

[186] R. A. Konoplya and A. Zhidenko, "Asymptotic tails of massive gravitons in light of pulsar timing array observations," *Phys. Lett. B*, vol. 853, p. 138685, 2024.

[187] A. Afzal *et al.*, "The NANOGrav 15 yr Data Set: Search for Signals from New Physics," *Astrophys. J. Lett.*, vol. 951, no. 1, p. L11, 2023, [Erratum: Astrophys.J.Lett. 971, L27 (2024), Erratum: Astrophys.J. 971, L27 (2024)].

[188] S. V. Bolokhov, "Long-lived quasinormal modes and oscillatory tails of the Bardeen spacetime," *Phys. Rev. D*, vol. 109, no. 6, p. 064017, 2024.

[189] K. A. Bronnikov, R. A. Konoplya, and A. Zhidenko, "Instabilities of wormholes and regular black holes supported by a phantom scalar field," *Phys. Rev. D*, vol. 86, p. 024028, 2012.

[190] A. Flachi and J. P. S. Lemos, "Quasinormal modes of regular black holes," *Phys. Rev. D*, vol. 87, no. 2, p. 024034, 2013.

[191] S. Fernando and J. Correa, "Quasinormal Modes of Bardeen Black Hole: Scalar Perturbations," *Phys. Rev. D*, vol. 86, p. 064039, 2012.

[192] B. Toshmatov, A. Abdujabbarov, Z. Stuchlík, and B. Ahmedov, "Quasinormal modes of test fields around regular black holes," *Phys. Rev. D*, vol. 91, no. 8, p. 083008, 2015.

[193] B. Toshmatov, Z. Stuchlík, B. Ahmedov, and D. Malafarina, "Relaxations of perturbations of spacetimes in general relativity coupled to nonlinear electrodynamics," *Phys. Rev. D*, vol. 99, no. 6, p. 064043, 2019.

[194] J. Rayimbaev, B. Majeed, M. Jamil, K. Jusufi, and A. Wang, "Quasiperiodic oscillations, quasinormal modes and shadows of Bardeen–Kiselev Black Holes," *Phys. Dark Univ.*, vol. 35, p. 100930, 2022.

[195] R. A. Konoplya, D. Ovchinnikov, and B. Ahmedov, "Bardeen spacetime as a quantum corrected Schwarzschild black hole: Quasinormal modes and Hawking radiation," *Phys. Rev. D*, vol. 108, no. 10, p. 104054, 2023.

[196] R. A. Konoplya, Z. Stuchlik, A. Zhidenko, and A. F. Zinhailo, "Quasinormal modes of renormalization group improved Dymnikova regular black holes," *Phys. Rev. D*, vol. 107, no. 10, p. 104050, 2023.

[197] A. Simpson and M. Visser, "Regular black holes with asymptotically Minkowski cores," *Universe*, vol. 6, no. 1, p. 8, 2019.

[198] A. Simpson and M. Visser, "The eye of the storm: a regular Kerr black hole," *J. Cosmol. A. P.*, vol. 03, no. 03, p. 011, 2022.

[199] B. F. Schutz and C. M. Will, "Black hole normal modes - A semianalytic approach," *apjl*, vol. 291, pp. L33–L36, Apr. 1985.

[200] N. Froeman, P. O. Froeman, N. Andersson, and A. Hoekback, "Black hole normal modes: Phase integral treatment," *Phys. Rev. D*, vol. 45, pp. 2609–2616, 1992.

[201] J. Matyjasek and M. Opala, "Quasinormal modes of black holes: The improved semianalytic approach," *Phys. Rev. D*, vol. 96, p. 024011, Jul 2017. [Online]. Available: https://link.aps.org/doi/10.1103/PhysRevD.96.024011

[202] R. A. Konoplya, A. Zhidenko, and A. F. Zinhailo, "Higher order WKB formula for quasinormal modes and grey-body factors: recipes for quick and accurate calculations," *Class. Quant. Grav.*, vol. 36, p. 155002, 2019.

[203] R. A. Konoplya, "Quasinormal behavior of the d-dimensional Schwarzschild black hole and higher order WKB approach," *Phys. Rev. D*, vol. 68, p. 024018, 2003.

[204] K. D. Kokkotas, R. A. Konoplya, and A. Zhidenko, "Quasinormal modes, scattering and Hawking radiation of Kerr-Newman black holes in a magnetic field," *Phys. Rev. D*, vol. 83, p. 024031, 2011.

[205] C. Gundlach, R. H. Price, and J. Pullin, "Late time behavior of stellar collapse and explosions: 1. Linearized perturbations," *Phys. Rev. D*, vol. 49, pp. 883–889, 1994.

[206] B. Toshmatov, Z. c. v. Stuchlík, J. Schee, and B. Ahmedov, "Electromagnetic perturbations of black holes in general relativity coupled to nonlinear electrodynamics," *Phys. Rev. D*, vol. 97, p. 084058, Apr 2018. [Online]. Available: https://link.aps.org/doi/10.1103/PhysRevD.97.084058

[207] G. R. de Prony, "Essai expérimental et analytique: Sur les lois de la dilatabilité de fluides élastiques et sur celles de la force expansive de la vapeur de

l'alcool, à différentes températures," *Journal de l'École Polytechnique*, vol. 1, no. 22, p. 24–76, 1795.

[208] J. Lin, M. Bravo-Gaete, and X. Zhang, "Quasinormal modes, greybody factors, and thermodynamics of four dimensional AdS black holes in critical gravity," *Phys. Rev. D*, vol. 109, no. 10, p. 104039, 2024.

[209] S. V. Bolokhov, "Black holes in Starobinsky-Bel-Robinson Gravity and the breakdown of quasinormal modes/null geodesics correspondence," *Phys. Lett. B*, vol. 856, p. 138879, 2024.

[210] M. A. Cuyubamba, R. A. Konoplya, and A. Zhidenko, "Quasinormal modes and a new instability of Einstein-Gauss-Bonnet black holes in the de Sitter world," *Phys. Rev. D*, vol. 93, no. 10, p. 104053, 2016.

[211] A. Dubinsky, "Overtones of black holes via time-domain integration," *Mod. Phys. Lett. A*, vol. 39, no. 21n22, p. 2450108, 2024.

[212] Z. Malik, "Analytical QNMs of fields of various spin in the Hayward spacetime," *EPL*, vol. 147, no. 6, p. 69001, 2024.

[213] M. Skvortsova, "Quasinormal Frequencies of Fields with Various Spin in the Quantum Oppenheimer–Snyder Model of Black Holes," *Fortsch. Phys.*, vol. 72, no. 9-10, p. 2400132, 2024.

[214] A. Al-Badawi, S. K. Jha, and A. Rahaman, "Hairy black hole, Fermionic greybody factors, Quasinormal modes, Hawking radiation, Power spectrum and sparsity," *Eur. Phys. J. C*, vol. 84, p. 145, 2024.

[215] S. Aneesh, S. Bose, and S. Kar, "Gravitational waves from quasinormal modes of a class of Lorentzian wormholes," *Phys. Rev. D*, vol. 97, no. 12, p. 124004, 2018.

[216] R. A. Konoplya, Z. Stuchlík, and A. Zhidenko, "Massive Fields Affected by Echoes: New Physics vs. Astrophysical Environment," *arXiv e-prints*, p. arXiv:2411.09014, Nov. 2024.